APPLICATION OF SURFACE SEVERE PLASTIC DEFORMATION TO $\alpha + \beta$ AND β TITANIUM ALLOYS FOR MICROSTRUCTURAL MODIFICATION

A Dissertation

Submitted to the Faculty

of

Purdue University

by

David A. Brice

In Partial Fulfillment of the

Requirements for the Degree

of

Doctor of Philosophy

December 2019

Purdue University

West Lafayette, Indiana

THE PURDUE UNIVERSITY GRADUATE SCHOOL
STATEMENT OF DISSERTATION APPROVAL

Dr.David Bahr, Co-chair

School of Materials Engineering

Dr. Kevin Trumble

School of Materials Engineering

Dr. David Johnson

School of Materials Engineering

Dr. Lia Stanciu

School of Materials Engineering

Approved by:

Dr. David Bahr

Head of the School Graduate Program

Dedicated to my grandmothers Rose Mackay and Lucía Gerstl, who are missed very dearly.

ACKNOWLEDGMENTS

I would like to express my appreciation of all the support I have received from many people throughout the years that has made it possible for me to continue my academic pursuits. Firstly, I would like to express my deepest thanks to my advisors professors David Bhar and Kevin Trumble. Without their continued input, support, knowledge and guidance the work shown in this document would not be possible. I also want to give thanks to the committee members Professors Lia Stanciu and David Johnson, both of whom provided advise throughout the project. I also must acknowledge the help I received from my fellow students who help in the execution of experiments or simply helped me talk through results. I would like to thank Raheleh Rahimi, Siavash Ganbari, Temitope Aminu, Ana Ulloa, Mojib Saei. I would especially thank Quin Shuck for allowing me the use of his shot peening cabinet after other facilities became unexpectedly unavailable. I would like to thank my parents(Albert and Beatriz) brother(Alvaro)who have all helped and encouraged me in many ways throughout the pursuits of my doctorate and before..Particularly I would like to thank my wife (Randa) who has been an invaluable ally through my graduate career and an immense support in all aspects of my life.

TABLE OF CONTENTS

Page

Page

LIST OF TABLES

Table Page

LIST OF FIGURES

Figure Page

Figure Page

Figure Page

ABSTRACT

Brice, David A. Ph.D., Purdue University, December 2019. Application of Surface Severe Plastic Deformation to $\alpha+\beta$ and β Titanium Alloys for Microstructural Modification. Major Professor: David Bahr and Kevin Trumble.

Grain refinement of metallic materials has become a popular topic for investigation because decreasing grain size improves mechanical properties; however, the production of large pieces/parts with refined grain structures is problematic. Early attempts to produce fine grained materials relied on gas condensation, or milling processes that produced nanocrystalline materials. These processes produced small specimens that had nanocrystalline structures, but exhibited decreased ductility. The use of severe plastic deformation processes, namely ECAP, have produced ultra fine grained materials; however, the uniform grain sizes still decrease overall ductility of the piece produced. Recently, surface deformation processes have produced localized refinement of the surface in metallic materials, and reported an increase in strength along with ductility. This study focuses on the use of shot peening(SP) as a severe plastic deformation and its application to Ti based alloys, and has varied goals. Firstly, this project has used SP as a deformation process that coupled with a post SP heat-treatment resulted in clear and consistent grain refinement in a variety of titanium alloys. The alloys used for this investigation were selected to represent classes of titanium alloys of interest to several industries, and more importantly to contrast the capabilities of lesser known alloys with Ti-64. Application of SP produced clear grain refinement of surface layers that measured several microns from the surface. Significant hardening of the surface was measured as a result of the layers produced. Other effects from the processing, such as precipitation of α-Ti in β-alloys, were examined and shown to be influenced by elastic residual stresses. Also,

the corrosion resistance of the layers was measured through cyclic potentiondynamic polarization under conditions that mimic biological environment. Proof of concept for self-peening is reported in this study. Self-peening is the practice of performing SP with shot media composed of the same (or similar) material as the part that is being treated. Production of shot media was successfully performed through the exploitation of titanium oxidation. Evidence is provided that clearly shows decreased surface contamination when using the Ti-based shot media to shot peen Ti alloys. Additionally the surface hardening and residual stress imparted by the different shot media , while being used with identical shot peening conditions were compared.

1. INTRODUCTION

Titanium alloys are valued materials due to their high strength to weight ratio, a fact that has been exploited by the aerospace industry for several decades. The medical industry has also exploited Ti alloys for the chemical resistance to corrosive environments. As seen in the aerospace industry [1], medical implants are mainly produced from commercially pure Ti and Ti-6Al-4V (Ti-64) [2].Ti-based materials in medicine are most notably used in implants for total hip and joint replacement. Titanium has been used in these applications primarily because Ti is inert (caused by passive oxide layer), is non-toxic in the body, and mainly due to the corrosion resistance it maintains its mechanical properties within the body [3]

A cursory look at the titanium industry reveals that Ti-6Al-4V (Ti-64) is the most widely available titanium alloy that is used in many far ranging applications. However, the popularity of Ti-64 has resulted in research and development focusing on varied compositions within the Ti-Al-V system. This is evidenced by the production of "newer" alloys such as ATI-425(4Al-2V-1.5Fe), and Ti-54M(5-Al-4V). The consequence is that innovation or development into alternative compositional systems that could result in better performing alloys has been stunted. This has resulted in the relegation of β alloys to niche applications, and the use of Ti-64 into applications that would be better performed by a β-alloy. This is clearly seen in the medical field where the material of choice for implants is Ti-64. This is problematic because Ti-64 has a (relatively) large elastic modulus (105-116 GPa [4]) that can contribute to stress shielding, and eventually bone atrophy. In fact, this very problem has lead to the development of β-alloys that have low elastic modulus such as TNZ (76-82 GPa) [5], Ti-15Mo(78 GPa) [6], and TMZF(82 GPa) [7]. The common theme among all of the bio-alloys is the decreased aluminum content for the simple reason that Al will stabilize the α phase that is far stiffer than β-Ti phase. Looking at an Ashby plot

of metallic materials used in medical applications (see Fig.1.1), it can be seen that materials that can exhibit high strength, low density and low modulus, to achieve good modulus matching with bone, will be β-alloys. Note that density is a necessary consideration because bone is a low density material ($1.9 g/cm^3$ [8]);consequently, the density of the implant material should be limited. This study represents an effort to show the versatility of β alloys in comparison to $\alpha + \beta$ alloys. Thus it is important to understand the capabilities of existing β alloys, in order to enable better selection of materials for a given application.

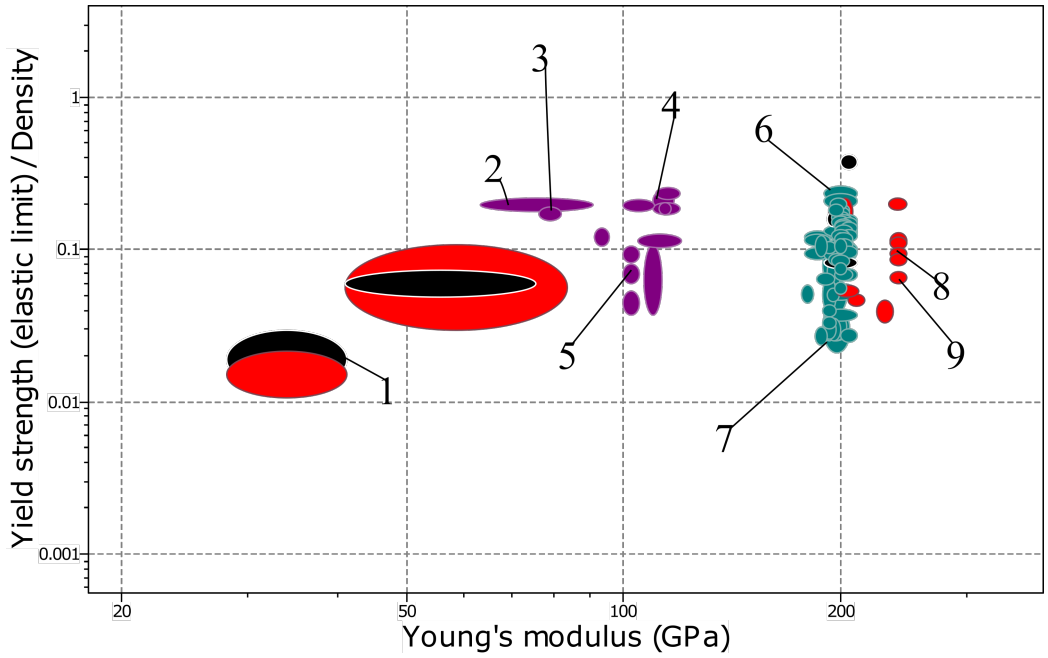

Fig. 1.1. Ashby plot of several metallic materials used in medical applications shows Young's modulus vs tensile yield strength/ density for (1) Ni-45Ti Nitinol, (2)TMZF (3)Ti-13Nb-13Zr(TNZ), (4) Ti-64, (5) CP-Ti grade 2, (6) AISI 440B, (7) AISI 316L, (8) BioDur CCM plus, (9) BioDur 108. Plot was created with CES Edupack

Surface modification of implant materials can be classified to patterning or the surface or chemical modification. Surface patterning tends to focus on producing features such as pores or other features at the surface that increase the roughness [3].

This study aims to use shot peening for surface modification of various titanium alloys. Shot peening(SP) is a well-established and relatively inexpensive surface modification technique that is used to produce strain hardening of the surface due to localized deformation of a small volume adjacent to the surface. A consequence of the localized deformation is the formation of residual stresses that can penetrate up to several millimeters into the material, and these stresses are compressive in nature. The compressive nature of the residual stress tends to improve fatigue life of parts processed with SP [9]. However, SP is a deformation process that can be exploited to induce surface recrystallization of the processed material. To induce recrystallization, heat-treatments may have to be performed after shot peening. This is usually avoided because post SP heat-treatments tend to relax away the residual stress that is providing the improved fatigue life.

This study will focus on modifying the surface of several titanium alloys to improve their performance as it relates to medical applications. The alloys selected for this project are: Ti-64, Ti-5553, and Ti21S. These alloys cover a wide range of β-stabilizer content. Again, this is done purposely to showcase the potential to get improved performance from β alloys when compared to $\alpha + \beta$ alloy for applications that have historically used CP-Ti or Ti-64. Each alloy was processed to produce different starting microstructures through a combination of heat treatments and deformation processes. The different conditions of each alloy were then subjected to shot peening. This was done to examine the response of different microstructures to localized severe plastic deformation of the surface. Following shot peening treatment of various alloys(and differing conditions), post-shot peening heat treatments were developed with the intention to produce fine scale structures at the surface.

2. LITERATURE REVIEW

2.1 Titanium Metallurgy

Titanium alloys are multi phase materials, generally, comprised of 2 primary stable phases: α-Ti and β-Ti (hexagonal closed packed and body centered cubic, respectively). α and β phases are allotropes of Ti that are present below and above the β-transus temperature (882°C), respectively. The presence of both α-Ti and β-Ti is caused by the alloying species.

2.1.1 Stabilizers and Phases

α-stabilizers

These are elements used as alloying additions that stabilize the α-Ti phase. Stabilization of the α-Ti phase is defined by the increase of the maximum temperature where α phase is present, as seen in Fig.2.1(a). Notable α-stabilizers include: Al, O, N, and C [10]. The most widely used α stabilizing alloying element is Al. Aluminum is potent solid solution strengthener in the α phase. Al is the most commonly used α-stabilizer because it is not an interstitial impurity like the others listed. It is important to note that Ti has a large solubility for O, close to 13wt% [11]. This is problematic because O embrittles the α phase [10]. Additionally, the chemical change caused by ingress of O can cause formation of other phases (e.g., Ti_3Al in Ti-6Al-4V) because it will stabilize α-Ti, and as a consequence drive other species out of solution in the α-phase, and may result in precipitation of a new phase [12].

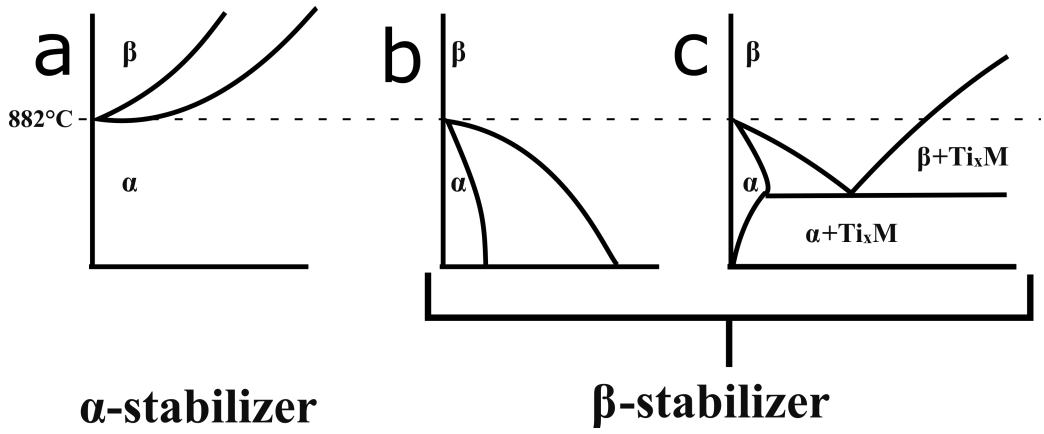

Fig. 2.1. Effect of alloying elements concentration(x-axis) on the β-transus temperature for (a) α stabilizer, (b) isomorphous β stabilizer (c) eutectoid β stabilizer. Adapted from [13].

β-stabilizers

β-stabilizers are those alloying species that stabilize the β phase, i.e. that the temperature at which the alloy can be comprised entirely of β phase decreases. Most transition metals tend to act as β stabilizers. There are 2 broad categories of β stabilizers: isomorphous and eutectoid, as seen from Fig.2.1b and c, respectively. Isomorphous stabilizing elements reduce the β transus temperature to a point where a large enough concentration of the alloying element produces a fully stable β phase at room temperature. The most widely used β-stabilizers are Mo and V [14, 15]. Alternatively, eutectoid stabilizers are those alloying species that exhibit a lowering of the β-transus temperature as solute composition increases, but below a certain temperature the β parent phase will decompose into α + intermetallic through a eutectoid transformation. These eutectoid stabilizers can be further subdivided into active (Cu, and Zn [16]) and sluggish (Fe, Cr, Si, etc) [17], depending on the rate of the eutectoid transformation.

Aluminium and Molybdenum equivalence

The properties of Ti alloys are largely based on their composition. It is convenient to compare alloys in relation to α or β stabilizer composition. The stabilizing effect is compared to a common alloying addition (Al for α-stabilizers and Mo for β-stabilizers). For example, an alloy that contains V and Fe (both β-stabilizers), there should be an equivalent composition of Mo that will produce the same volume fraction of β seen in the alloy. Thus Mo and Al equivalence can provide a quick way to estimate and compare volume fraction of alloys.

$$[Mo]_{eq} = [Mo] + 0.2[Ta] + 0.28[Nb] + 0.4[W] + 0.67[V] + 1.25[Cr] + 1.25[Ni] + 1.7[Mn] + 1.7[Co] + 2.5[Fe] from\ [4, 10] \tag{2.1}$$

$$[Al]_{eq} = [Al] + 0.17[Zr] + 0.33[Sn] + 10[O] from\ [4] \tag{2.2}$$

Mo equivalence (Eq. 2.1) is derived from the concentration (in wt%) of the alloying species needed to suppress the martensite start temperature (M_s) below room temperature [10] [4]. This also gives a measure of how potent a β stabilizer is, e.g., Fe is the most potent β stabilizer seeing as it takes 2.5 times less concentration of it to produce the same volume fraction of β-Ti when using only Mo. Similarly, the Al equivalence (Eq. 2.2) shows the relative potency an alloy species has to stabilize α-Ti.

2.1.2 Phase transformations

In addition to α-Ti and β-Ti phases, Ti alloys display several metastable phases that develop as a consequence of quenching or isothermal heat treatments.

Martensite

Martensitic phases are typically produced as a consequence of rapid quenching the alloy directly from a temperature above the β transus. This rapid quenching results in a transformation by shear motion of atoms that displaces lattice planes causing a distorted crystal lattice to be quenched in. The motion of atoms is restricted, making this phase transformation a diffusionless process, where the composition of

the product and parent phases remains the same [13]. There are 2 variations of the martensitic phase: hexagonal-α' and orthorhombic- α". The transition from α' to α" is due to increased solute content that crystallographically distorts the hexagonal lattice to a lower symmetry orthorhombic structure.

Omega phase

ω-Ti is typically seen in heavily β-stabilized Ti alloys, and exhibits a hexagonal crystal structure. The ω phase can be categorized by the process used to create it: athermal when produced by quenching and isothermal when produced by heat treating [13]. Athermal ω is produced through a displacive process, similar to martensite, and usually retains the composition of the parent phase because this is a diffusionless process. The relevance of this phase comes from its role in α precipitation during subsequent heat treatment [18], where ω-Ti affects dispersion of α precipitates. Isothermal ω is produced through a diffusion controlled decomposition of *beta*-Ti, and the volume fraction of ω produced depends on the time allowed for reaction [13].

2.1.3 Ti Alloy classification

Titanium alloys are classified in accordance to the relative fraction of phases present in them. Fig.2.2 shows the classification of alloys as it relates to the concentration of β-stabilizer in the alloy. The alloy classes are presented in Fig.2.2 and are described as follows:

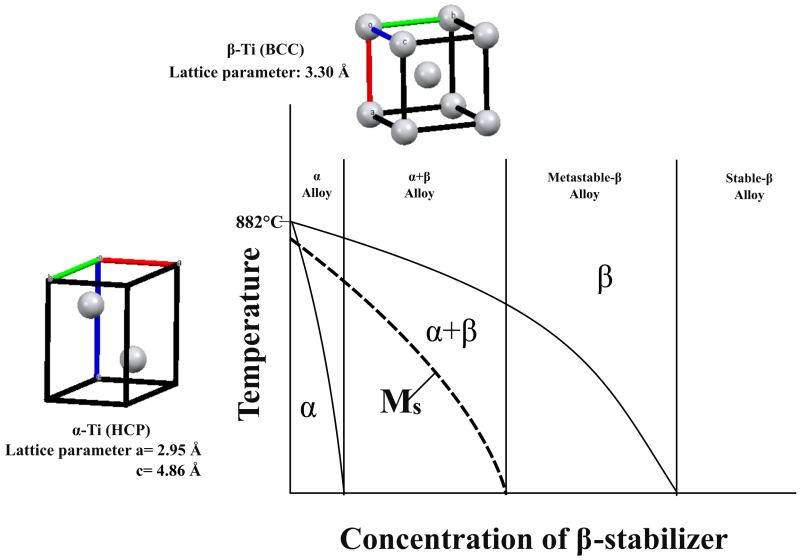

Fig. 2.2. Schematic binary titanium phase diagram in relation to β stabilizer content. Here the different alloy classes are placed, generally, in relation to their phase fractions of α and β phases. Adapted from [10]and [4].

- α **alloys**

  These alloys are comprised almost entirely of α phase. Most compositions of this class of alloy are commercially pure Ti and alloys containing large concentrations of α stabilizers such as Al.

- $\alpha + \beta$ **alloys**

  By far, this is the most common class of Ti alloys due to the prevalence of Ti-6Al-4V (Ti-64). As the name suggests, these alloys are composed of a mixture of α and β phases. These alloy show a variety of possible microstructures depending on processing and heat-treatment parameters, and will be discussed in a later section.

- **β alloys**

  This category is comprised of both metastable and stable β alloys. Generally, β alloys are those compositions that have enough β stabilizing content to suppress the martensite transformation. Bypassing the martensite transformation one produces a material that is fully composed of stable or metastable β-Ti.

2.2 Processing, Microstructure and Properties

Different classes of titanium alloys require different processing routes to get the desired microstructures and properties. The following is a review of common processing routes for $\alpha + \beta$ and β alloys.

2.2.1 $\alpha + \beta$ Alloys

$\alpha + \beta$ alloys have the capacity to produce a variety of microstructures that can be broadly divided into lamellar and equiaxed (see Fig.2.4). What follows is a brief review of processing routes used to produce these microstructures in Ti alloys.

Lamellar structures are formed through the use of processing temperatures above the β-transus temperature of the alloy(see Fig.2.3-a). There are two types of lamellar structures: (1) colony, where packets of α-laths are arranged parallel to each other within prior β-grains(Fig.2.4-a), and (2) basket weave, where α-laths form in various orientations with laths interpenetrating each other (see Fig.2.4-b).

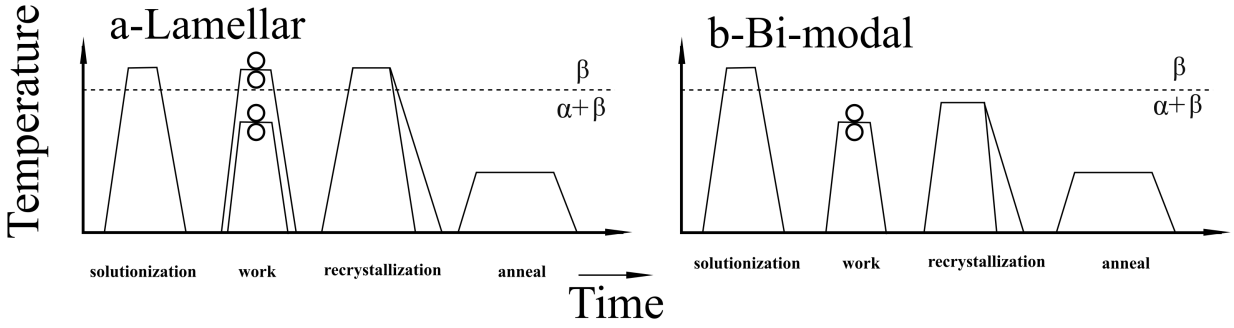

Fig. 2.3. Schematic of processing schedules to produce (a) Lamellar and (b)Bi-modal structures in $\alpha + \beta$ alloys as seen from [10]. Here the two circles identify processing steps where the material is deformed.

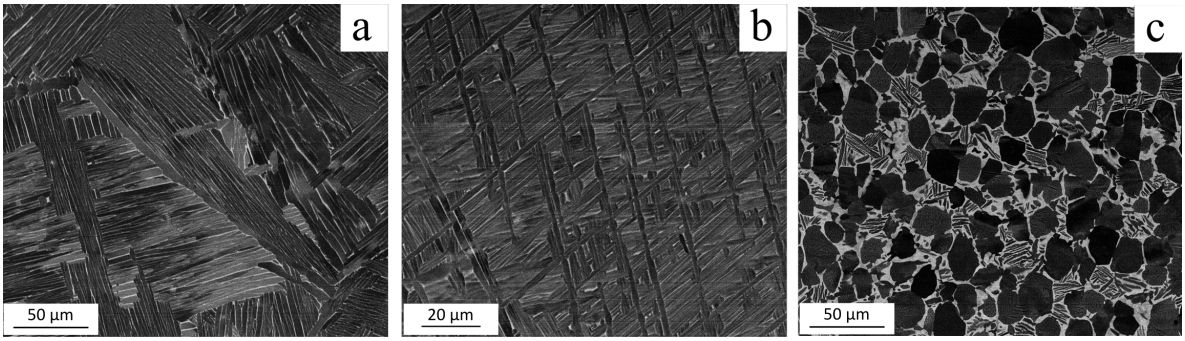

Fig. 2.4. Microstructures of Ti-64 lamellar (a) colony, (b) basket weave , and (c) bimodal equiaxed [19].

Lamellar Structures

The properties of lamellar structures are dictated by the lath thickness, prior beta grain size and colony size. The β grain size is determined by the amount of time spent above the β transus [10]. Time above the β transus is limited because fast diffusion caused by the high temperature produces large grains. The colony size and lath thickness will be determined by cooling rate from β phase field. Lütjering reports

that fast cooling rates will produce finer α laths, and restricts growth of colonies [10]. Decreasing colony size increases yield stress and resistance to macrocrack propagation [10] [20]. This is expected because the decreasing of lath thickness and colony size will serve to decrease the possible length for slip that a dislocation has [10,21,22].However, one should note a major failing present in literature: the implication that colony and basket weave have same mechanical behavior [10]. It is true they are both lamellar structures, but the larger variation in crystallographic orientations in the basket weave structure would suggest that it would be stronger than a colony structure. In IMI 685, the basket weave structure shows a slightly greater yield, UTS, and low cycle fatigue(LCF) when compared to the colony structure formed in the same alloy [23]. Therefore, the application of a severe plastic deformation process would be expected to yield different results if applied to a basket weave versus a colony structure. It would be considerable to think that the preferential textures of colony structures, that can occupy entire grains, would result in an increased resistance to deformation.

Bimodal Structures

Accompanying the lamellar structures, the bimodal structures are characterized by the formation of equiaxed α-grains along with lamellar domains (see Fig.2.4-c). Deforming the material within $\alpha+\beta$ phase field produces a primary equiaxed α-grains (α_p) due to a recrystallization event. The volume fraction of α_p produced depends on the amount of strain (dislocations) added to the material, e.g., Ti-64 can produced 10% volume fraction α_p after undergoing a 40% reduction, and 40% α_p after 65% reduction [24]. It should be noted that Semiatin reported results of thermomechanical processing, meaning that the material was hot worked. Equiaxed α-Ti forms during a recrystallization step below the β-transus temperature, where β-Ti forms along α/α boundaries, breaking up the α-laths to produce equiaxed α-grains [10,24]. Decreasing the size of the α_p can increase several properties, particularly yield strength and UTS. This is explained by the decreasing slip length provided by the formation of α_p; additionally, decreasing the size of α_p will dampen crack growth rate [10, 20]. The volume fraction and size of α_p grains are determined by recrystallization temperature

and subsequent cooling rate, respectively. The formation of α_p is linked to solute partitioning of the lamellar structures causing their softening. Initial β-grain size will affect the diffusion length of solute atoms to produce equiaxed structures, thus small β-grain sizes will produce a larger volume of α_p [24]. For both lamellar and bimodal structures, decreasing lath thickness will increase yield strength. Comparing the properties obtained from lamellar and bimodal structures obtained from IMI 834 shows that the bimodal structures can reach higher yield and UTS (995 and 1060 MPa, respectively) than lamellar structures (925 and 1015 MPa, respectively) [10].

2.2.2 β alloys

Compared to $\alpha + \beta$ alloys, the processing temperatures needed for β alloys is lower because the β-transus temperature is decreased by the increased β-stabilizer content. A clear advantage in processing β alloys (in relation to $\alpha + \beta$ alloys) is the decreased work temperatures and flow stress of the material due to the larger fraction of β-Ti [25]. There are several processing routes to produce desired microstructures and properties (see Fig.2.5).

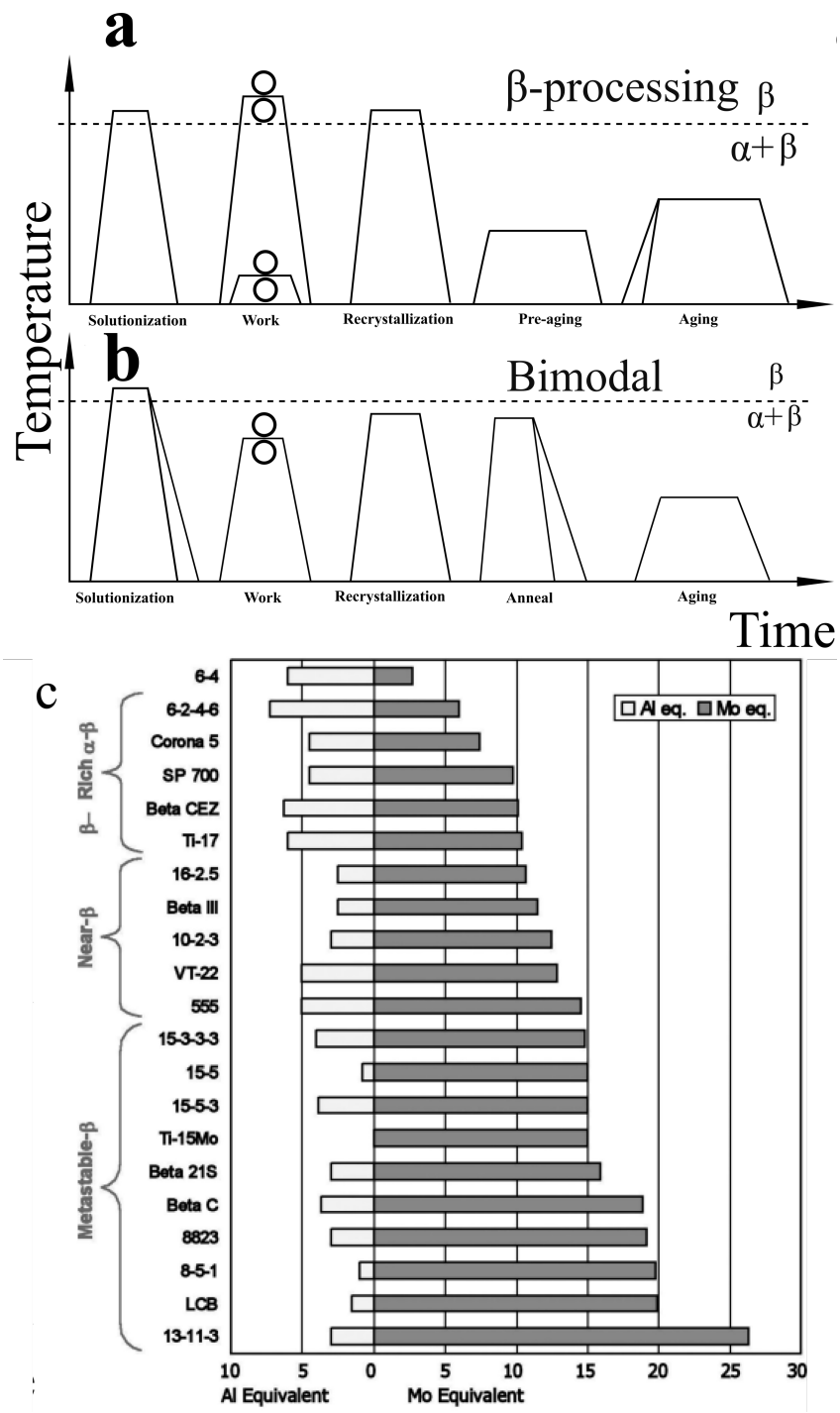

Fig. 2.5. Processing for β alloys though (a) β process and (b) Bimodal routes (adapted from [10])(c) Mo equivalences of several β-Ti alloys [26]. Here the two circles identify processing steps where the material is deformed. Figure b is used with permission from Springer Nature.

β Anneal

β anneal processing (see Fig.2.5-a) is usually used for heavily stabilized titanium alloys (Ti-21S, Ti-1023, Beta-C), where deformation is done in the β phase field because a fully β structure has a lower flow stress when compared to alloys containing α-Ti [10, 25]. A large degree of β stabilization (see Fig.2.5-c) can allow an alloy (like Ti21s) to be water quenched from above β-transus to room temperature and retain a fully-β structure devoid of α, and allow for cold working of the alloy (see Fig.2.6-a). This is highly advantageous for processing because it avoids the formation of grain boundary α-Ti that would embrittle the alloy [10]. A consequence of grain boundary α is the formation of precipitate-free zones (PFZ)(see Fig.2.6-b inset).Therefore, a recrystallization step is performed above transus temperature for a limited amount of time to limit grain growth, and avoid formation of α phase that will increase the flow stress of the material [10]. The aging step is done to precipitate α-Ti to harden the material, and can be preceded by a pre-aging step (see Fig.2.5-a). Pre-aging is done to form isothermal ω-Ti. The ω-Ti will serve as a potent nucleation site for α during the aging step (done above the solvus temp for ω-Ti), and will produce a uniformly dispersed precipitation of α-Ti [10, 13, 18, 25]; however, these fine precipitates tend to embrittle the material.

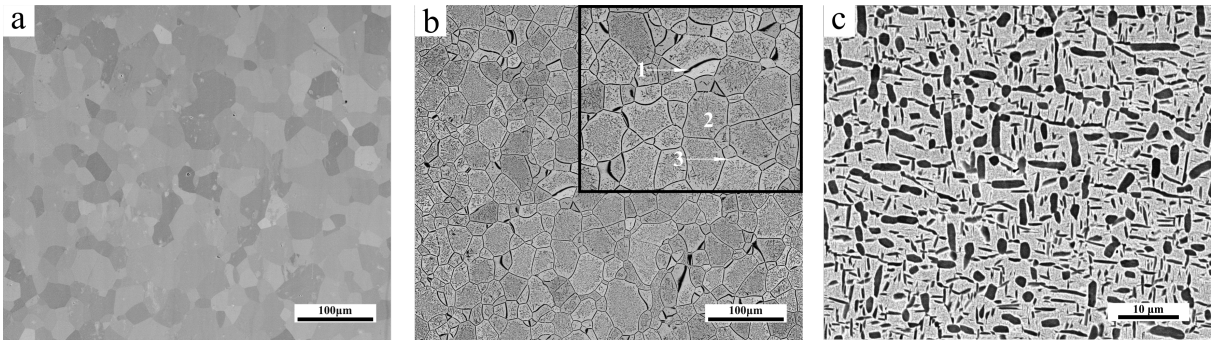

Fig. 2.6. Microstructures for of heavily stabilized in (a) β-solutionized Ti-21s, (b) β processed Ti-21s showing 1-grain boundary-α, 2-α-Ti precipitates,3-Precipitate free zones; and (c)Bimodal processed Ti-5553. [27]

Bimodal

Bimodal processing is done on β alloys that possess a large fraction of α phase, such as β-CEZ and Ti-5553. These are classed as near β alloys, and have a lesser β-stabilizer content than metastable β alloys (see Fig.2.5-c). Deformation and recrystallization happen at temperatures below β-transus temperature to produce equiaxed α grains (see Fig.2.5-b). The volume fraction of equiaxed grains will be determined by the temperature used in the annealing step, and the subsequent aging step is done to precipitate fine α plates. The increased α phase fraction in the β alloys makes them susceptible to grain boundary α formation regardless of cooling rate [10, 25].

The processing routes discussed above affect the mechanical properties by virtue of the microstructural features produced. Alloys that form grain boundary α, irrespective of processing, will have a decreased strain to fracture. The grain boundary α allows dislocation pile up against the α/β boundary causing resistance to further dislocation motion and stress concentration [21]; however this is a problem for β-rich $\alpha+\beta$ (e.g., Ti-6246) and near-β alloys(e.g., Ti-5553) rather than metastable β alloys (Ti-21s) because of the decreased volume fraction of α precipitation possible. The size of β grains does not affect the yield strength significantly between microstruc-

tures, but the volume fraction of precipitates formed during aging will affect the yield strength because it will determine inter-particle spacing [21]. Decreasing grain size influences high cycle fatigue (HCF) where finer grain size will sustain larger stresses at 10^7 cycles [10].

2.3 Corrosion

Corrosion is the gradual degradation of a material thorough interaction with the environment that cause chemical changes to the surface. For metals, corrosion can be caused by contact with aqueous solutions that contain ions such as Cl^-, H^+ and OH^-; or thermal oxidation where oxygen ingress at high temperature modifies surface chemistry. This section will focus on aqueous corrosion.

2.3.1 Reduction-Oxidation reactions and Thermodynamics

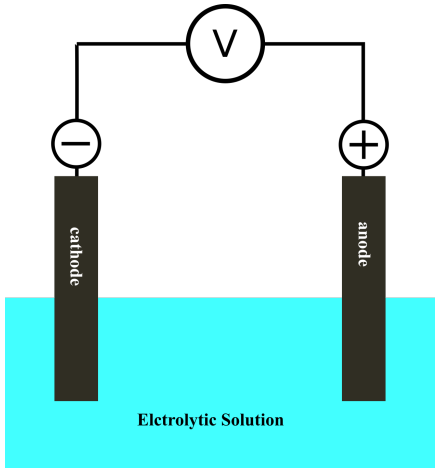

Fig. 2.7. Schematic view of electrolytic cell.

A cell can be classified as galvanic or electrolytic, the distinction is that electrolytic cells have an external voltage applied to induce a current flow [28]. In an

electrolytic cell (see Fig.2.7) there is a distinction between each electrode depending on the chemical reactions taking place. The positively charged electrode, where the electrons (e^-) flow into, is the anode. Conversely, the negatively charged electrode, where positively charged ions flow into, is the cathode. The distinction between the two electrodes is important because different reactions will take place at each electrode. At the cathode, reduction will take place, and oxidation will take place in the anode.

$$H^+ + e^- \rightarrow \frac{1}{2}H_2 \text{ [28]} \tag{2.3}$$

$$Al \rightarrow Al^{3+} + 3e^- \text{ [28]} \tag{2.4}$$

Reduction and oxidation (REDOX) are chemical reactions that involve the motion or exchange of electron. An example of a reduction reaction is presented in Eq.2.3, here the H^+ ion is reduced by gaining an electron. Conversely, oxidation (see Eq.2.4) is the loss electrons. REDOX reactions are not necessarily spontaneous processes, and may require energy input to happen. The Nernst equation (see Eq.2.5) uses the cell potential of a given REDOX reaction to determine the Gibbs energy associated with the reaction. Therefore Nernst determines whether the reaction is likely to happen, but like most thermodynamics it does not take time into account.

$$\Delta G = -nFE_cell \tag{2.5}$$

Here n is the number of electrons participating in the reaction, F is Faraday's constant, and E_{cell} is the potential of the reaction. This means that reactions having a negative E_{cell} will not be spontaneous. The galvanic series (see Fig.2.8-a) is an arrangement of metals in relation to how spontaneous their reduction reaction is, as measured by the cell potential or electromotive force (EMF). With highly positive EMF the metal is more noble, i.e., less likely to corrode.

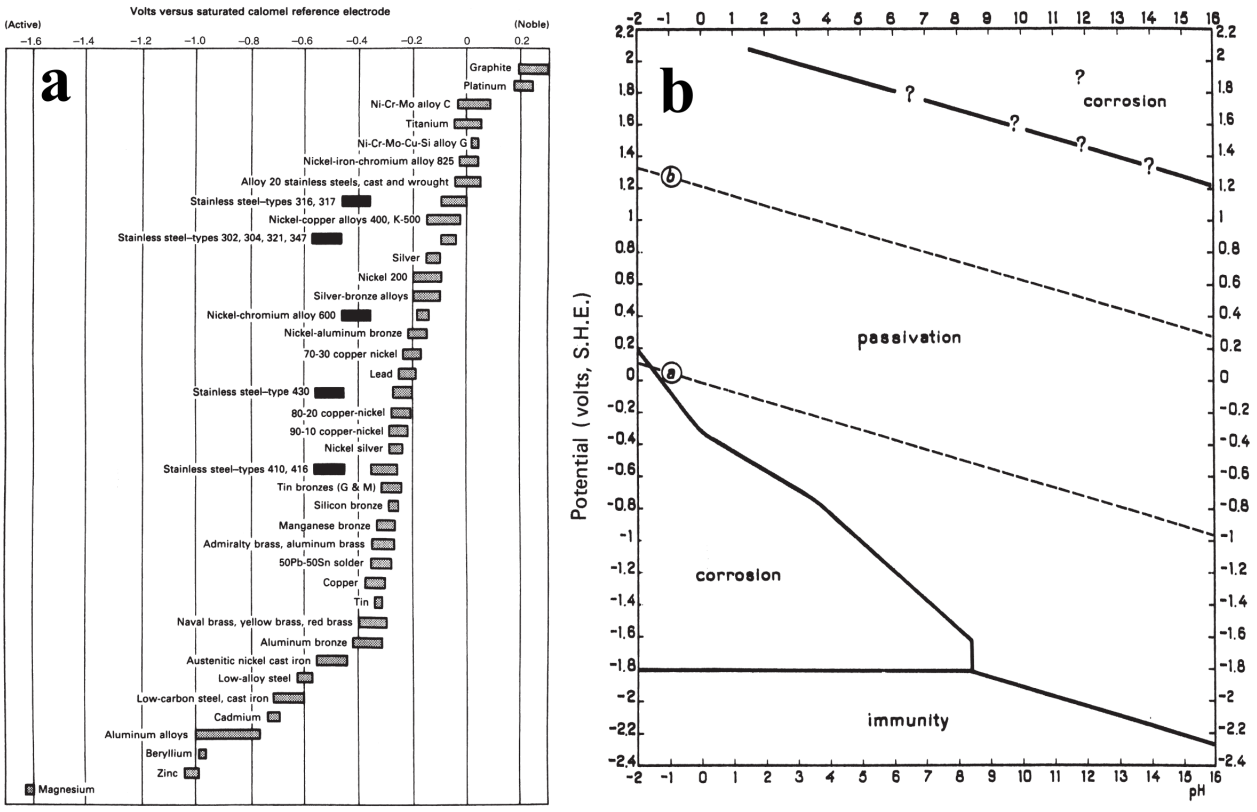

Fig. 2.8. (a)Galvanic series and (b) simplified version of the Pourbaix diagram of titanium as presented by Revie [28]). Both Figures used with permission from Wiley and Sons Publishing Co.

Pourbaix diagrams

Similarly to phase diagrams, Pourbaix diagrams show the stable conditions for a material given environmental inputs of pH and potential(V). The Pourbaix diagram of Ti (Fig.2.8-b) shows several areas marked as corrosion, immune and passive. The borders of these areas are created when the different reactions are in equilibrium by using a modified version of the Nernst equation (see Eq.2.6). In Eq.2.6 ϕ and ϕ^0 are the system and reference potential, respectively, and q is the equilibrium constant. Because the equilibrium constant is a ratio of the concentrations of products and reactants this can account for pH. In the corrosion area, Ti^{2+} are produced as Ti

oxidizes. In the immune region Ti does not react, and in the passivation region Ti produces a protective oxide film that halts any further corrosive processes.

$$\phi = \phi^0 - \frac{RT}{2F} log(q) \tag{2.6}$$

2.3.2 Potentiondynamic Polarization

Polarization is a process where the passing of current through electrodes causes their potential to shift or polarize. The direction of potential change will be in opposition to the current. Both electrodes will experience a change of potential until reaching a common potential designated as corrosion potential(E_corr) [28]. REDOX reaction will take place at different electrodes; however, it is assumed that the rate of reactions will be equal. There are several types of polarization:

Concentration polarization

Here the change in potential at an electrode will be determined by the concentration of metal ions in solution and on the surface of the electrode. The polarization of an electrode will depend on the supply of ions, but this can be expressed though the Nernst equation in terms of current densities (see Eq.2.7). Here i_L is defined in Eq.2.8, and is dependent on diffusion (D) of ions and concentration (c) [28].

$$\phi_2 - \phi_1 = -\frac{RT}{2F} log \frac{i}{i_L - i} \tag{2.7}$$

$$i_L = \frac{DnF}{\delta t} c * 10^{-3} \tag{2.8}$$

Activation polarization

This type of polarization needs to overcome an activation energy in the form of the application of a potential, referred to as overpotential [28]. Increasing the temperature of the solution can decrease the overpotential needed to corrode, and ultimately result in faster corrosion rate since overcoming the overpotential is a rate-limiting process [28].

The results of polarization experiments are curves that express the potential in terms of the current density (see Fig.2.9)-a), and the curves can be used to differentiate between different corrosion processes taking place, similarly to a Pourbaix diagram, however, this is for a fixed pH). The active area is seen in potentials just above the E_{corr} transitioning into a passive regime where the current will no longer change with increasing potential, and lastly at elevated potentials the passive film formed in the passive regime breaks down and corrosion continues. Corrosion rates can be calculated from polarization curves shown in Fig.2.9-a by measuring the slope of the linear portions of the active regions in the anodic curve (see Fig.2.9-b). This value is then input into the Tafel relation (Eq.2.9),

$$I_{corr} = \frac{\beta_a}{2.3} \frac{I_{app}}{\Delta\phi} \tag{2.9}$$

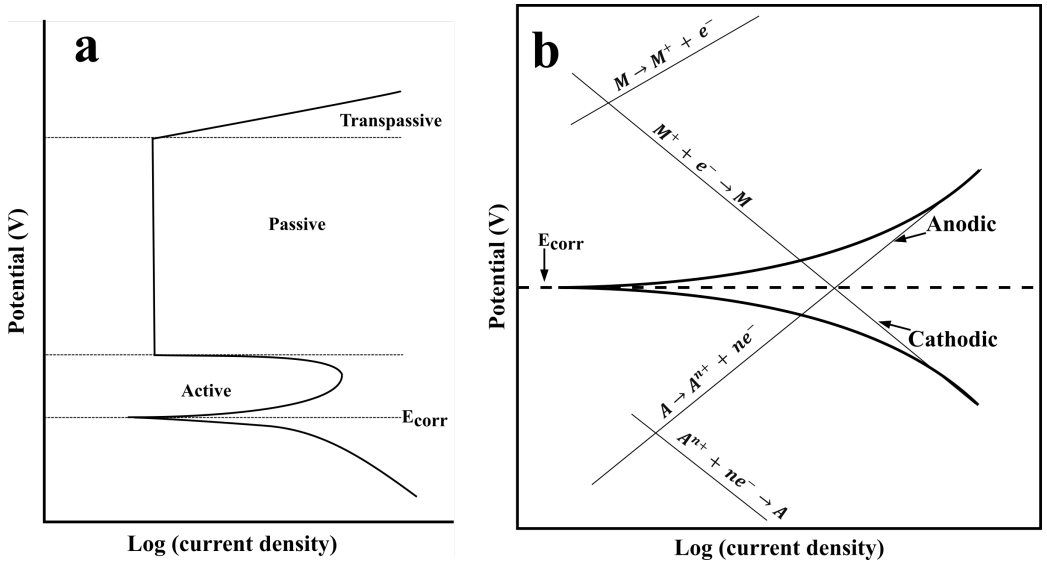

Fig. 2.9. (a) schematic of a polarization curve showing the different corrosive behaviors, and (b) Schematic of multiple electrode cell for Tafel fit. Revie [28])

2.4 Oxidation of Titanium

Oxidation of titanium differs from most other metals because oxygen exhibits an enormous solubility in α-Ti, with a maximum oxygen content reported up to 15wt% O [29](see Fig.2.10a). However, like most metals, oxidation of titanium directly limits the service temperature because the alloy degrades by producing and spalling off an oxide layer (TiO_2). Production of TiO_2 in a Ti alloy is a gradual process where O ingress into the metal stabilizes α phase at the surface. Remember O is a potent α stabilizer, and the mechanism of oxidation changes between $\alpha + \beta$ and β alloys.

$\alpha + \beta$ Alloy Oxidation

Alloys like Ti-64 and Ti-6242 tend to behave similarly during oxidation. Both alloys have similar Mo and Al equivalences, and can produce the same microstructures (basket weave, colony, etc). The ingress of O will displace β-Ti from the surface and stabilize the α. This will result in a displacement of the β-Ti phase, and the production of an oxygen rich α-Ti (see Fig.2.10-band c). With increasing temperature Ti-64 will precipitate out Ti_3Al; however, the presence of O will drive out all other alloying species out of α-Ti (in addition to drive out all β-Ti) and results in the formation of V-rich Ti_3Al [12]. In addition to microstructural changes in the metal, an oxide layer is produced from the heat exposure. This oxide layer will not be composed of a single oxide species but several because there is an effective O compositional gradient from the surface into the metal [30]. In alloys the presence of several alloying species results in the formation of oxide species different to TiO_2, such as Al_2O_3 when Al is a solute addition [31].

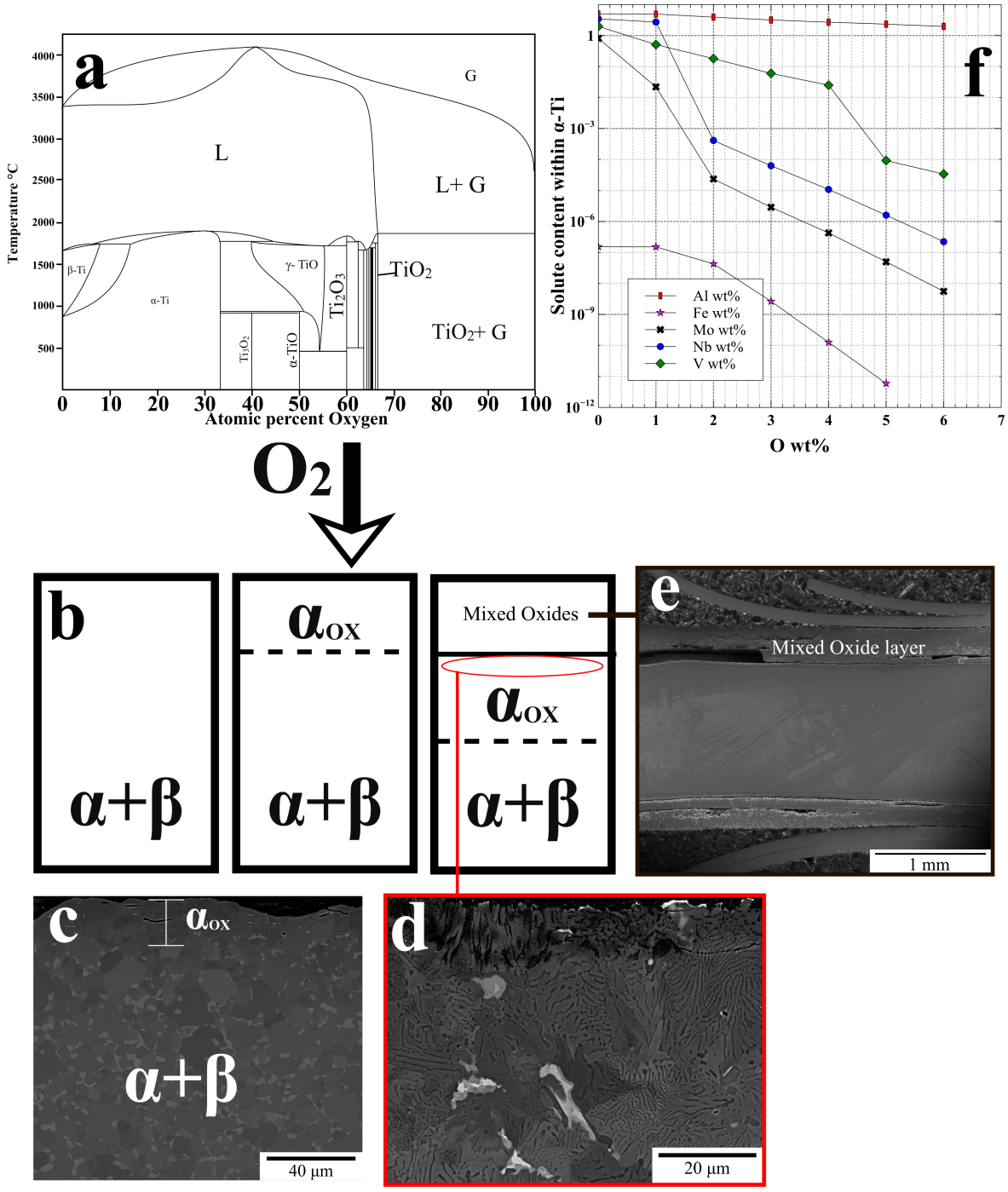

Fig. 2.10. (a) O-Ti binary phase diagram as reported by Okamoto [29]. (b) Schematic of oxidation microstructural changes. (c) Ti-64 oxidized at 750°C for 50 hrs [12]. (d) Ti-64 oxidized at 950 for 50 hrs [12]. (e) Oxide scale produced on Ti-64 oxidized. (f) PANDAT calculation of solubility of solute additions in α-Ti as O wt% increases. All referenced figures are used with permissions from Elsevier.

β Alloy Oxidation

The increased solute concentration in β-alloys changes the diffusion of oxygen, consequently the changes in microstructure during oxidation will differ between $\alpha + \beta$ and β-alloys. A study on oxidation of Ti-21S at 600°C in air showed an oxide layer primarily composed of TiO_2 and small amounts of Al_2O_3 [32]. This is also seen in oxidation of Ti-Cr compositions that show $TiCr_2$ embedded in the oxide scale [33]; this would be relevant to oxidation of Ti-5553. β-alloys also differ in how the α-case is formed. There is no continuous α-case, but instead there is an increased amount of α-laths at the metal oxide interface (see Fig.2.11) that with enough time and temperature for oxidation will result in a continuous alpha case and oxide scale formation.

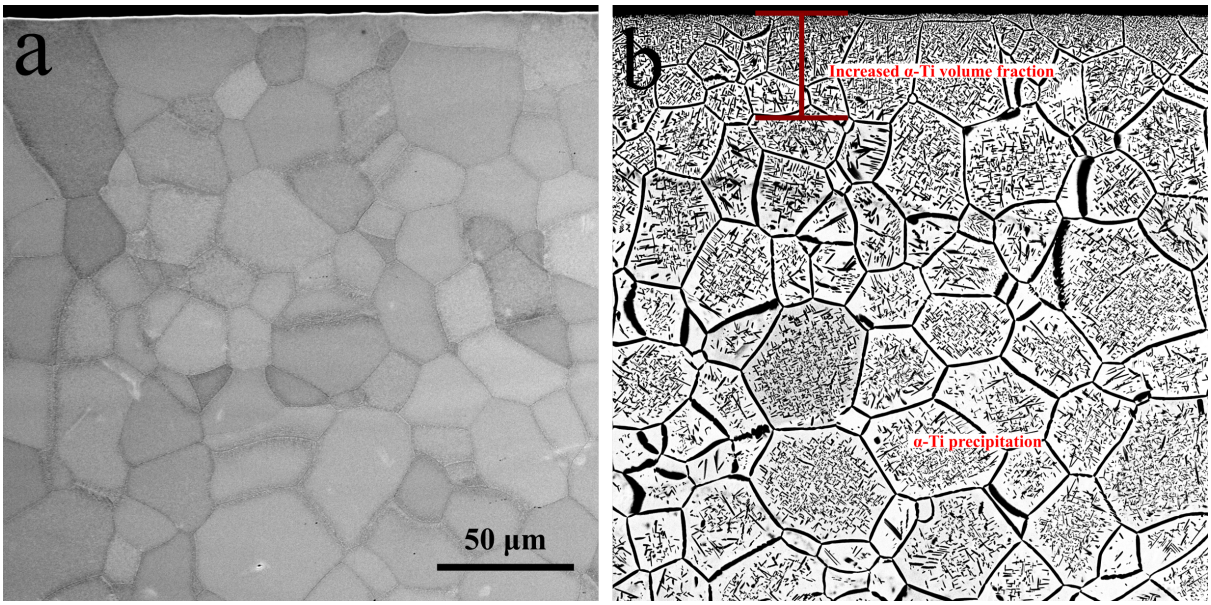

Fig. 2.11. Backscattered SEM images from Ti21S oxidized from fully β structure at (a) 550°C and (b) 750°C, for 50 hours [27]

2.4.1 Exploitation of Oxidation

Oxygen ingress into titanium can be exploited because it results in hardening of the surface. This is caused by solute strengthening of α-Ti and stabilization of α-

Ti. There have been several successful processes that have been developed to exploit surface hardening of Ti. Dong et al. [34,35] and Sarma [36] have shown that exposing Ti to high temperatures (800-1000°C) in air to produce an oxide layer followed by a vacuum heat treat to dissolve the oxide into the metal results in hardening of the surface. The depth of the hardened layer can measure several hundred microns in thickness; however, the high temperatures means that this type of processing is restricted to bulk materials. To harden Ti-based particles, one would need to avoid any sintering or forming an oxide layer, and will be discussed in Chapter 7.

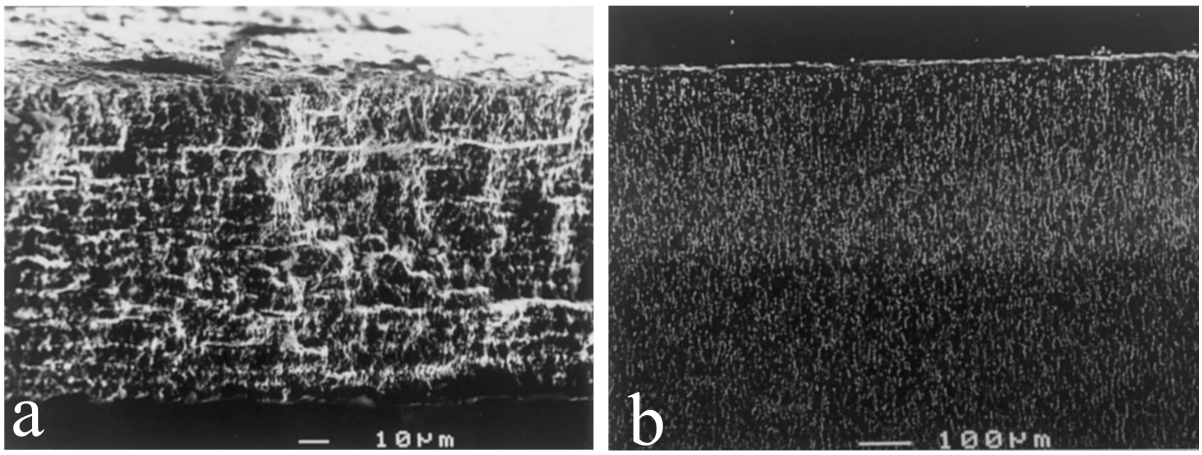

Fig. 2.12. Images of (a)oxide scale produced on Ti-64, and (b) oxygen stabilized α-case in Ti-64. All images taken from study performed by Dong et al. [35]. Images used with permission from Elsevier.

2.5 Severe Plastic Deformation

2.5.1 SPD processes

SPD processes were developed to produce materials with fine grain sizes that improve mechanical properties. Fine grain sizes can be split into ultra fine grained(UFG) and nanocrystalline (NC) with grain diameters (d) of 100<d<500 nm and d<100 nm, respectively [37]. The production of materials with such fine grain sizes has

proved difficult. Initial processing to produce bulk UFG/NC materials relied on inert gas condensation processes; however this limited the size of components made to several millimeters [38–40]. Additionally, ball milling and mechanical alloying of nano-particles was also attempted, but suffered from retained porosity and contamination [40]. Recently, the development of equal channel angular pressing(ECAP) has provided a viable way to produce bulk UFG materials, and has also lead to the development of criteria needed for a SPD process: (1) the production of large fraction of high angle grain boundaries, (2) uniform UFG microstructure, and (3) no damage to the materials (e.g. cracks) [41]. From these requirements it seems that #2 is not strictly needed, meaning that a distribution of grain sizes may be better than having a grain size distribution that has a very narrow spread [37, 42].

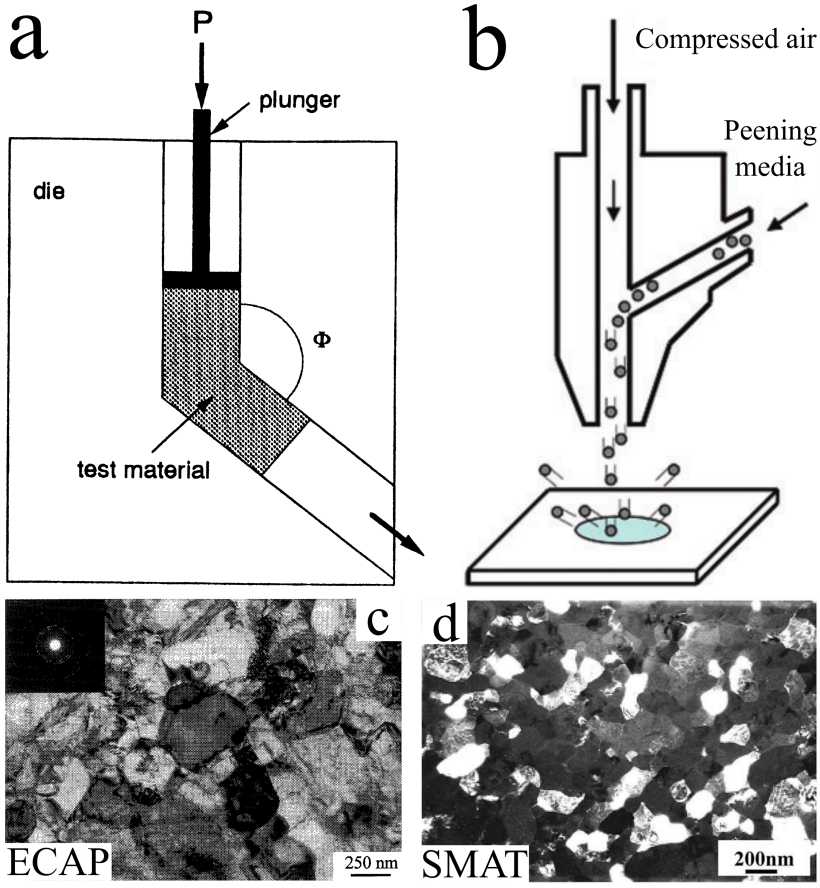

Fig. 2.13. Schematic view of SPD processes (a)ECAP [41], (b) Shot peening [9], and the resulting UFG microstructures for CP Ti processed by (c)ECAP [43] and (d) SMAT [44]. Images displayed with permissions from Elsevier(a,d), Taylor Francis (b).

2.5.2 Equal-Channel Angular Pressing (ECAP)

ECAP has become a popular SPD process to produce UFG materials because it produces large specimens with uniform UFG structure. ECAP process is done by passing a material through a channel that intersects a second channel (see Fig.2.13-a) at an angle (Φ). Angle Φ determines the shear strain imposed on the material per pass, [41, 45] as seen from Eq.2.10.

$$\epsilon_s = \frac{2}{\sqrt{3}} * cot(\Phi/2) \text{ [41]} \tag{2.10}$$

ECAP is a shear deformation process [46], this allows the material to pass multiple times and accumulate strain after each pass. For materials that are hard to deform (e.g. Ti) Φ can be increased (>90°) to reduce strain per pass, or material can be passed through at an elevated temperature.

2.5.3 Shot Peening(SP)

Shot peening is an established process used for increasing the fatigue life of components by introducing a compressive residual stress on the surface that acts against crack propagation. SP is carried out by blasting the surface of a specimen with hard media(see Fig.2.13-b) to deform the surface. There are several parameters that can be controlled to change the effects on material:

Media material

Cast iron, stainless steel, glass and ceramic shot are conventionally used for SP [47]. Hardness of the shot needs to be greater than the specimen to deform the surface; however, there seems to be a hardness threshold for the material undergoing SP at which the process is ineffective [48]. this means that with large enough surface hardness of the target material there is a necessary threshold of peening intensity needed to impart deformation on the surface and a residual stress on the part [48].

Media size and velocity

Size and velocity of shot is critical because it dictates the kinetic energy that will strike the specimen surface [49]. Shot sizes can vary from 4.75mm to 75 μm [50].

Coverage and Almen strip

Coverage is the fraction of the surface covered by dimples from shot impact. The coverage is described by the following equation;

$$C = 100(1 - exp(-\pi r^2 Rt)) \text{ [51]} \tag{2.11}$$

where r is the radius of the shot, R is the "rate of creation of impressions" and t is time. This relation would suggest that 100% coverage would require infinite time, but

100% coverage is commonly reported and required [52]. In practice, 100% coverage, in Almen strips, is determined by reaching a saturation point where a 10% increase of Almen intensity would require twice the time [53]. Almen intensity is measured through the Almen strip test, where a strip of 1070 steel of a given geometry (see [54]) is peened for a given time. Once the Almen strip is released, it deforms, turning into an arc. This arc height is measured (termed Almen intensity), and used to approximate peening conditions. It is accepted that the piece has been processed to 100% coverage once the change in arc height is lass than 10% after doubling exposure time [54]. Alternatively, SAE has established a standard for coverage measurement where a fluorescent coating is added prior to peening , and the area of removed coating is measured after peening to measure coverage [55]. Both of these methods are highly qualitative, and would be better replaced by a x-ray diffraction method that at least measures surface stress.

2.5.4 Consequences of SPD

Strength and Ductility

The grain refinement caused by the large strain introduced from SPD results in changes to many properties. The microstructures in CP-Ti, produced from both ECAP and Surface Mechanical Attrition treatment (SMAT)(see Fig. 2.13-c and d, respectively) show similar globular fine grains being produced as a consequence of the processing. SMAT results are shown because this process is comparable to SP where a surface is struck by spherical media to induce deformation. For multi-phase systems (Ti-64), ECAP processing showed the break up of the bimodal structure (see Fig.-2.4-c) into fine globular grains due to dislocation slip and twining that resulted in the formation of UFG 200-500 nm in diameter [56, 57]. However, both of these studies do not explain the role of the β-Ti phase during deformation, though one could assume that it can aid in the accommodation of strain, given that it is softer than α-Ti. ECAP processed specimens with a uniform UFG grain size result in pronounced increase of

strength at the cost of ductility [46]. The common expectation is that decreasing grain size should improve strength without deteriorating ductility [58];however, ECAP processed materials show a clear decrease in ductility. The embrittlement is caused by a lack of strain accommodation in the grains after deformation that contain a large fraction of high angle grain boundaries that formed by dislocations at the grain boundaries [41]. Additionally, the maximum strain as a function of distance from the grain boundary is seen not at the grain boundary, but adjacent to it (see Fig.2.14-a). Thus, if the grain size is small enough, a large portion of the grain is experiencing a large strain and probably causing the brittle behavior of UFG materials [41]. However, Fang et al [59] showed that a Cu specimen subjected to surface mechanical grinding at cryogenic temperatures developed a gradient of grain sizes that increased from surface to the specimen interior. The mechanical properties of this gradient nano-grained(GNG) material were measured through conventional uni-axial tensile testing of bars surface treated to produce a gradient of grain sizes. Fang [59] showed both improved strength and ductility when comparing the GNG material with the coarse grained Cu. Fang also tested , in uni-axial tension, material that was extracted from the treaed surface that was entirely NC, and showed that it displayed large yield strength but extremely limited elongation to fracture. Koch explains that the large grains provide ductility by allowing accommodation of the dislocations, through twining and strain hardening, while smaller grains stay in a "confined multi stress state" [37, 42]. The formation of a GNG structure in a titanium alloy has not been reported (to the best of the author's knowledge), and should be possible through the use of shot peening.

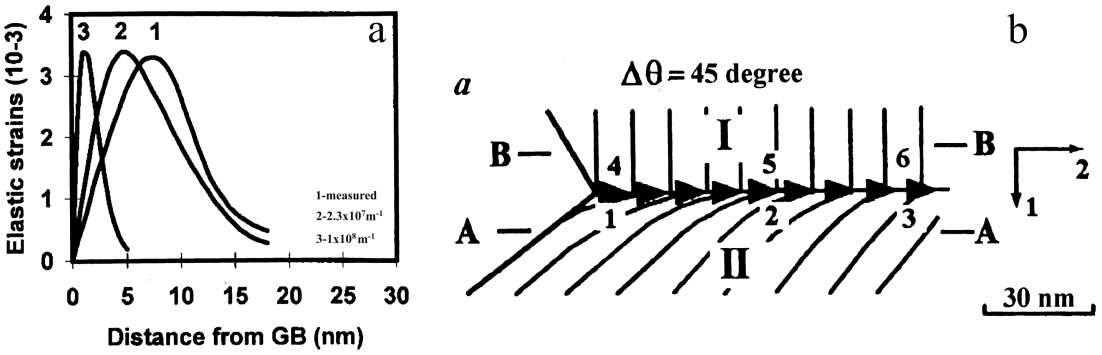

Fig. 2.14. (a)Strain versus distance from the grain boundary in depending on dislocation density at the grain boundary. (b)Visualization of lattice distortion adjacent to grain boundary as a consequence of increased dislocation density. Images shown with permissions from Elsevier. [41]

Modulus

Modulus of the material seems to change as a consequence of SPD processing. ECAP processed Cu and Cu composites show a decrease in modulus of roughly 10% [41, 60–62]. The decreased modulus could be due to it differing at the grain boundary with respect to the inside of the grain because of lattice bending in the area adjacent to the grain boundary (see Fig.2.14-b), thus the total modulus of elasticity is a combination of grain boundary and inside grain, and would suggest that the modulus at the grain boundary is much lower than the inside. Conversely, SMAT-treated CP-Ti [63] showed an increase in elastic modulus when compared to untreated CP-Ti of roughly 15%. Huang et al. suggest that residual stress does not play a role increasing the modulus because annealing treatments that relaxed the residual stress showed no decrease in modulus. Alternatively, texture from processing may be responsible for changes in modulus because modulus of elasticity is anisotropic and dependent on crystal orientation. the texture argument seems to be the most reasonable explanation for any change in modulus previously reported, and is a piece of information missing from most of the authors cited. From Nanopeened© (a shot-

based process similar to SP that intentionally used fine particles (40-150 μm) as shot media) processed materials, the UFG layer on the surface has no preferential texture [64], while ECAP processed materials [65] can inherit a preferential texture caused by the directional pressing.

Diffusivity and Thermal Stability

Diffusion rates in UFG materials produced by either ECAP or SP are markedly increased in relation to coarse grained materials. This is a direct consequence of the grain refinement causing an increase in volume occupied by grain boundaries [9, 41]. Grain boundaries act as short circuit diffusion paths [66]. One consequence of increased diffusivity is a limited thermal stability. Thermal stability is the temperature threshold needed to induce considerable coarsening or grain growth. Experiments performed on NC Fe, Pd and Cu showed grain growth at 0.26, 0.23 and 0.27 T_m (homologous temperature), respectively. For the case of Fe the starting grain size of 10 nm did not change significantly until temperatures were increased above 200°C ($\sim 0.25 T_m$) for hold time of 10 hr (seen Fig. 2.15-a). This would limit the use of UFG materials to applications to temperatures below threshold of grain growth, and for Ti it would mean that applications should not exceed 200°C(after accounting for homologous melting temperature). Note the similarity between Fe and Ti thermal-stability is due to their similar melting temperatures 1538 and 1660°C, respectively. However, annealing of UFG materials can take place at higher temperatures without significant grain growth if annealing time is limited, and is consistent with conventional processing (Fig.2.3 and 2.5) where the service temperature is lower than the annealing temperature. The effect of annealing in SPD (ECAP) processed materials (see Fig.2.15-b) showed that dislocations tended to migrate towards grain boundaries [40].

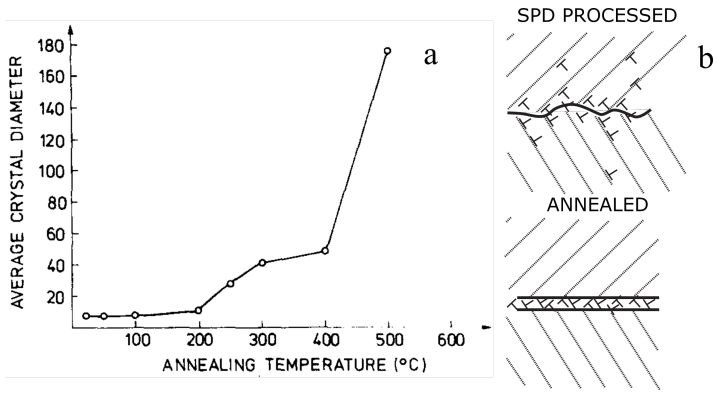

Fig. 2.15. (a) Grain growth of nanocrystalline Fe showing a marked increase in growth at temperatures past 200°C [38].(b) Schematic of dislocation migration to the grain boundaries during annealing [40]. Images shown with permissions from Elsevier(a), and Springer Nature(b).

3. PROCEDURES

3.1 Shot Peening

For this study, shot peening is being used as a cold working process to enable recrystallization in a subsequent heat-treatment step. Previous works [9, 48, 67] have shown that shot peening can produce UFG structures; however, there is no consensus on effective peening conditions that result in grain refinement. Todaka et al. argues that coverage is crucial for producing grain refinement at the surface [48]. However, most studies used higher peening pressures than normally used, where Maleki et al. used ∼80 psi propelling pressure [67] and Berger et. al used ∼100 psi to peen Ti-21S [68]. With this in mind, the parameters that used in this study prioritized high propelling pressure because propelling pressure is directly proportional to the energy imparted into the material.

Coverage was selected by peening a dummy specimen for 10 seconds and measuring the coverage optically [69]. Then using using the coverage expression(see below) [69].

$$C_n = 1 - (1 - C_1)^n \tag{3.1}$$

Here C_1 is the area covered before shot peening, n is the number of cycles and C_n is the resulting coverage.Eq 3.1 is a simplified version of Eq 2.11, and allows SP users to extrapolate exposure time needed to achieve the desired coverage. The exposure time was increased to achieve ∼80% coverage on the surface. It was decided it was not necessary to peen the material to 100% because the manner in which the subsurface volume is deformed coincides with the cavity model used in contact mechanics [70], meaning that not all the surface has to be peened, but enough of the surface has to be peened to result in overlap of the volumes being deformed. The parameters chosen are presented in Table.3.1. Alloys and microstructural condition of the alloys being shot peened are detailed in Table.3.2.

Table 3.1.
Parameters used for shot peening.

Peening Material	Shot Size(μm)	Propelling Pressure(psi)	Exposure Time (sec)	Coverage
Soda-lime glass	250-370	80	40	∼83%
Ti	50-150	80	40	∼83%

Table 3.2.
Alloys and their respective microstructural conditions that were peened. Ti-peened with Ti shot. Si-peened with glass shot.

Alloy	quenched	basket weave	colony	Bimodal
Ti64	Si, Ti,	Si	Si	Si
	quenched	lamellar	bimodal	
Ti-5553	Si,	Si	Si	
Ti-21S	Si, Ti	Si		

3.2 Alloy processing

Heat treatments

This section will focus on the procedures used to perform the heat treatments. A later section in this document will focus on the temperatures and hold times used for producing particular microstructures. A Lindberg tube furnace(see Fig.3.1-a) was used to heat treat all specimens. This furnace was selected because it allows the user to connect a gas cylinder onto it and establish an inert atmosphere for the duration of the heat-treatment. Before inserting the specimens, the furnace was raised to the temperature required for the heat treatment. Once the temperature was reached, Ar flow was started. This resulted in a temperature drop that was corrected by increasing

temperature setting of the furnace. The temperature was monitored with an external k-type thermocouple until the desired temperature was achieved, and was stable for 10min prior to inserting any specimen.

Specimens were thoroughly cleaned in ultrasonic baths of ethanol, and dried. After drying, the specimens were wrapped tightly in commercially pure Ti foil (0.25mm thick). Care was taken to seal the foil around the specimen prior to heat-treatment. The wrapped specimen was placed in an Al_2O_3 boat(see Fig.3.1-b). In addition, Ti sponge was placed with the specimen in the boat. The foil, Ti sponge, and Ar were all used to prevent oxidation of the specimens during the heat-treatment.

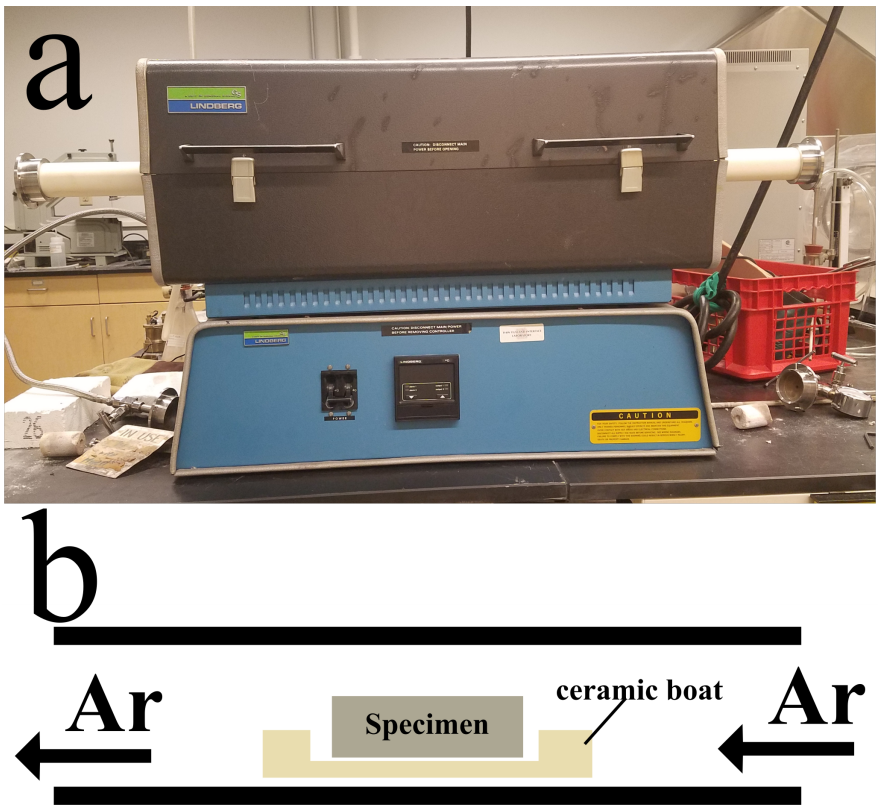

Fig. 3.1. (a) Tube furnace used for heat-treating Ti under a controlled atmosphere. (b) Schematic of tube furnace showing specimen sitting on ceramic boat.

3.3 Sample preparation

Test coupons specimens were wire EDM cut from billet(Ti-5553), plate(Ti-21S) and sheet (Ti-64) to produce test coupons that measured 20 X 20 X 1.60 mm. These coupons were then subjected to various heat treatments detailed in chapter 5.

Metallographic preparation

Specimens were cut from the test coupons to reveal the cross-sectional area. This was done to evaluate microstructural changes that resulted from shot peening and subsequent treatments. the specimen was mounted in phenolic resin, and ground with SiC sandpaper of increasing grit (320-800 grit). Final polishing was done with 0.03 μm colloidal silica. The silica slurry was diluted to 50-50 solution with water. This process was sufficient for SEM characterization; however, for optical imaging specimens were etched after polishing with silica. Kroll's(distilled water 92ml, nitric acid 6ml, and hydrofluoric acid 2 ml) reagent was used to etch all specimens for 30 seconds.

3.4 Characterization and Testing Techniques

Vickers hardness

Vickers hardness testing is a common micro-indentation technique. The indenter uses a pyramidal shaped tip(see Fig.3.2-a). The load applied by the indenter can be varied as seen in Fig.3.2-b. For this study a Wilson Hardness Tukon 1202 hardness tester was used to measure surface hardness. For all hardness measurements a load of 500g was used, and a separation of 500μm between each indent. Before each indentation session, the hardness tester was checked to make sure that it was still within calibration. the calibration check was done by measuring the hardness of a LECO hardness standard.

a

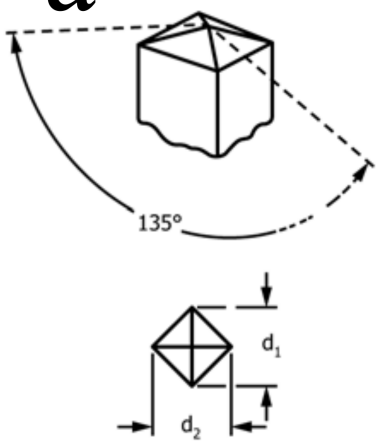

b

Vickers scale	Knoop scale[A]	Test force (N)	Approximate Test force (kgf)	Approximate Test force (gf)
HV 0.001	HK 0.001	0.009807	0.001	1
HV 0.01	HK 0.01	0.09807	0.01	10
HV 0.015	HK 0.015	0.1471	0.015	15
HV 0.02	HK 0.02	0.1961	0.02	20
HV 0.025	HK 0.025	0.2451	0.025	25
HV 0.05	HK 0.05	0.4903	0.05	50
HV 0.1	HK 0.1	0.9807	0.1	100
HV 0.2	HK 0.2	1.961	0.2	200
HV 0.3	HK 0.3	2.942	0.3	300
HV 0.5	HK 0.5	4.903	0.5	500
HV 1	HK 1	9.807	1	1000
HV 2	HK 2	19.61	2	2000
HV 3		29.41	3	
HV 5		49.03	5	
HV 10		98.07	10	
HV 20		196.1	20	
HV 30		294.1	30	
HV 50		490.3	50	
HV 100		980.7	100	
HV 120		1177	120	

Fig. 3.2. (a) Vickers indenter tip geometry. (b) Table of possible tests forces in Vickers hardness testing.all images and data taken from [71]. Images shown with permission from ASTM

Glow Discharge Spectrometer

Glow Discharge Spectrometer (GDS) is a destructive characterization method for measuring composition of metallic and nonmetallic materials. An Ar plasma is generated and by passing a potential on Ar atoms, this ionizes the Ar. The ionized Ar atoms are propelled towards the specimen by the potential, because the specimen serves as the cathode. The collision of Ar atoms with the specimen result in material being sputtered out of the specimen. Ejected cathode atoms will endure further collisions with the Ar in the lamp, resulting in the excitement of these atoms, and returning to a de-excited state through the emission of light with a characteristic wavelength(see Fig.3.3b-c) [72]. The light passes through a grating that refracts light of particular wavelengths to hit a photo-multiplier tube (PMT), that measures the intensity of the light.

For this study, a LECO GDS 850A (see Fig.3.3-a)was used for high precision compositional measurements to compare compositional changes at the surface caused

different shot peening media. Specimens are usually ground with 120 and 320 grit SiC sandpaper; however, for this study shot peened surfaces have not been ground before GDS measurements because this would destroy the deformed and contaminated layers. Quantitative depth profiling was carried out on specimens shot peened with glass, titanium-based, and iron-based shot media.Depth profiling works by measuring mass from sputtering rate, and by knowing the density of the material the volume sputtered out of the material is calculated. This gives the depth sampled because the cross-sectional area sampled is constant. The species of interest measured in the depth profiles was changed depending on the shot media used: Si for glass, O for Ti, shot. Maximum depth reached by a contaminant will be marked by the position at which the contaminant equals the maximum allowable composition in the alloy.

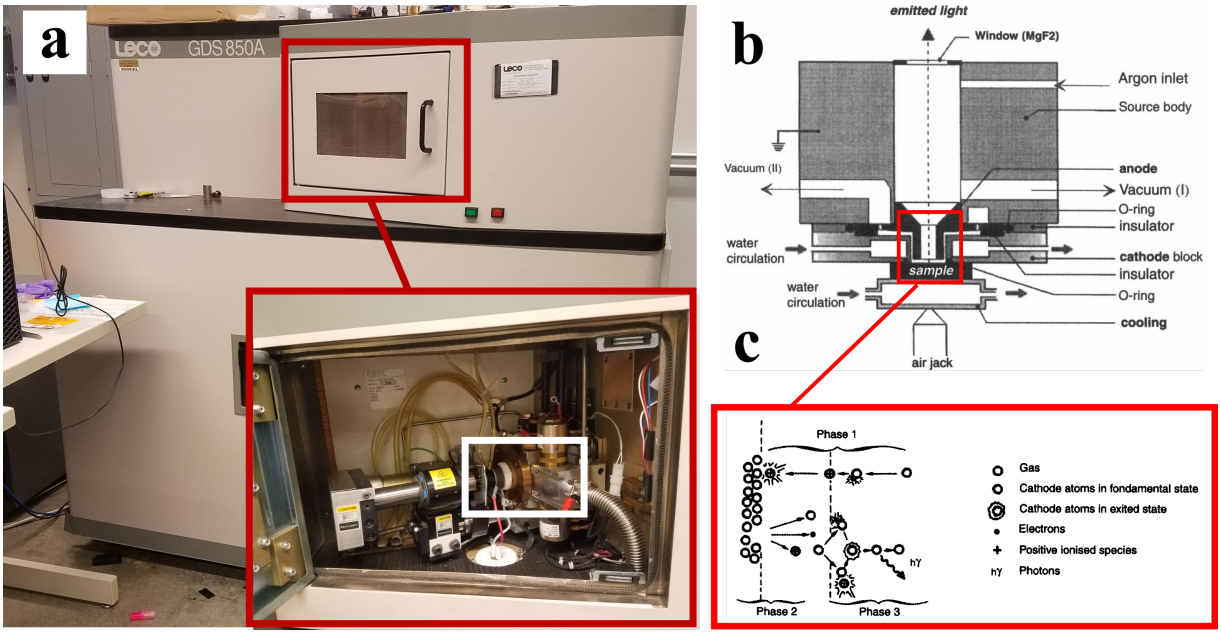

Fig. 3.3. (a) Image LECO GDS 850A, inset shows the lamp holding a specimen (b) Schematic of the lamp construction, and (c) Schematic of the sputtering and emission process caused by collisions of atoms. Images b and c taken from [72]. Images Shown with permission from the Royal Society of Chemistry (b,c).

Nanoindentation

The nature of the study required the measurement of mechanical properties from fine scale microstructural features. Consequently, specimens were tested with a Hysitron Ti 950 Triboindenter with Berkovich tip with an effective radius of 300 nm. Maximum load and loading functions varied depending on specimen and purpose for testing, so this information will be given for each respective test.

Scanning Electron Microscopy

Scanning electron microscopy was used to evaluate microstructures. All alloys selected for this study are composed of a mixture α-Ti and β-Ti; consequently, back-scattered imaging was used because the contrast generated from the back-scattered detector provides compositional information of the phases present through z-contrast. Z-contrast reflects the penetration of back-scattered electron into the material.Where phases rich in high Z elements will appear brighter because the electrons do not penetrate deeply.

X-Ray Diffraction

X-ray diffraction was performed using a Bruker D8 diffractometer. 2-theta omega scans were performed on all specimens using a Cu source with a 1.54Å wavelength. Diffraction of Ti powders was performed by attaching the powder to a piece of double sided tape, and attached to a polymer diffraction block. this was done to avoid any peak generation from crystallographic phases that were not present in the powder. This technique was sued to determine the crystallographic phases present in the powder specimens before and after treatment.

Corrosion testing

Potentiondynamic anodic polarization measurements were performed to measure corrosion rates of material processed and compared to unprocessed material. procedure followed is detailed in ASTM G61 [73],ASTM G5-14 [74] and F2129-17b [75]. Processed specimens were cut into 4 X 4 X 1.60 mm. These specimens were cold mounted in epoxy. A copper wire (1mm diameter) was placed in contact with the specimen (in

the back), and allowed to set in place in the epoxy. The wire serves as the contact in the electrolytic cell. Hank's solution was used to immerse the specimens.

4. ALLOY SELECTION AND MICROSTRUCTURE PROCESSING

The microstructural variability observed in titanium alloys (introduced in Chapters 3.1-3.2) is an exploitable feature that was explored in this study. Selection of materials to study was based on the knowledge that Mo equivalence in titanium alloys will dictate what microstructures are able to be formed through heat-treatment. Consequently , it was necessary to select Ti alloys that would represent a large swathe of Mo equivalence. To this end Ti-64, Ti-5553, and Ti-21S were selected, each having a Mo equivalence of 2.67, 9.60 and 12.8 [25], respectively. What follows is a description of heat-treatments and processing involved in the production of microstructures that were selected to be shot peened. Compositions of each alloy are presented in Table4.1.

Table 4.1.
Nominal compositions of alloys used in this study.(All compositions are expressed in wt%)

Alloy	Ti	Al	Cr	Fe	Mo	Nb	V	Si
Ti-6Al-4V	89.6	6.0	n/a	0.4	n/a	n/a	4	n/a
Ti-5Al-5Mo-5V-3Cr	71.6	5.0	3.0	0.4	5.0	n/a	5.0	n/a
Ti-21S	78.3	3	n/a	0.4	15.0	3.0	n/a	0.3

Ti-64

Ti-64 is the most widely produced and used Ti product accounting for at least 50% of Ti produced by tonnage. Ti-64 is the most common Ti-based material for medical implants, and it is used for full hip, knee, and jaw replacement implants. Ti-64 is used even though the alloy has significant Al and V content that when introduced to

the body may result in chronic diseases [76]. Ti-64 an $\alpha + \beta$ alloy that can produce several microstructures (as discussed in Ch3.2) depending on temperatures used for heat-treatment; consequently, β-transus temperature (see Table. 4.2) of the alloy is an important consideration for processing.

Table 4.2.
General properties reported for Ti-64 [4]

Modulus GPa	Yield Strength MPa	β-transus temperature(°C)	Density (g/cm^3)
105-116	862-903	955-1010	4.43

Ti-5553

T-5553 or Ti-555 is the adaptation of a Russian alloy (VT22) [77]the difference between VT22 and Ti-5553 is the addition of Cr to replace Fe, both elements are strong β strengthners. As a near-β alloys, Ti-5553 is capable of producing many microstructures through a combination of recrystallization and heat-treatments(see Ch3.2.2). This alloy has been primeraly used in laod bearing airframe components and more notably in landing gears [25]; however, the use of Ti-5553 in the medical field would be beneficial because in a fully β condition will have a lower Young's modulus compared to Ti-64. In fact, this is a great motivation to develop beta alloys such as TNZT. Mechanical properties for Ti-5553 are shown in Table.4.3, one should note that this is for the solutionized and aged condition which will have a larger modulus than a fully β microstructure.

Table 4.3.
General properties reported for Ti-5553 as solutionized and aged [4,25,78]

Modulus GPa	Yield Strength MPa	β-transus temperature(°C)	Density (g/cm^3)
112	1100-1220	820-880	4.65

Ti-21S

Ti21-S was developed in the 1980's to produce with the intention of making an alloy that is resistant to high temperature corrosion [25]. This alloy exhibits good corrosion resistance at low and high temperatures. In fact, Ti-21S has been used as a replacement of certain Inconel 625 [25]. Similarly to Ti-5553, this alloy has been predominantly used in the aerospace industry; however, this alloy would benefit the medical field because it can exhibit a lower modulus than the previous alloys described above, and has a great corrosion resistance.

Table 4.4.
General properties reported for Ti-5553 as solutionized and aged [4,25,79]

Modulus GPa	Yield Strength MPa	β-transus temperature(°C)	Density (g/cm^3)
74-85	795-913	807	4.93

4.1 Processing $\alpha+\beta$ Alloy

Lamellar Structures

The alloy selected for this class of Ti-based alloy was Ti-64. The reason being that this is the most common Ti product in existence today, and in the past has accounted for over 60% of titanium produced in industry [1]. More importantly, Ti-64 is an ac-

cepted material for use in medical implants currently being used. Lamellar structures are produced by cooling down directly from a temperature above the β-transus temperature, and cooling rate controls the microstructure development. Heat treatments performed on Ti-64 are presented in Table.4.5.

Table 4.5.
Heat-treatments performed on Ti-64.All specimens were wrapped in Ti foil and heat treated in an Ar atmosphere.

Desired Microstructures	Solutionization (Temp(°C)/time)	Aging (Temp(°C)/time)	Cooling
Martensite	1060/ 4 hrs	none	Water Quench
Basket weave	1060/ 4 hrs	none	Air Cool
Colony	1060/ 4 hrs	none	Furnace Cool
Bimodal	none	925/ 2 hrs	air cool

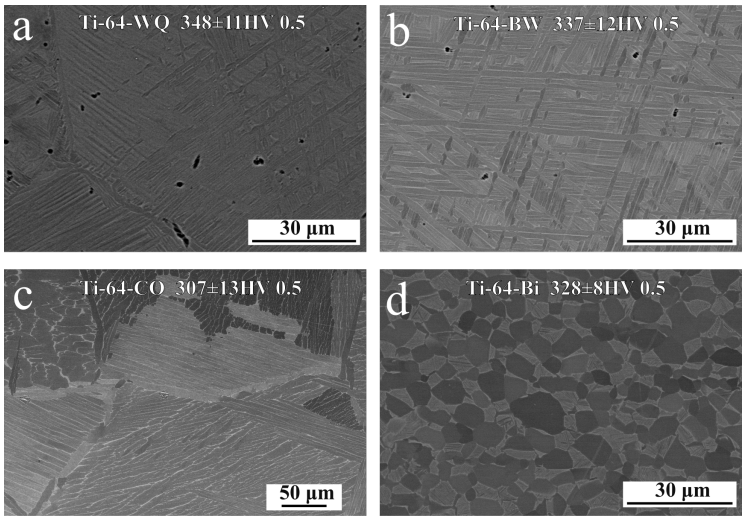

Fig. 4.1. SEM backscattered images of the following microstructures: (a) Martensitic lamellar structure(b) Basket-weave,(C) Colony, and (d) Bimodal.Note all structures show their average hardness.

The resulting microstructures from heat-treatments detailed in Table.4.5 are presented in Fig.4.1. The average hardness of each microstructure is displayed in Fig.4.1. Note that there is a slight increase in hardness when comparing lamellar martensite and basket-weave. This is a far-cry to Fe-C martensite that shows large hardening because in titanium the lattice is supersaturated with β-stabilizers, that are usually substitutional elements in the lattice and not interstitial as is the case in Fe-C alloys [80]. Microstructural features of interest were measured for all structures and are presented in Table4.6

Table 4.6.
Measured Microstructural Features from Ti-64 Microstructures.

Microstructure	α Volume Fraction	α-lath Thickness (μm)	Pior-β grain size (μm)	Equiaxed-α Vol. Frac	Equiaxed-α grain size (μm)
Martensite	-	0.65	863	-	-
Basket weave	0.86	0.86	1113	-	-
Colony	0.83	4.20	790	-	-
Bimodal	0.77	0.25	-	0.74	4.60

Bimodal Structure

To form the bimodal structure (see Figure.4.6-D), a piece of Ti-64 that was in the as rolled condition(see Figure4.2) was heat-treated as seen in Table4.5. The temperature was selected because it is below the β-transus temperature, but still within a $\alpha + \beta$ phase field within the Ti-Al-V system. The heat-treatment reuslted in the formation of equiaxed α-grains(primary-α) along with α-laths. The features measured from this microstructure are listed in Table4.6.

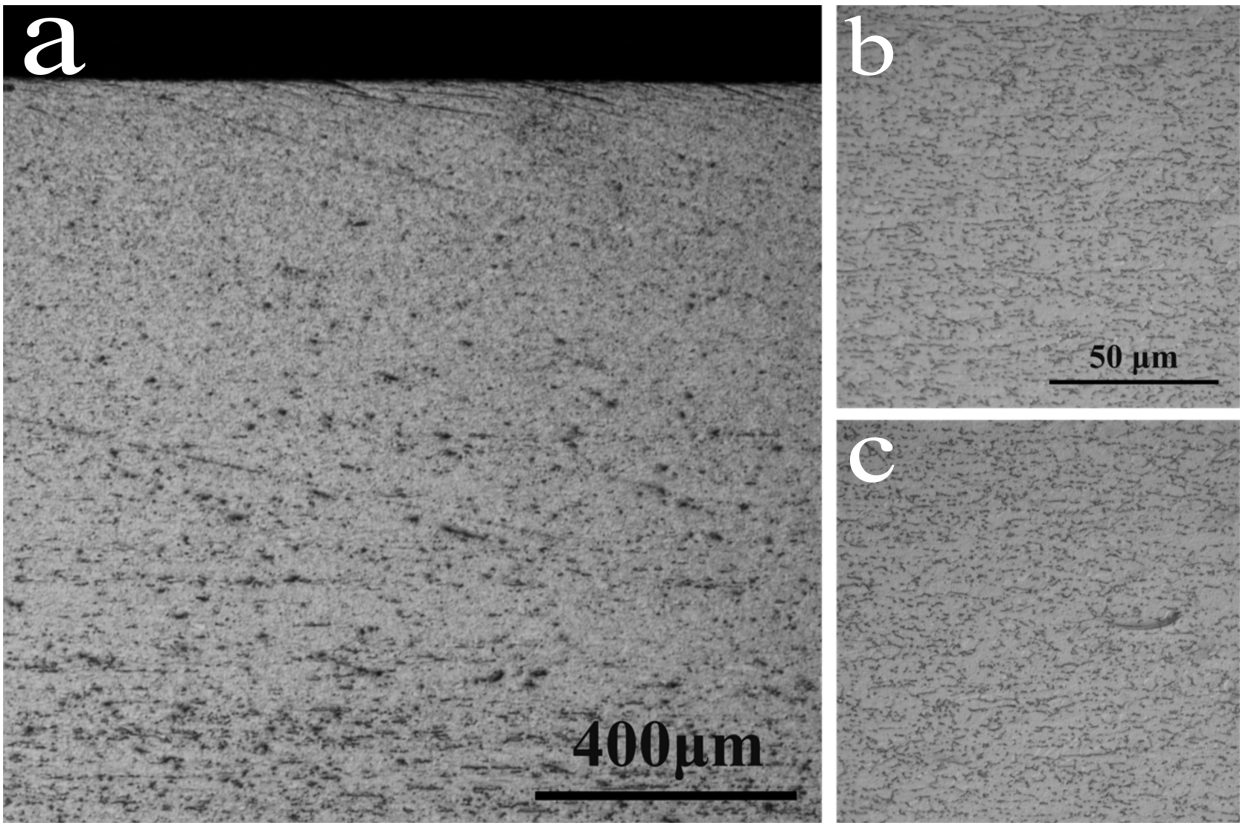

Fig. 4.2. SEM backscattered images of Ti-64 in the as rolled condition(a)Low magnification (b) and (c) show higher magnification. Note figures b and c were taken at the same magnification.

4.2 Processing β-Alloys

The processing of Ti-5553 and Ti-21s is similar because both alloys have a large Mo equivalence. The following sections explain processing of Ti5553 and Ti21s to produce: Fully quenched-in β structure, lamellar structures, and bimodal structure.

Fully β and Lamellar Structure

Table 4.7.
Heat-treatments performed on Ti-5553 and Ti-21s. All specimens were wrapped in Ti foil and heat treated in an Ar atmosphere.

Alloy	Desired microstructure	Solutionization (Temp(°C)/time)	Aging (Temp(°C)/time)	Cooling
Ti-5553	Fully β	950/ 6hrs	none	Water quenched
	Lamellar	950/ 6hrs	650/ 3hrs	Air cooling
Ti-21S	Fully β	950/ 6hrs	none	Water Quenched
	Lamellar	950/ 6hrs	650/ 3hrs	Air cooling

To produce the the fully β structures in both Ti-5553 and Ti-21S, the specimens were heat-treated above their respective β-transus temperature(solutionized), and water quenched. To produce the lamellar the specimens were aged following solutionization. the particular times and temperatures used to heat-treat the specimens are seen in Table.4.7. Note that the same solutionization conditions were used for both Ti-5553 and Ti-21s because temperature was above the β-transus temperature for both alloys, and allowed for a shorter hold time. The microstructural features of interest for Ti-5553 and Ti-21S are shown in Tables.4.8 and 4.9, respectively.

Table 4.8.
Measurements of microstructural features in Ti-5553 .

Microstructure	α Volume Fraction	β Grain Size (μm)	α-Lath Thickness (μm)
Fully β	0	630	n/a
Lamellar	0.45	730	0.177
Bimodal	0.45	1170	0.120

Table 4.9.
Measurements of microstructural features in Ti-21S .

Microstructure	α Volume Fraction	β Grain Size (μm)	α-Lath Thickness (μm)
Fully β	0	150	n/a
Lamellar	0.41	400	0.08

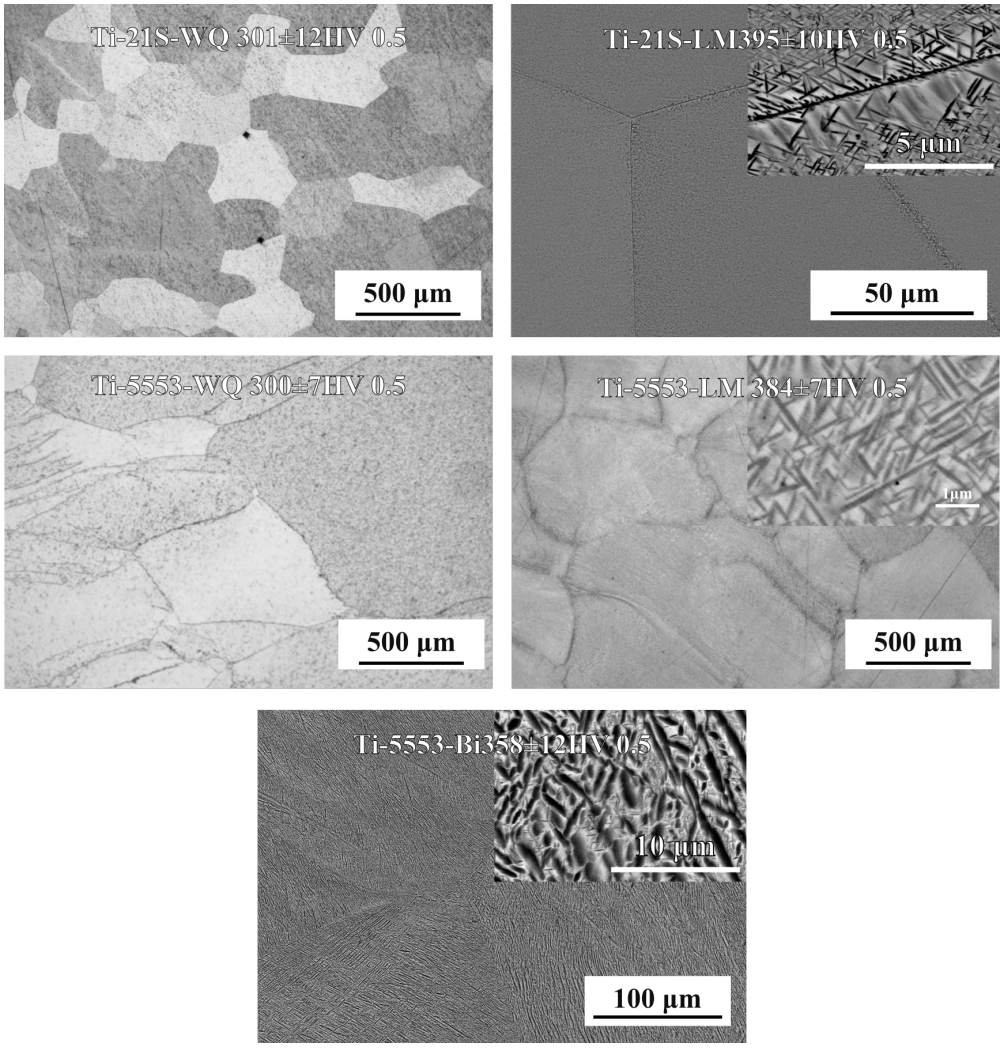

Fig. 4.3. Optical and SEM backscattered images for the microstructures produced. (a)Ti-21S water quenched,(b) Ti-21S Lamellar, (c) Ti-5553 water quenched,(d) Ti-5553 Lamellar, and (e) Ti-5553 bimodal. The initial hardness of each structure is given for all structures.

Bimodal Structure

As discussed in Ch3.2, bimodal structures are the result of a recrystallization following a deformation event. Only Ti-5553 was processed to produce a bimodal structure because it has a lesser Mo equivalence compared to T-21S. A piece of Ti-5553 was solutionized and water quenched to produce a fully β structure. This was done

because β-Ti is far more ductile than α-Ti. The fully β structure was cold rolled to 25% reduction. The deformed specimen was heat-treated to induce recrystallization at 750°C for 3 hrs. This was followed by an aging treatment at 550°C for 3 hrs. The resulting microstructure is shown in Figure.4.3.

5. SURFACE PROCESSING OF TITANIUM ALLOYS FOR MICROSTRUCTURAL REFINEMENT

5.1 Abstract

This study has utilized conventional shot peening as an effective method to modify a variety of microstructures in several Ti-based alloys. SEM images of cross-sectioned surfaces show the comparative ease of deformation of different microstructures. The evolution of residual stresses in distinct microstructures within several alloys was evaluated using nanoindentation. Significant grain refinement was obtained by subjecting shot peened conditions to a post shot peening heat-treatment that resulted in formation of ultra-fine-grained layers. Post SP heat-treatments showed that α-Ti precipitation is influenced by residual stress within the material.

5.2 Introduction

In recent years several researchers have shown that deformation incurred in different metals through shot peening(SP),and other shot based processes such as Surface Mechanical Attrition Treatment, can result in the formation of fine microstructures in the volume adjacent to the surface [9, 67, 81]. Similarly, processes such as surface grinding (at cryogenic temperature) have produced gradations of grain size from the surface of the material into the interior that have resulted in a marked increase in tensile properties without any meaningful sacrifice of ductility [59]. A gradient of grain sizes allows for better accommodation of strain in the coarse grains while maintaining the strength of the fine grains thus avoiding the early onset of plastic instability seen in entirely nanocrystalline (NC, sub-100 nm) or ultrafine grain (UFG, 100-1000 nm) materials [37, 42, 82, 83].

SP conditions suitable for formation of fine scale structures are debated in literature. Some authors contest that increasing coverage results in enough strain accumulation to induce recrystallization of the surface [9, 48, 81].However, coverage is a poor parameter to choose as a measure of SP intensity let alone an accurate measure of deformation imparted on the work piece surface because residual stress and surface deformation tend to be saturated at coverage values near 80% coverage[10]. Additionally, studies that claim coverage is the crucial to surface grain refinement seem to ignore the fact that strain hardening will limit the strain imparted on the sample and cold work of the piece will saturate [84]. Other studies claim that propelling pressure of and shot size are more relevant because these two parameters dictate the total kinetic energy imparted to the work piece by each shot impact [67].

There is a problem in the world of titanium metallurgy in that Ti-64 has concentrated research interests for alloy development on alloy compositions within the Ti-Al-V ternary system. This is clearly seen when analyzing the tonnage of titanium produced shows that the majority is comprised by Ti-64[11]. This has consequently relegated β titanium alloys to small niche applications, in spite of many β alloys showing tensile that are comparable or surpass properties seen in Ti-64 [25, 26]. One of the purposes of this study is to showcase the versatility of β alloys in comparison to Ti-64 as it relates to surface severe plastic deformation.

This study analyses application of SP as a surface severe plastic deformation to induce localized recrystallization of surfaces by careful selection of parameters, with no consideration for coverage. Three alloys were selected to represent the main alloy classes in titanium i.e. α+β alloys, near β, and metastable β alloys; represented in this study by Ti-64,Ti-5553, and Ti21S, respectively. In an attempt to characterize differences in microstructural response to shot peeing, the starting microstructure before shot peeing was varied in all alloys.

5.3 Procedures

This study used Ti-64, Ti-5553 and Ti-21S (see Table.4.1) were selected because it allowed for the analysis of a wide range of molybdenum equivalences([Mo]) in titanium alloys, 2.67, 9.60 and 12.80 [Mo] for each alloy, respectively [25]. The response to SP of differing microstructures produced in these alloys is of interest, and has not been studied directly previously. To this end each specimens of each alloy were processed to produce: quenched, lamellar, and bimodal types of microstructures(see Tables5.1,5.2, and 5.3).

Table 5.1.
Heat-treatments to produce quenched in structures prior to shot peening.Note WQ stands for water quenched .

Alloy	Temperature(°C)/ Time	Cooling	Target microstructure	Specimen label
Ti-64	1060/ 4hrs	WQ	martensite	61
Ti-5553	950/ 6hrs	WQ	Fully-β	51
Ti-21S	950/ 6hrs	WQ	Fully-β	21

Table 5.2.
Heat-treatments to produce lamellar microstructures prior to shot peening
.

Alloy	Solutionization (°C/ hrs)	Cooling	Aging (°C/ hrs)	Target Microstructure	Label
Ti-64	1060/ 4	AC	N/A	Basket weave	64-BW
Ti-64	1060/ 4	FC	N/A	Colony	64-CO
Ti-5553	950/ 6	WQ	650/ 3	lamellar α preciptates	52
Ti-21S	950/ 6	WQ	600/ 3	lamellar α preciptates	22

Table 5.3.
Heat-treatments to produce bimodal in structures prior to shot peening.

Alloy	Solutionization	Cooling	Recrystallization	Cooling	Aging	Cooling	label
	(°C/ hrs)		(°C/ hrs)		(°C/ hrs)		
Ti-64	N/A	N/A	925/ 2	AC	N/A	N/A	64
Ti -5553	960/ 4	WQ	750/ 4	AC	550/ 4	AC	53

Table 5.4.
Post Shot peening heat-treatments to induce recrystallization.

Specimen	Temperature/ time (°C/ min)	Cooling
61 64-BW 64-CO 53	700/ 20	AC
51 21	575/ 20	AC

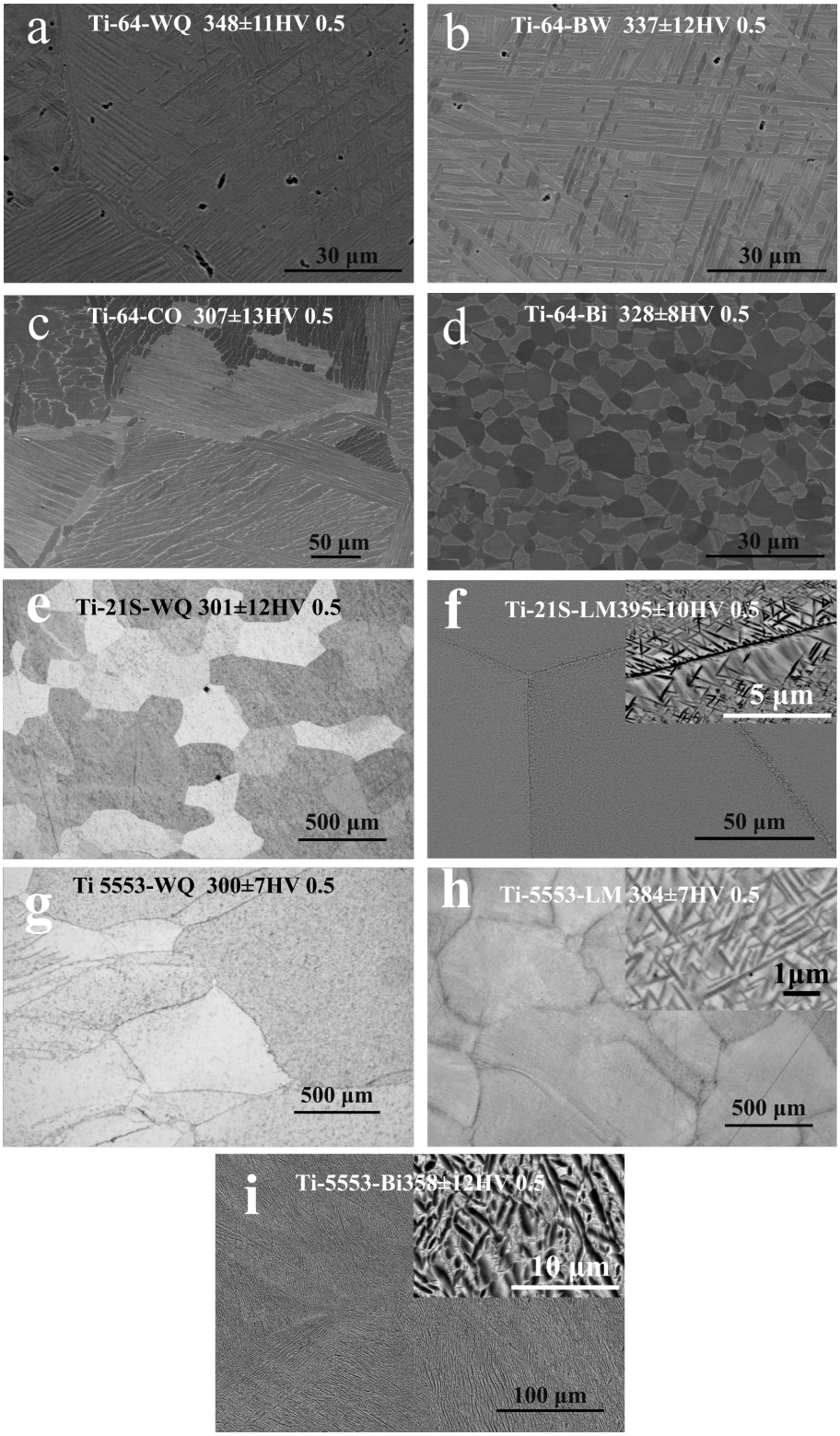

Fig. 5.1. Backscattered SEM images show the resulting microstructures from the processing detailed in tables 2-4. The resulting surface hardness for each microstructure is presented for each specimen.

Solutionization conditions for each alloy were selected by considering the β-transus temperature of each alloy 955-1010°C [4], 850°C [77] and 807°C [78] for Ti64, Ti-5553 and Ti-21S, respectively. For each alloy a solutionization temperature above the β-transus was selected to ensure specimens reached a fully-β condition prior to cooling. It should be noted that all heat-treatments were performed in a tube furnace with a controlled atmosphere that allowed for a positive pressure of Ar to be maintained through out the duration of every heat treatment Testing coupons 20mm by 20mm and 1.8mm (thickness varied among all alloys due to differences in material stock used) were produced from all alloys and conditions. These testing coupons were subjected to shot peeing to selectively deform the surface and impart a residual stress on each specimen. Specimens were peened with using ∼550KPa (80 Psi) for 40 seconds at a standoff distance of ∼25 cm (10 in). Duration of SP was selected to produce a SP coverage of ∼80%. Coverage was determined by subjecting a test coupon to SP for 10 sec . Subsequently, the peened surface was analyzed with optical microscopy to measure the area covered by peen marks as specified in SAE J2277 [69]. Knowing the coverage produced allows for extrapolation using the following relation:

$$C_n = 1 - (1 - C_1)^n \text{ [69]} \tag{5.1}$$

Specimens subjected to SP were sectioned to reveal the cross-sectional area. Cross sections of each specimen were metallographically prepared and polished with SiC paper (320-800 grit), and 0.03 μm silica suspension. The cross-sections were analyzed with scanning electron microscopy (SEM) and optical microscopy. Further analysis of specimen cross-sections was done with nanoindentation to measure residual stress produced by SP. Residual stress was measured in the same fashion as done by Ghanbari et al [85]. Indentations were performed on a specimen before shot peening i.e. stress free condition (SFC) , and the indentation depth was corrected to account for the pile up of material at the edges of the indentation (see Fig.5.2 a-c). It is important to correct for pile up because residual stress is calculated from comparing the contact area produced by using the same loading parameters in a stress free sample and a stressed (shot peened). So the corrected depth (hc) (see Eq.5.2) is used to

calculate the corrected contact area(see Eq.5.3) for the stress free specimen. The corrected contact area is used to calculate a corrected hardness(see Eq.5.4) that is input into Eq.5.5-5.6 and used to calculate residual stresses. Determination between tensile and compressive states for the residual stress is done by comparing the load of each indentation to that of the stress free specimen; if the load in the shot peened specimen is larger than that of the stress free condition at the same depth(270nm), then the shot peened specimen contains a compressive stress.

$$h_c = h_p + \frac{h_1 + h_2 + h_3}{3} \tag{5.2}$$

$$A_c = \pi * tan\psi * h_c^2 \tag{5.3}$$

$$H = \frac{P_{max}}{A_c} \tag{5.4}$$

$$\sigma_C = H(\frac{A_0}{A} - 1) \tag{5.5}$$

$$\sigma_T = \frac{H}{sin\alpha}(1 - \frac{A_0}{A}) \tag{5.6}$$

A stress free(not shot peened) specimen of all microstructural conditions was indented and the pile up resulting from the indentation is used to calculate a correction to the projected contact area. Pile up height was measured for all three sides(see Fig.5.2-b and c.) of the indentation and the average value used to correct the projected area resulting from material pile up. The pile correction is necessary because the presence of a compressive or tensile residual stress will increase or decrease the value of reduced modulus measured because the projected contact area will be changed by the material pile up at the edges of the indentation(see Fig.5.2-c).

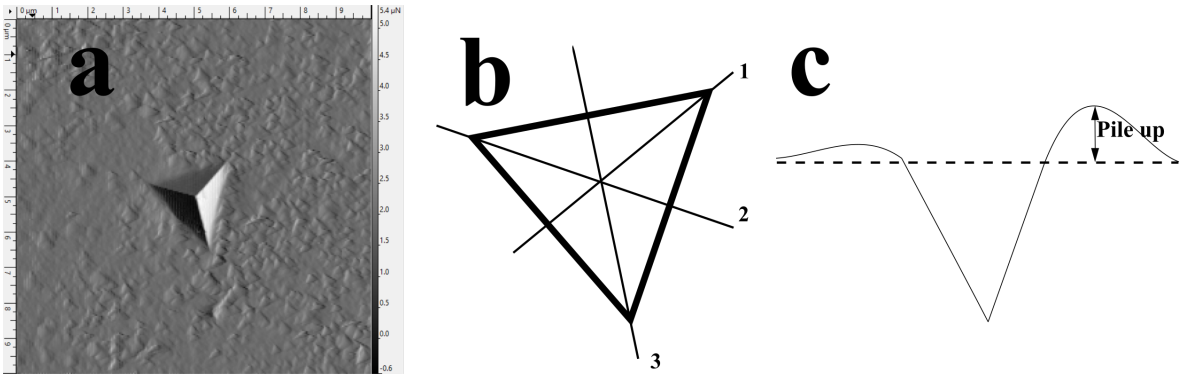

Fig. 5.2. (a) surface imaging done by scanning probe on the surface (similar to AFM) (b) pile up measurements done on each side of the indentation (c) depth profile used to measure pile up.

Post-shot peeing heat-treatments were performed on specimens that showed clear signs of deformation. The times and temperatures employed were selected to induce recrystallization of only the volumes adjacent to the surface. Ti-21S was heat-treated500°C for 30 min and Ti-5553 and Ti-64 specimens were heat-treated at 700°C for 20 min. The difference in temperature is due to the undercooling each alloy would experience in relation to β-transus temperature of each alloy. The times used for each heat-treatment were kept short to avoid or limit precipitation in the bulk of the material. Residual stress was measured (as detailed above) after heat-treatment to analyze relaxation of residual stress caused .

5.4 Results and Discussion

5.4.1 Microstructural Response to Shot Peening and Residual Stress

Ti-64

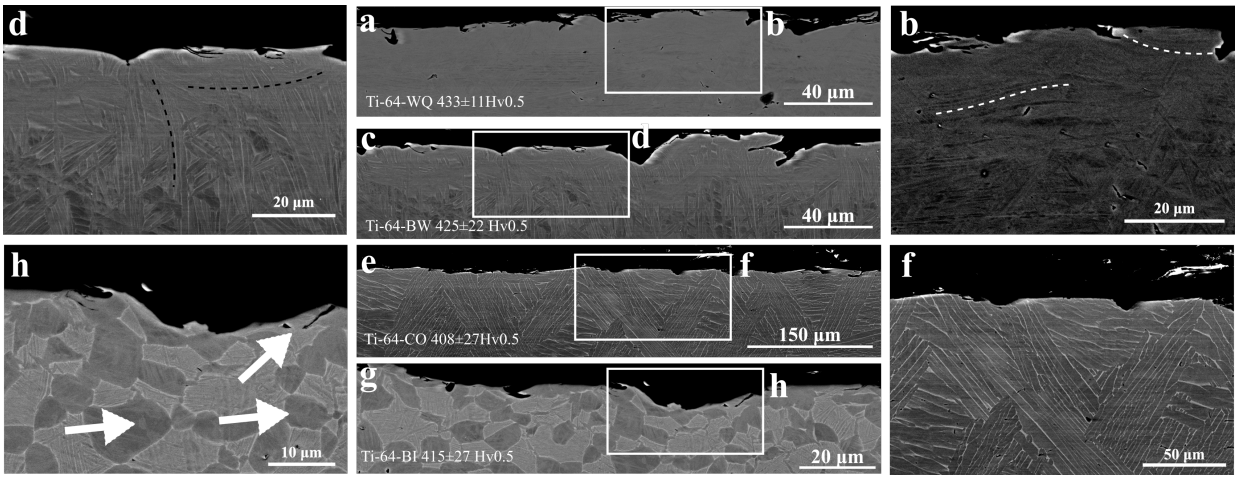

Fig. 5.3. SEM backscattered images of Ti-64 specimens cross-sections used to analyze microstructural changes caused by shot peeing in (a -b) Ti64- WQ, (c-d) Ti64 BW, (e-f) Ti64-CO, and (g-h) Ti64-BI.

Martensite and basket weave structures (see Fig.3 b,d,h) display bent or distorted α-laths the in areas near the surface and can be seen at 20 and 10 μm from the surface in martensite and basket weave, respectively. In contrast, colony structure does not show a clear morphological change of the α-laths(see Fig.5.3 e-f). This is surprising because the colony microstructure tends to be softer than the other structures does not show clear signs of deformation. Alternatively the bimodal structure (see Fig.5.3-g and h) shows distortion of laths and the partitioning of equiaxed grains into smaller.

Ti-5553

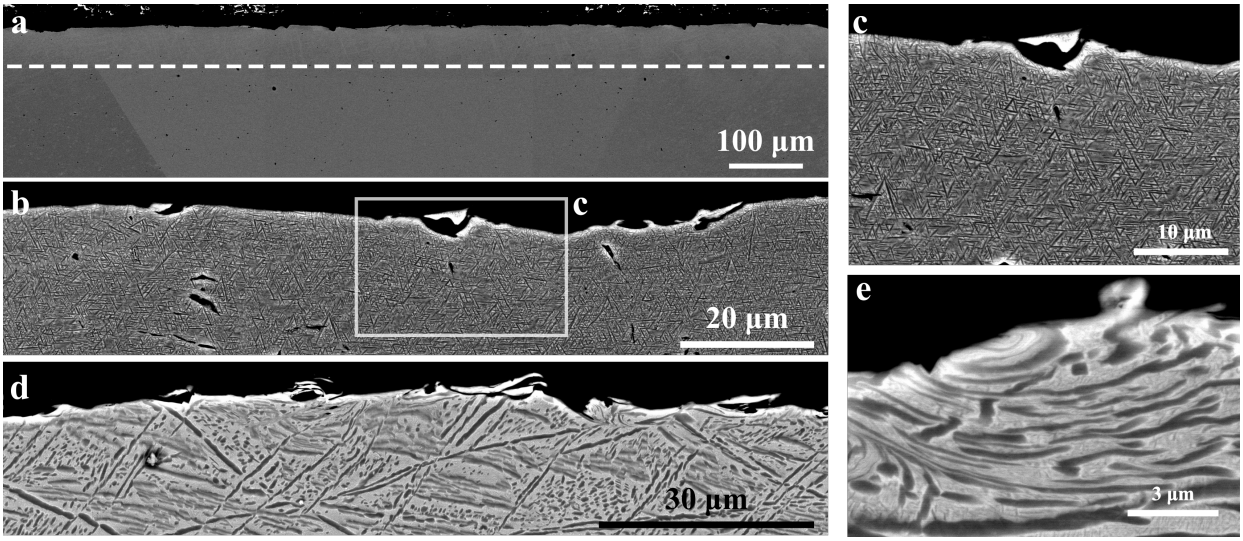

Fig. 5.4. SEM backscatter images of Ti-5553 showing response of different microstructures to shot peeing (a) Fully β, (b-c) fine lamellar, and (d-e) bimodal.

SEM imaging of the Ti-5553 fully solutionized shows faint marks in areas adjacent to the surface of the shot peened material that are shear bands. These bands extend roughly $\sim$50 μm into the specimen (see Fig.5.4-a). The fine lamellar structure does not show clear signs of microstructural deformation as seen in Ti-64, meaning that the fine lamellae do not show any bending(see fig4-c). Interestingly, the bimodal(see Fig.5.4 d-e) structure shows clear deformation (bending) of primary α-laths, but it is unclear if the fine precipitates have undergone a shape change.

Ti-21s

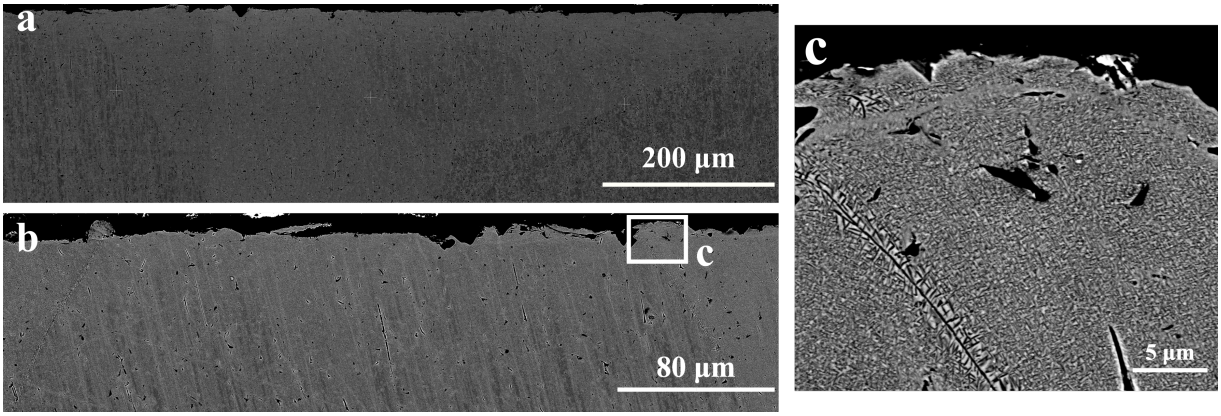

Fig. 5.5. SEM backscattered images of Ti21S showing (a) fully β and (b and c) fine lamellar structures after SP.

Fully-β (see Fig.5.5-a) Ti-21s similar response to SP as seen in Ti-5553 (see Fig.5.4-a) similarly there is a faint area adjacent to the surface that measures $\sim$50 μm that seems to be populated by shear bands(similarly to Ti-5553). Note the measurement of the layer composed of shear bands is measured from the surface to a point at which grain boundaries are discernible, given that grain boundaries are not resolvable within this layer. The fine lamellar condition of Ti-21s(see Fig.5.5 b-c) does not show clear signs of deformation

It should be noted that for all specimens (see Fig. 5.3-5.5) display significant discontinuities on their surfaces. Though there is an expectation for surface roughness to increase in specimens that undergo shot peening, some samples display signs of fracture localized to the surface. these cracks originate on the surface and tend to divert back towards the surface. It is reasonable to expect that these features would ahve a deleterious effect on performance (depending on the application); however, it may be possible to aovid the localized surface fracture through the use of several peening steps with decreasing media size in each step to decrease roughness.

5.4.2 Surface hardness

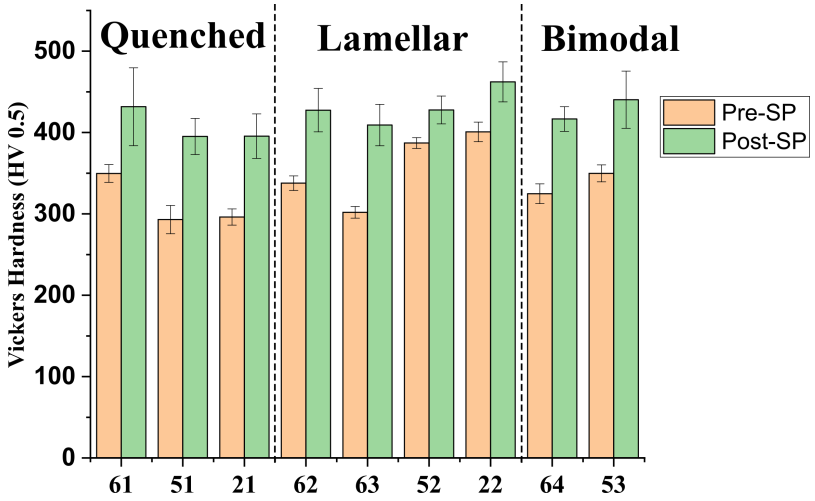

Fig. 5.6. Vickers hardness measurements of surfaces from(a) quenched,(b) lamellar, and (c) bimodal structures.Specimen naming given in tables 5.1,5.2 and 5.3.

Hardness for all microstructural conditions has increased after SP as seen from surface hardness measurements (see Fig.5.6). The largest increase in hardness was seen in the fully β conditions of Ti-5553 and Ti-21s, showing an increase in surface hardness of $\sim$100 HV0.5. this is followed closely by the fully martensitic structure. Lamellar conditions(Fig.5.6-b) displays a lager variation of hardening caused by SP. β-alloys with lamellar conditions displayed the least hardening of all conditions with a 40-60 HV0.5 increase. This is caused by the fine α-lath precipitates that reinforce the β-matrix, and oppose decrease hardening by limiting the dislocation motion. On the other hand, Ti-64 lamellar conditions (basket weave and colony) show that the colony structure hardened slightly more than the basket weave condition, this was expected due the larger variation in lath orientation in basket weave structure, and coarser structures in colony structure. Lastly, the bimodal structures in Ti-64 and

Ti-5553 for displayed similar hardening. It should be noted that the post-SP hardness for all specimens seems to saturate near 430HV0.5 .

5.4.3 Residual Stress

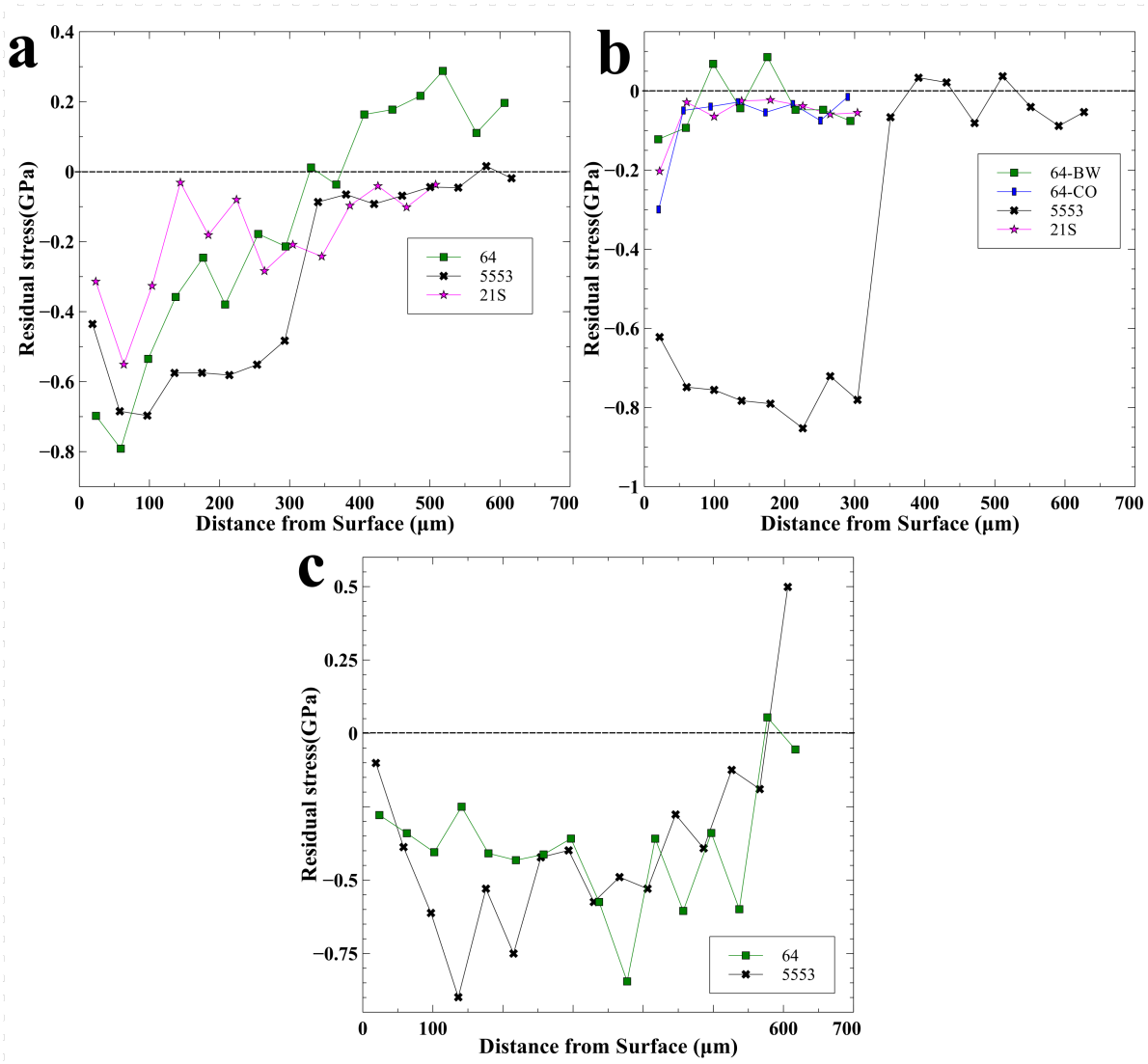

Fig. 5.7. Residual stress profiles measured through nanoindentation for (a) quenched, (b) lamellar, and (c) bimodal microstructures.

Coupling microstructural changes with residual stress produced in each specimen shows that there is a dependence of distance from surface and magnitude of residual stresses reached. Residual stresses due to SP are formed by the plastic deformation of the surface being restrained by the rest of the material, resulting in an elastic distortion for the material beneath the plastically deformed layer. Fig.5.7 shows that all alloys and structures achieved a compressive residual stress, but with varying magnitude of stress and distance penetrated the material. Residual stresses formed in quenched conditions of all alloys(Fig.5.7-a show a peak compressive residual stresses between 500 MPa (Ti- 21s) and 800 MPa (Ti-5553). Lamellar structures, see Fig.5.7-b, displayed shallow penetration and low magnitude of compressive residual stress. The exception being TI-5553 that displays a high compressive residual stress that penetrates roughly 300 μ into the material Lastly, bimodal condition. Lastly, bimodal microstructures (see Fig.5.7-c) in Ti-5553 and Ti-64 displayed the deepest penetration of residual stress within the material. There is a dependence of residual stress evolution to the starting microstructure. The quenched and bimodal specimens displayed the largest magnitude compressive RS, and large penetration of RS from the surface. For all quenched conditions, this suggests that homogeneous microstructures are more receptive to RS formation. In contrast, bimodal structure are not homogeneous because these conditions are composed of both α+β; however, both TI-64 and Ti-5553 bimodal structures contain primary α-precipitates and fine α-laths. Comparing the alpha phase content in each specimen to the maximum residual stress and maximum depth of penetration of residual stress(see Fig.5.7) shows that intermediate fractions of alpha phase will result in maximum RS generated and distance from the surface the residual stress is present. It seems that residual stress produced in the material depends on the α-Ti phase fraction of the alloy; however, specimens with intermediate α-phase fraction contain strengthening mechanisms that surely affect development of residual stress.

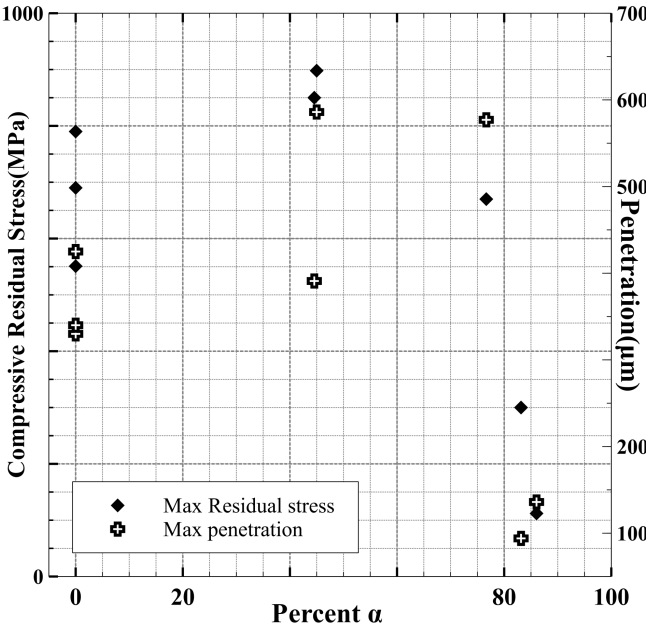

Fig. 5.8. comparison of α-phase percent present in each specimen to (a) maximum residual stress created in each specimen, and(b) maximum distance from surface of compressive residual stress penetration.

5.4.4 UFG Layers

Previous works have shown that surface processing techniques can result in dynamic recrystallization of metallic materials [59,67,86] during processes like SP, SMAT and SMG; however, the SP parameters presented thus far in this study have not resulted in a UFG structure. Consequently, specimens from each alloy that exhibited clear signs of plastic deformation on the surface were selected to perform heat-treatments (see table.5.4). Ti-64 martensitic and basket weave conditions(see Fig.5.9 a-b) showed clearly defined UFG layer within the first 2 μm from the surface. In contrast, Ti-64 colony structure did not produce any recrystallization products (see Fig.5.9-c). Ti-5553 bimodal structure (see Fig. 5.9-d-e) displayed a continuous layer of UFG. Lastly Ti21s fully β structure(see Fig.5.9-f-h) displayed fine scale α-Ti formed

at the surface of the specimen, however, unlike TI-64 and Ti-553 the morphology of the grains within the layer changes from a mixture of equiaxed α and β grains(zone 1 in Fig.5.9-h) to slightly elongated β-grains surrounded by grain boundary-α (zone 2 Fig.5.9-h).

It is evident that shot peening has induced enough strain on the surface of the material because equiaxed grains are present in the surfaces of all alloy microstructural conditions, the exception being Ti-64 colony. Formation of equiaxed α-grains has long been reported to be the result of thermomechanical processing [10, 24, 87], where strain introduced to the material will induce formation of equiaxed grains through the break up of α-laths. The α-laths are broken into small equiaxed particles by the accumulation of dislocation within the α-lath that results in the formation of an α/α interface, followed by the penetration of β-phase into the laths, thus microstructures with wide laths will deter the formation of equiaxed grains [87]. This explains the ease of recrystallization seen in Ti-64 martensitic and basket weave microstructures because they possessed average α-lath thicknesses of 0.6 and 0.8 μm(respectively) , and the colony structure has coarser laths with an average thickness of 4.20μm. for Ti-5553, the same mechanism seems to be responsible for the formation of the fine scale equiaxed grains because most of the α-grains formed within the UFG layer tend to follow the shape of the lath they previously formed; however, some α-grains are not clearly separated from each other β-grains. This could be due to several reasons:1- the mechanism of equiaxed-α separation is driven by the equilibration of α/β interfacial energy and diffusion, both of these quantities will change with composition of the material . previous works show that diffusion of Mo in Ti (both α and β) [10, 88, 89] is slow, and could limit the length the β-Ti penetrates into the α-lath. 2- the α-lath break up process could be caused by localized shear and rotation of parts of the α-lath [87], and this phenomenon was seen in Ti-64 bimodal structures shot peened in this study (see Fig.5.3-h) and this same process cold have taken place in Ti-5553 bimodal structure. These two mechanisms that are proposed by Weiss explain the process of equiaxed grain formation at elevated temperature; however, shot peening

is a localized cold working process affecting only the surface so the piece itself does not generate a significant increase in temperature to cause diffusion, this coupled with the fact that strain generated by SP will be maximized near the surface and can reach large strains (3-7 as reported by Bagherifard et al. [90]) it makes sense that a shear dependent grain rotation mechanism would produce the α/α interface and the diffusion available during annealing allows for the penetration of β into the α/α interface, but the short duration of the post SP anneal does not allow for the complete separation of all newly formed equiaxed α-grains.

The UFG layer produced in Ti-21s clearly differs from the other alloys in that there is a morphology change of the α-precipitates(see Fig.5.9-h), but more importantly this is not caused by any pre-existing microstructure because the initial microstructure is homogeneous single phase β-Ti. The structure seen in Ti-21S (see Fig.5.9-h) is likely not a product of diffusional processes, or rather diffusion plays a small role, because this alloy has a considerable Mo concentration (15 wt%). Mo is a slow diffuser in Ti and thus would increase transformation times [10]. So the appearance of 2 distinct regions in the UFG layer suggests that the plastic deformation was not entirely responsible for the subsequent α-Ti precipitation, and must have been aided by the residual stress present in the material.

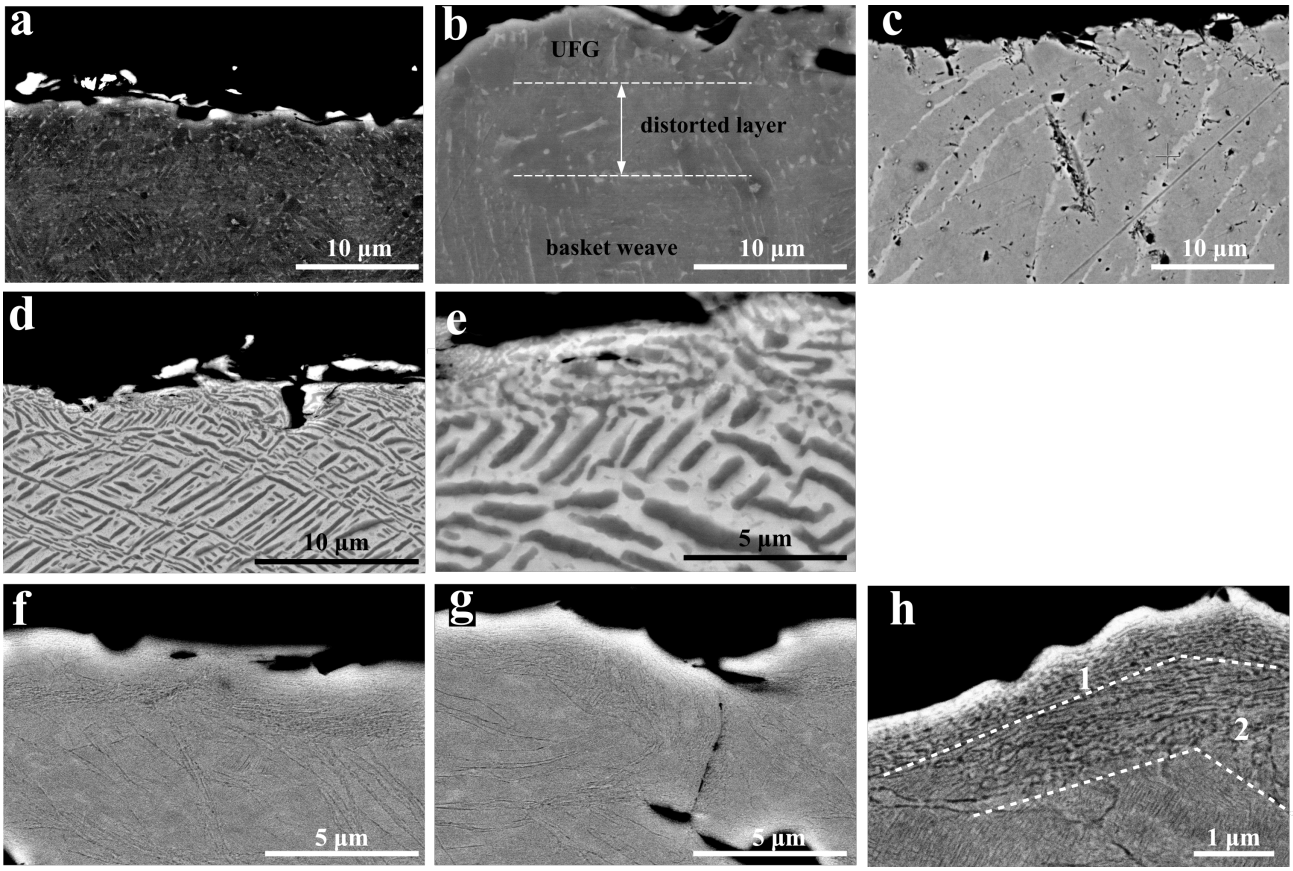

Fig. 5.9. SEM backscattered images taken from s specimens that were shot peened and subsequently heat treated that had starting microstructures of (a) Ti -64 martensite, (b) Ti-64 basket weave, (c) Ti-64 colony,(d and e)Ti-5553 bimodal, and (f -h) Ti-21S fully β where zones 1 and 2 show a morphology change within the layer.

Properties of UFG Layers

Measurements of microstructural features (see Table.5.5) and mechanical properties measured through Nanoindentation performed within the UFG layers seen in Fig.5.9 (see Table.5.5) are presented here. Across all specimens there is an increase in hardness, as expected by the decreased grain size; however, there seems to be an increase in modulus for Ti-5553 and Ti-21S. This should be attributed to the increased alpha phase fraction at the surface in comparison to the original state of the material. in

comparison, Ti-64 specimens did not show a significant increase in modulus compared to the untreated condition. The modulus measurements shown in this study contrast those reported by Huang et al. [63], where they report a 16% increase of the elastic modulus of Cp-Ti(fully α) specimens processed by SMAT. Similarly to this study, Haung et al. used nanoindentation to measure the elastic modulus, however, they measured the material using a high load (510mN) and a single load un load segment. The present study has used a lower load coupled with multiple load/unload segments. This was done as a self check of each indentation site, and only indentation measurements were reported if the modulus did not vary with 0inedntation depth, something that cannot be known from Huang et al.'s work. Another distinction is the fact that the grain sizes achieved by Haung et al.'s study are significantly finer than the ones produced here (150nm vs 700nm respectively); however, modulus of the material should vary with crystallographic orientation not grain size .

Effect of SP parameters

The processing parameters that affect SP "intensity" are: propelling pressure, exposure time (coverage), and shot size. This study employed a uniform shot size ($\sim$300 μm), pressure (80 Psi) , and exposure time of 40 sec (to produce 80% coverage). The pressure and shot size used are somewhat common, but the coverage (80%) is somewhat low when compared to the industry expected 100%. However, deformation and penetration of the deformation is dependent on pressure and shot size, as demonstrated by Maleki et al. [67]. Other studies have argued that increasing coverage was necessary to form fine scale features on a surface [48]; however, the present study shows that below 100% coverage has produced UFG layers in Ti. This result is in agreement with Prevey et al. [84], who argued that 20 and 80%coverage will result in similar fatigue performance to 100% coverage. The utility of coverage is seen in the formation of uniform/continuous layers this is clearly seen when the resulting UFG layers produced in this study is compared to Todaka's and Maleki's results [48, 67], studies that show uniform UFG layers.

Table 5.5.
Resulting measurements and properties of UFG layers recrystallized. Specimen naming given in tables 5.1,5.2 and 5.3.

Specimen	Layer Thickness	Average Grain	Pre-SP		Post-SP	
	(μm)	Size (nm)	Modulus (GPa)	Hardness (GPa)	Modulus (GPa)	Hardness (GPa)
61	2.05	710	119.6+/-10.8	3.64+/-0.76	119.7+/-10.8	5.08+/-1.12
62	1.88	740	112.4+/-3.6	3.59+/-0.52	111.9+/-8.2	4.30+/-0.52
53	3.58	350	128.6+/-5.3	4.73+/-0.40	112.4+/-10.3	4.98+/-1.06
21	2.10	500	98.3+/-4.0	3.93+/-0.30	103.1+/-10.1	5.00+/-1.04

RS effect on precipitation

The recrystallization of the UFG to nanocrystalline layers in all titanium alloys is clearly a result of plastic deformation localized to the surface; however, the transition zone seen in Ti-21S (fig.5.9-h) indicates that the plastic deformation dissipated rapidly and necessarily the residual stress is affecting the precipitation of α-Ti this particularly evident in the fully-β conditions of Ti-5553 and Ti21s. SEM microscopy of Ti-5553 fully-β condition (see Fig.5.10) that was processed, shows the formation of UFG domains in areas adjacent to the surface, surrounded by a large field of α-laths in a β-matrix. Curiously, the presence of α-laths disappears after $\sim$500μm, this coincides with the decrease of residual stress as distance from the surface increases. Similarly, Ti-21S reveals a similar trend of decreasing α-volume fraction with decreasing RS (see Fig.5.11). This would suggest that the residual stress is facilitating the nucleation and growth of α-Ti during the post-SP heat-treatments. The elastic strain stored in the material could be reducing the nucleation energy barrier needed to produce α-Ti, by contributing to the strain energy term of the Gibbs free energy. THe results seen in Ti-5553 and Ti-21S suggest that the residual stress is solely responsible for the precipitation gradient as the increased α phase fraction seems to follow the residual stress profile . Additionally, the fact that the α-phase fraction gradient is seen in an alloy that has a sluggish $\beta \rightarrow \alpha$ transformation (Ti-5553) due to the significant Cr content [10], and after a short heat treatment would strengthen the argument that RS during annealing produced the precipitation. However, this study does not show conclusively that the RS is the sole cause of this phenomenon, and more in depth work needs to be done regarding this point.

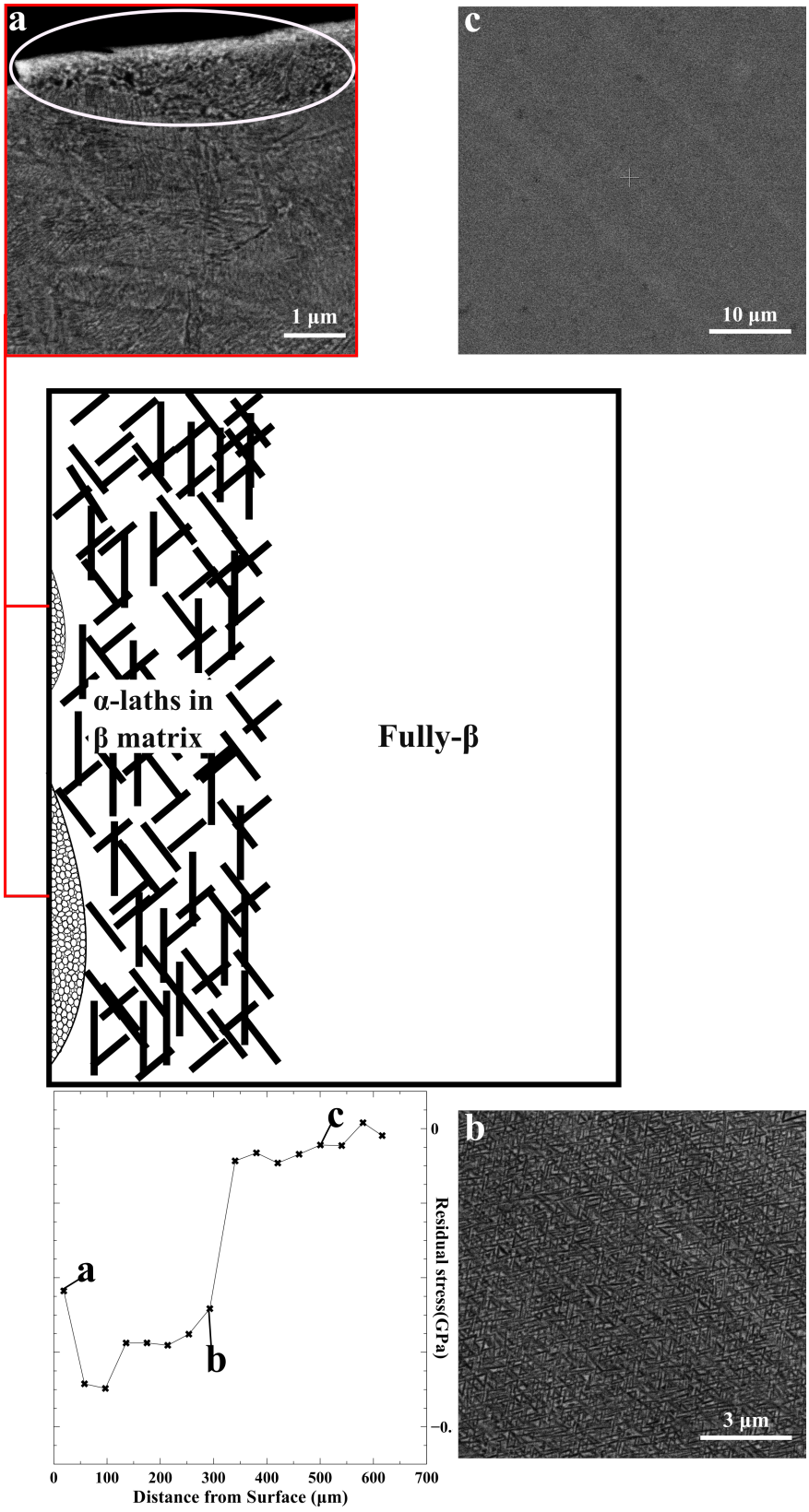

Fig. 5.10. Structures produced from post SP heat treatment of Ti-5553 fully . Schematic and backscattered SEM images shows variation in microstructures seen as (a) nanocrystalline equiaxed α+β grains, (b) β matrix with fine α-lath precipitates and (c) fully β.

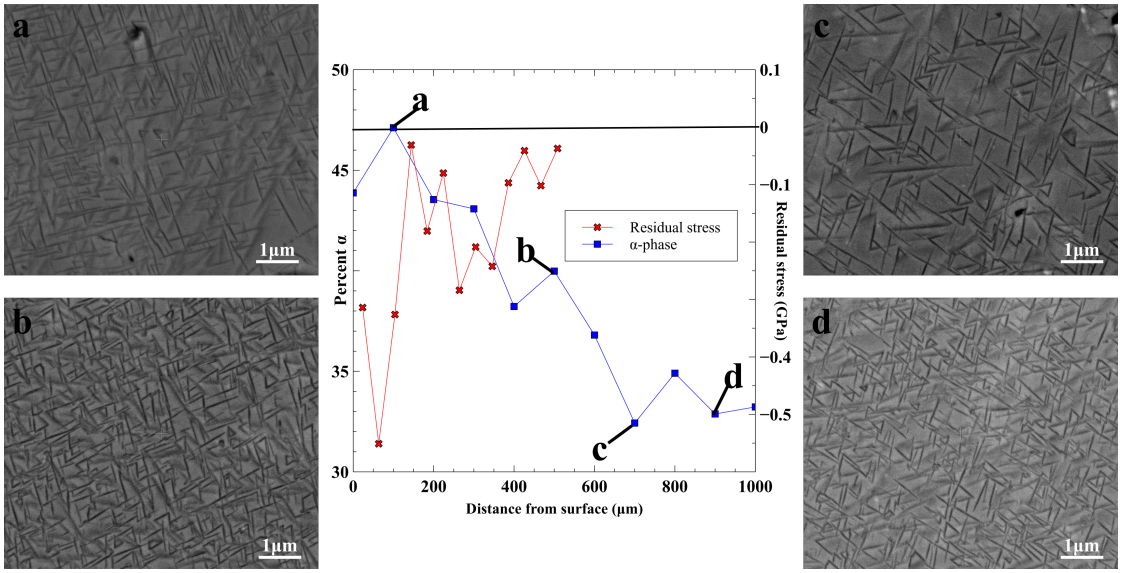

Fig. 5.11. Plot of residual stress and volume fraction of α-Ti both in relation to distance from surface. The backscattered SEM micrographs are taken from (1)100 μm, (b) 500 μm, (c) 700 μ , and (d) 900 μm from the surface.

5.5 Conclusions

The present study has employed conventional shot peening surface processing to a variety of titanium alloys that cover a large range Molybdenum equivalencies . The degree of deformation incurred on each sample varied with the microstructures showing that all but Ti-64 colony, and the lamellar conditions of both β-alloys did not show significant changes after SP. Residual stresses developed within the studied structures was assessed with nanoindentation, and showed that quenched conditions of the alloys (Ti-64 martensite, and fully-β Ti-5553 and Ti-21s) along with bimodal structures developed high magnitude and deeply penetrating residual stresses. The study clearly showed that the addition of a post SP heat-treatment can be done at relatively low temperatures, and with processing ease to create UFG layers on the surfaces of all alloys. The addition of a heat-treatment is a counter intuitive choice

because it sacrifices the compressive residual stress within the material; however, the hardness of the surface layer significantly increased. The application of a post SP heat treatment has resulted in a graded precipitation of α-Ti. The presence of residual stress seems to stabilize the α-Ti phase in Ti-5553 and Ti-21s, and a decreasing volume fraction of α-Ti has been measured in TI-21s as distance from surface increases. This suggest that compressive residual elastic stresses from SP can be used to selectively form precipitate regions within a single specimen through thoughtful application. Therefore a surface could be designed to have gradation of precipitation of varied penetration and in selected areas of the surface by masking/protecting areas that one would not need peened; however, more evidence is needed to establish a causal relation between RS and the precipitation gradient.

6. HARDENING PARTICULATE TI MEDIA THROUGH CONTROLLED OXIDATION

Portions of this chapter were previously published in Metallurgical and Materials Transactions A DOI: https://doi.org/10.1007/s11661-019-05326-6

6.1 Abstract

Oxygen in titanium is an alpha stabilizer that provides significant solid solution strengthening. This study presents a method of exploiting surface hardening of titanium particulate media. Appropriate thermal exposure parameters resulted in the doubling of surface hardness due to the ingress of oxygen, from ∼3 GPa to over 8 GPa, as measured through nanoindentation. This process produced solid solution strengthening without creating a distinct oxide layer or significant sintering of particles.

6.2 Introduction

Shot peening is a well-established surface treatment commonly used to impart a compressive residual stress on a part to improve the fatigue life [9,91,92]. The possible drawbacks of this surface engineering process, depending on the final application, include increased surface roughness from the indentations caused by shot media and the potential for contamination of the workpiece surface from material transfer of the shot residue. Shot contamination can have deleterious effects on properties. As a common shot media is iron-based particles, shot peened surfaces of corrosion resistant alloys tend to have poorer corrosion resistance when compared to their untreated counterpart; such as the case when Fe-based peening media is used on Al [93]and Mg

alloys [94]. Clemens et al. reported that the Fe concentration in shot peened AZ91 was as high as 1.5wt% on the peened surface. Other researchers [95] have attempted using ceramic peening media for shot peening, and using this media results in no measurable corrosion or fatigue deficit; however, Schuh et al. showed that ZrO_2 shot still results in contamination of the surface when used to shot peen Ti-64 [96]. One route to circumvent surface contamination would be to use Ti-based shot to peen Ti alloys; this would require Ti-based shot that is harder than the target alloys. Titanium displays a large solubility for oxygen in the α-Ti phase [29]and the addition of oxygen to α-Ti is a potent hardener [35, 88]. Oxidizing (distinct from oxidation) of titanium should produce a Ti-based shot media that is both hard and will avoid surface contamination because of the large solubility of oxygen in α-Ti before producing an oxide layer. Avoiding oxide formation would decrease the potential for incorporating Ti-oxides in any media transfer. This study proposes a method to produce Ti-based shot peening media via solid solution strengthening with oxygen.

6.3 Procedures

Pure titanium powder (99.8% metal basis) was obtained from Atlantic equipment engineers (AEE) with an initial composition presented in Table.6.3. The powder had a particle size range between 50-150μm. In order to harden the powder, there has to be a controlled diffusion of O into the powder particles. Surface engineering of Ti alloys via case hardening procedures are well established, but often the goal is to incorporate a case with a thickness on the order of 100's of microns [36]. Previous researchers developed a hardening mechanism for Ti structural parts where the material is oxidized at high temperature to produce a distinct oxide layer between 700°-1000°C [34–36]. The oxide layer is then dissolved into the alloy by a second heat treatment in an inert atmosphere or vacuum [12]. The method presented in the current study differs substantially from the process described by Dong et al. since the processing temperatures are much lower, and the hardening through O ingress is

taking place in powder material as opposed to bulk material. Dilution of O into the Ti must be done without sintering because the powder must remain loose to be an effective shot peening media. However, the goals of incorporating O ingress into Ti and not sintering fine particles are processes in opposition to each other; oxidation will occur at a faster rate as temperature increases, but sintering will also be more effective at elevated temperatures, leading to a decrease in spherical morphology which is desired for shot media. Therefore, processing temperatures should be kept below the oxidation start temperature of 550°C, to minimize TiO_2 formation [10]. To clarify, this start temperature is a temperature that limits the diffusion flow of oxygen into Ti, and does not decrease the thermodynamic driving force for oxidation. Thus by limiting diffusion of oxygen into the Ti oxide formation can be limited.

Table 6.1.
Composition of as received powder and bulk CP-Ti used in this study, all values in wt%.

	H	C	N	O	Ti
Powder	0.01	0.02	0.02	0.18	Balance
Bulk CP-Ti	0.015	0.08	0.03	0.25(max)	Balance

Powder processing

It was decided to exploit oxidation of Ti to produce a hardened Ti-based powder. Oxidation of Ti happens readily at elevated temperatures (above 550°C); however, for the purposes of this study it is desirable to avoid any sintering of the powder so it can be used as shot peening media. To this end, it was decided to expose loose powder to temperature just below the reported oxidation start temperature. This is done to avoid sintering, and have a controlled oxidation of the powder that does not result in the formation of an oxide layer. As mentioned in chapter 3.4.1 previous researchers have exploited oxidation in titanium to produce a hardened surface; however they rely on the production of an oxide layer that is then dissolved into the underlying metal in a subsequent vacuum annealing step. The process explained here would use a single heat exposure step to produce the hardened powder(times and temperatures are presented in Table6.2). A Vulcan A-550 box(see Fig.6.1-a) furnace was used to expose the Ti-powder to oxidizing conditions. The furnace was preheated to the temperatures before placing the powder in the furnace. To avoid contamination the powder was placed in a container, referred to as a boat, that was made out of commercially pure Ti foil (see Fig.6.1-b). The boat was treated in the same manner the powder was to be processed. This was done to limit the oxygen being absorbed by the boat during the heat exposure. By using the boat it was possible to produce a 500 g batch of powder in one run. The temperature of the furnace was monitored with an external thermocouple.

Table 6.2.
Oxidizing parameters used to harden Ti powder.

specimen	Time (hrs)	Temperature (°C)
1	24	430
2	20	530

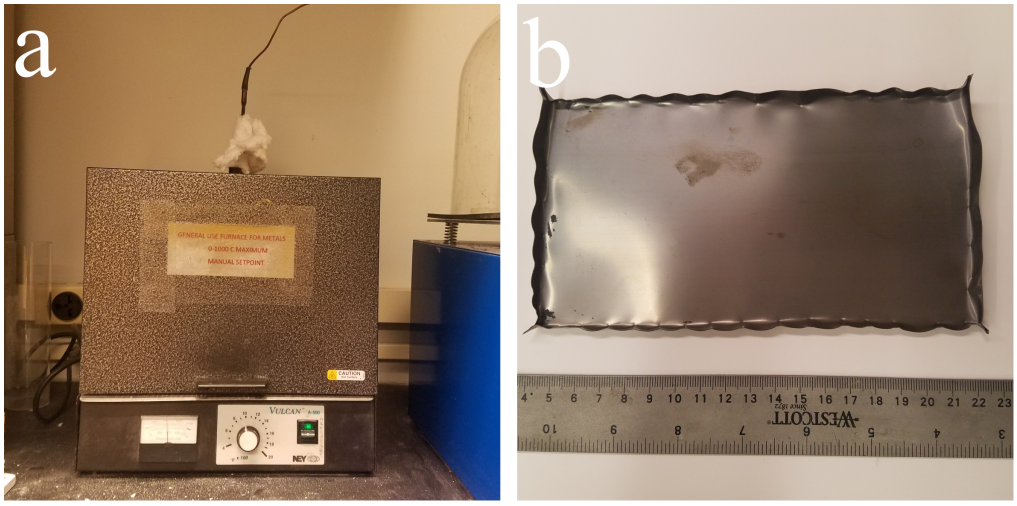

Fig. 6.1. (a) Furnace used to oxidize powder. (b) Furnace boat used to hold powder during heat-exposure.

To evaluate the extent of hardening from O ingress into Ti at these moderate temperatures, a bulk piece of CP-Ti (commercially pure Ti grade 2 obtained from Mcmaster Carr) was ground and polished with colloidal silica, and cleaned by immersing the specimen in ultrasonic baths of acetone, propanol, and methanol. The specimen was then heat treated in air at 530 °C for 20 hours. This duration should allow a diffusion length on the order of 2-5 μm for O into Ti [10]. The hardness of the surface as treated, and a metallographically prepared cross-section, were evaluated with nanoindentation using a Hysitron Ti 950 Triboindenter with Berkovich tip with an effective radius of 600 nm, and a maximum load of 10 mN. All hardness measurements were calculated using the Oliver and Pharr technique [14]. A partial load-unload method was used to acquire hardness as a function of depth of the indentation; for the results presented in this work only the hardness at a depth of $\sim$200 nm is presented (see Fig.6.2) since by using a fixed depth any differences due to indentation size effects are minimized.

The powder was processed at 430°C for 24 hours and 530 °C for 20 hours. The lower temperature processing (430°C) was done to determine a window of conditions

which minimize the risk of sintering. Following the thermal exposure, the powder was milled (rotating roller mill in a Nalgene bottle with no milling media) for 24 hours. The milling step was performed to break up any small clumps of powder that formed during heat exposure. The loose powder was cold-mounted in epoxy and polished to reveal a cross-sectional area of the particles. Polished specimens were tested with nanoindentation to measure hardening caused by O ingress, and electron microscopy was performed using a FEI Quanta 650 SEM. Phase analysis of loose powders was done through X-ray diffraction with a Bruker D8 diffractometer. Quantitative depth profiling measurements were taken from the bulk CP-Ti piece using a LECO 850 GDS (glow discharge spectrometer). GDS measurements were conducted on the bulk piece and are assumed to be representative of the oxygen ingress into the powder particles.

6.3.1 Results and Discussion

Hardness measurements from bulk specimen (Fig.6.2-a) show that the 530 °C thermal treatment has created a hardened layer near the surface. Surface hardness in the bulk specimen increased from ∼3.00.81 GPa to ∼8.41.5 GPa. GDS measured an appreciable O concentration within the first 1 μm of the material. The maximum oxygen concentration does not reach 60wt%, the threshold composition for TiO_2 This matches the expected penetration depth when using diffusivity data presented by Liu and Welsch [4]. Nanoindentation experiments on cross sections of the powder also show that there is a clear hardening of the surface (indents were placed within 3μm of the surface) in relation to the center of powder particles tested (schematically noted in Fig.6.2-b). Hardness measurements performed on powder and nanoindentation measurements made on the cross section of the bulk piece show good agreement for the hardness measured at 3 μm from the surface of powder processed at 530°C. Hardness measurements were extracted from the load-displacement data, shown in Fig.6.3; the load-depth curves of indentations on the powder cross section at 3 μm from the surface of the powder and indentations on the cross section of the bulk Ti at

a distance of 4 μ from the surface are very similar, suggesting there are no deleterious effects from the mounted powder on the frame compliance. This also suggests the surface hardness measured from the bulk piece should be a valid representation of the powder surface hardness. The hardness of the powder processed at 530 °C at a depth of 3 μm from the edge is approximately 20% higher than the bulk particle hardness, and this difference is statistically significant. The hardness of the powder processed at 430°C at the same depth from the surface is not statistically different than the center of the powder, indicated the increased hardness in the higher temperature powder must be due to compositional or microstructural changes and not a geometric effect of the measurement method. The hardness, when measured at an indentation depth of ∼200 nm is approximately 3 GPa in the as received material, is higher than would be conventionally measured with bulk indentation due to the indentation size effect; however the relative differences in hardness between the oxidized and as-received materials are statistically significant.

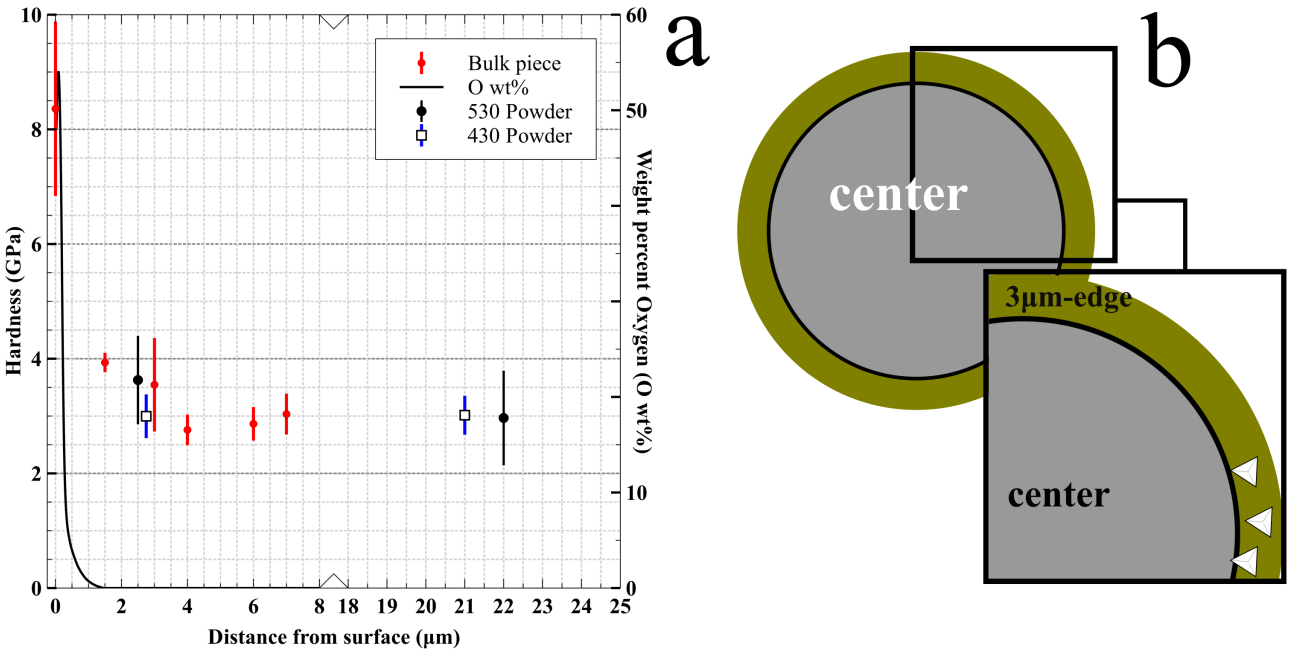

Fig. 6.2. (a) Hardness as measured from bulk and powder specimens treated at 430°C and 530°C. The bulk specimen shows a gradual decrease in hardness with increasing distance from the surface, and is closely matched by powder processed at 530°C. Powder processed at 430°C showed no significant change in hardness.(b) Schematic of powder particle cross-section shows that indentations were performed within 3μm from the surface of the particle and individual indentation locations varied within this band from particle to particle.

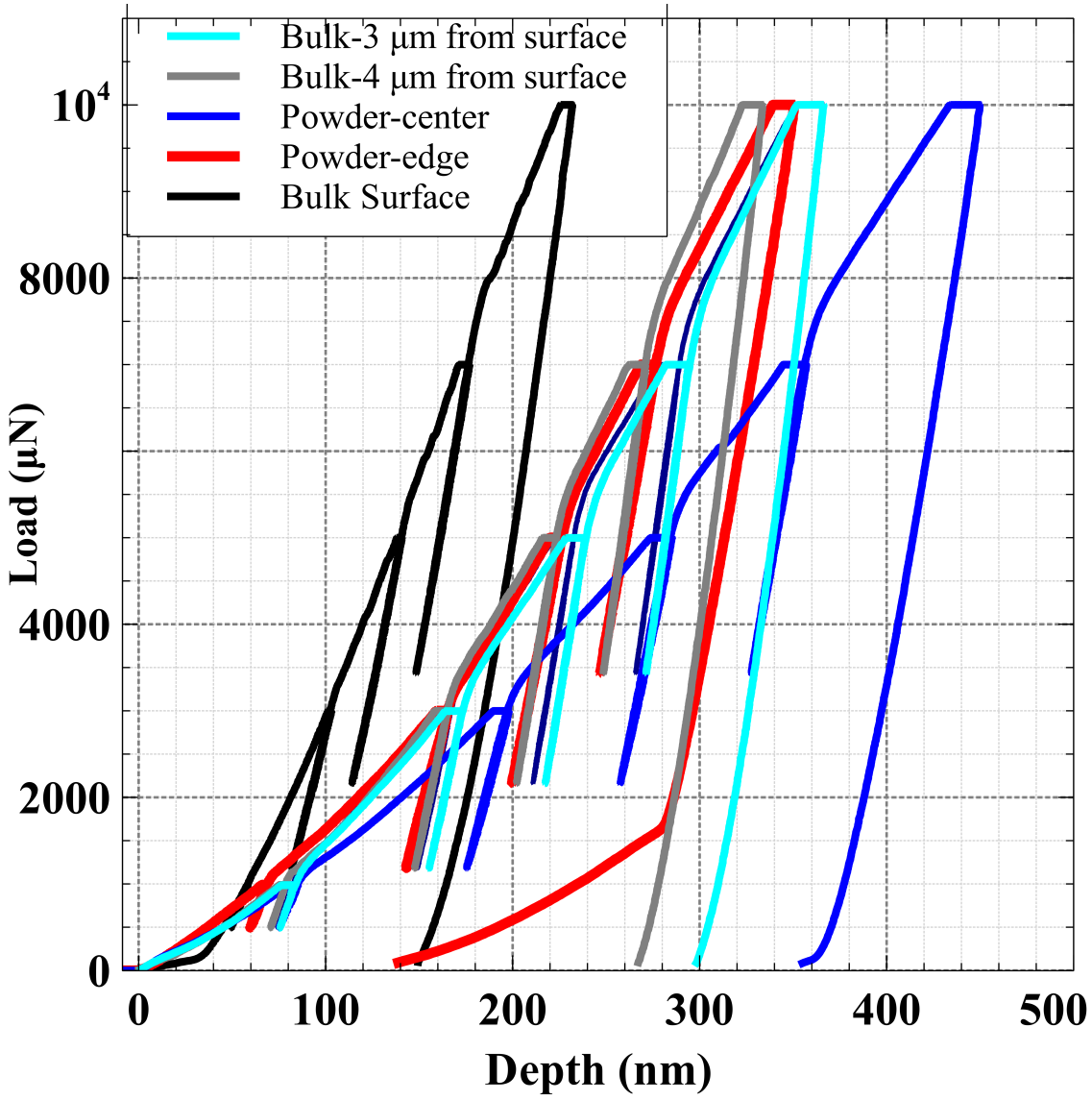

Fig. 6.3. Load-depth curves from indentations of bulk and powder processed with same oxidation treatment. The load depth curve for a typical indentation of the case, ∼3 μm from the edge of a spherical particle are bracketed by indentations between 3 and 4 μm deep on the cross section of the bulk material, both of which greatly exceed the hardness of the core.

Powder diffraction measurements (see Fig.6.4) were conducted on as-received powder (AR), powders processed at 430°C for 24 hrs, and 530°C for 20 hrs. Powder pro-

cessed at 430°C showed no signs of oxide formation, while powder treated at 530°C showed small peaks attributable to TiO_2 at 27.4° and 73.8° 2θ. To determine the relative amounts of metallic α-Ti phase compared to TiO_2, the direct comparison method of peaks was used [97] (See Eq.6.1,Eq.6.2, and Eq.6.3).

$$\frac{I_\alpha}{I_{ox}} = \frac{R_\alpha C_\alpha}{R_{ox} * C_{ox}} \tag{6.1}$$

where

$$R = \frac{1}{\nu^2}[F^2 \rho \frac{1 + cos^2(2\theta)}{sin^2(\theta) * cos(\theta)}]e^{-2M} \tag{6.2}$$

and

$$C_\alpha + C_{ox} = 1 \tag{6.3}$$

ν is the volume of the lattice, F is the structure factor, ρ is the multiplicity of the plane chosen. The exp(-2M) factor has been neglected in this study because it is a temperature factor not valid at room temperature. Cox and Cα are the fractions of the oxide and α-Ti phase. Table. 6.3 shows values used for calculation of the volume fraction.

Table 6.3.
Values used for volume fraction calculation

Diffracted Peak	νˆ2 (nmˆ3)	Fˆ2	ρ
α-Ti-(101)	0.0351	478	12
TiO_2	0.06243	1417.65	4

X-ray spectrum taken from powders processed at 530°C revealed that there is $\sim$0.03 volume fraction of TiO_2; however, SEM imaging of the surface and cross-sectional SEM imaging of powder exposed to 530°C (see Fig.6.5-b-c) does not show

clear microstructural evidence of an oxide on the surface of the material when compared to AR powder (Fig.6.5-a). This is fortunate because this avoids the issue of an oxide layer spalling off during shot peening and depositing impurities on the target material as seen in previous studies. The fact that this is a solid solution of O and Ti would suggest that even if portion of the power/shot were to be deposited on to the targeted surface the resulting compositional change to the workpiece would be minimal. Additionally, this result suggests that similar processing could be done on other valve metals such as Ta, V , Zr, Hf [98–101]; because these are elements that show appreciable solubility for oxygen in a metallic phase. Fig.6.5-c shows that minor necking has occurred during thermal treatment at 530 °C (that was easily separated during self-milling conditions which also did not lead to significant powder deformation), this sets an upper temperature / time processing window for creating a case hardened Ti powder. Cross sections of as received and material treated at 430 C exhibit no clear necks and reflect random sections of spheres.

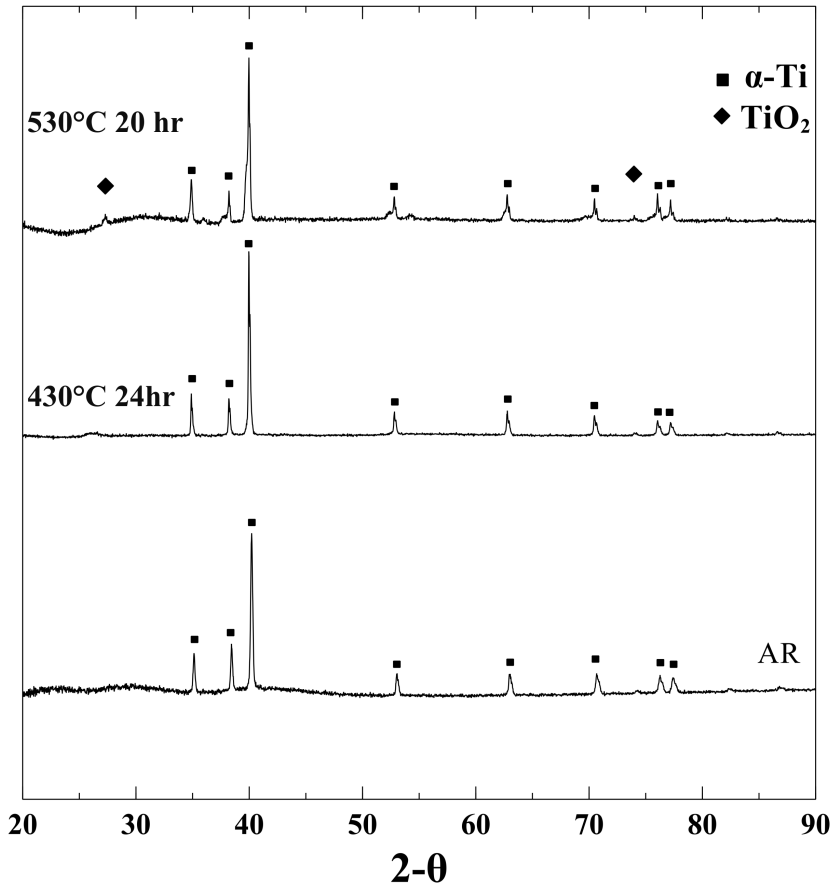

Fig. 6.4. (a) X-ray spectra taken from powders from as received Cp-Ti powder(AR), and powders subjected to heat exposures at 430°C for 24hr , and 530°C 20 hr.

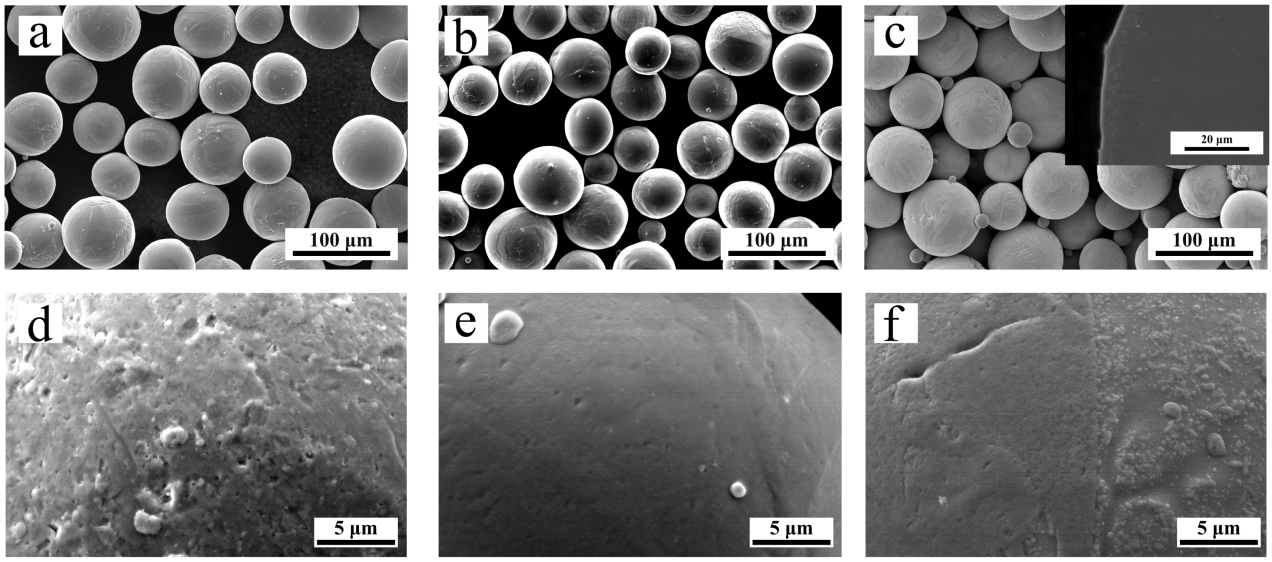

Fig. 6.5. (a and d) SEM image(taken with Everhart-Thornley detector) of Cp-Ti powder in the as received condition (b and e) SEM image (taken with Everhart-Thornley detector) of powder subjected to 430C for 24 hr. (c and f) SEM image (taken with Everhart-Thornley detector) of the powder subjected to 530C for 20 hr. Inset (backscattered SEM image) shows that oxide formed on surface is thin.

6.3.2 Conclusions

To summarize, this work has demonstrated a method to case harden Ti powder, with the potential for creating fine shot peening media to self-peen Ti systems. The time/temperature processing conditions for significantly hardening the case (almost tripling the surface hardness (∼8 GPa) over the core (∼3 GPa) hardness) in ambient atmosphere with no mechanical agitation while not significantly sintering nor significantly oxidizing the Ti powder is between 430°C / 24 hours to 530°C / 20 hours. The effective case depth created with a 20 hour oxidation at 530 °C is on the order of 2-3 μm, sufficient to harden powders with diameters between 50 and 100 μm.

7. COMPARISON SHOT MEDIA FOR SURFACE MODIFICATION OF TITANIUM ALLOYS FOR USE IN MEDICAL APPLICATION

7.1 Abstract

This study employed a newly developed Ti-based shot media for use in shot peening of titanium alloys and compared to glass shot in an attempt to provide proof of concept for the benefit of self peening processes. Resulting surface contamination from each shot media was evaluated with glow discharge spectrometry, and residual stresses produced by each shot media were measured through nano-indentation. Lastly, using the Ti and glass based media shot peening was used to develop ultra-fine grained layers on several Ti-based alloys. The corrosion rate of the UFG layers in conditions simulating the human body were used to show viability of use in medical applications.

7.2 Introduction

Titanium is a material of importance in several industries due to its low density and high strength. The value of titanium in the medical field was established by its chemical inertness that makes it biocompatible in the body. Even though Ti alloys have a lower modulus($\sim$112GPa) in comparison to CoCrMO(210 GPa) alloys and steels(207 GPa),Ti-alloys still have an elevated modulus in comparison to bone making it susceptible to stress shielding [102, 103]. This has created interest in developing low modulus Ti-alloys that are usually heavily alloyed with Nb. Additionally, Nb is a β-stabilizer in Ti [10] and most β-Ti alloys display a lower modulus than Ti-64 depending on their thermal history. Thus leading to the hypothesis that β-alloys

would be better suited for medical application so long as mechanical properties are acceptable. Therefore, the present study aims to compare Ti-64 to β-alloys(Ti-5553 and Ti-21S) used in the aerospace industry to show that currently available β-alloys can be suited for use in medical applications. Shot peening (SP) is a well-established surface modification process commonly used in a variety of industries. SP is valued for the compressive residual stress that the process imparts on the surface of the material that results in an increased fatigue life [91]. However, the aim of this study is to exploit the highly localized deformation incurred in the surface to enable grain refinement. Previous works have shown that surface microstructures can be refined to produce nanocrystalline(NC) and ultrafine grained (UFG) layers on the surface [48, 59, 63]. A drawback of SP is the surface contamination produced by the deposition of shot material onto the surface. The drawback is usually seen as a decrease in corrosion resistance as seen in previous works pertaining to Al, Mg and Fe alloys [93–95]. To circumvent surface contamination caused by SP it would seem necessary to use shot media that is composed of the same or similar material, essentially performing a self-peening of the material. previously, self-peening of Ti was not possible due to the lack of Ti-based shot. Self-peening of Ti alloys has become possible thanks to newly produced hardened Ti particulate media [104]. This study will show if the surface modification affects performance as it relates to corrosion resistance in a biological environment by performing cyclic potentiodynamic polarization on treated samples This study employed conventional SP as a surface deformation processes in combination with post SP heat-treatments to produce grain refinement on several Ti alloys, and evaluated the effects of the microstructural modification have on properties that affect biocompatibility.

7.3 Procedures

Several Ti-based alloys (see Table.4.1) were subjected to SP. The alloys were subjected to varied SP parameters (see Table.2). The study focuses on the effects of

peening media on the material by using SiO_2, and hardened titanium shot media. In this study both glass shot was used to compare against hardened Ti-based shot [104]. Surface contamination was measured through compositional depth profiles performed with a LECO glow discharge spectrometer (GDS 850A). GDS is a destructive compositional characterization technique that produces a plasma by sputtering material and analyzing the ionized atoms through a spectrometer. The GDS instrument is well suited to analyze interstitial inclusions such as C, O, and N. Specimens were Select specimens were subjected to post SP heat-treatments to produce UFG layers. Specimens of Ti-64 and Ti-5553 were heat-treated at 700°C for 20 min after SP. Ti-21S specimens were heat-treated to 575°C for 30 min. All heat-treatments were carried out under flowing Ar ; additionally, specimens were wrapped in Ti foil and covered in Ti sponge to avoid oxygen contamination.

Table 7.1.
Shot peening parameters. Previously presented in Table4.1, but presented here for the reader's convenience.

Shot Media	Density (g/cm^3)	Average diameter (μm)	Pressure (PSI/KPa)	Coverage(%)
SiO_2	2.52	300	80/552	83
Ti	4.5	100	80/552	83

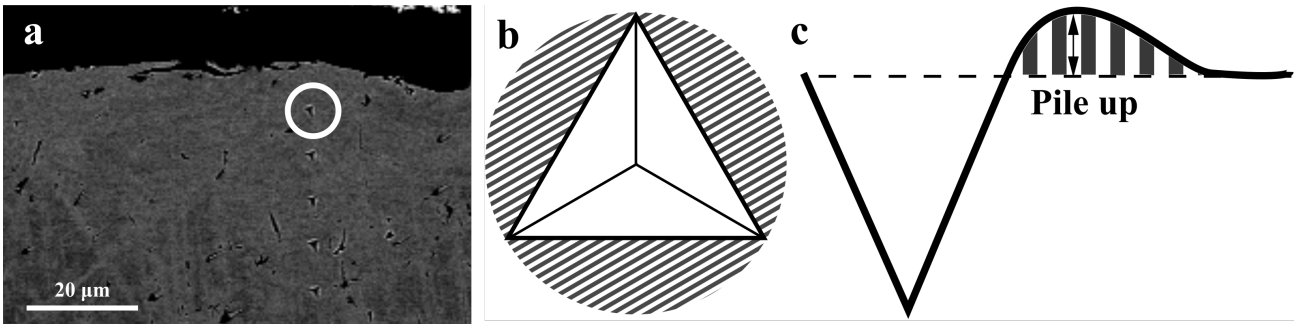

Fig. 7.1. (a)SEM backscattered image of Ti-specimen subjected to nanoindentation for RS measurement. Schematics of (b) plan view indentations, and (c) cross-sectional view showing the pile up height measured for RS measurements. The shaded areas indicate the pile up regions.

Following SP, specimens were cut to reveal the cross-sectional area, and prepared metallographically to produce a polished surface. Residual stress(RS) produced in the specimens were measured through nanoindentation using a method established by Ghanbari et al. [85]. A Hysitron Ti 950 Triboindenter with Berkovich tip with an effective radius of 300nm was used for RS evaluation. The residual stress profile is produced by placing a row of indents that samples different positions relative to the shot peened surface. A stress-free condition of each specimen was indented to measure the average pile up height (see Fig.7.1). This is then added to the measured height from the indentation (Eq.7.1), where h1,2,3 are pile up measurements on different sides of the indentation. The pile up height is used to correct the final depth achieved by the indentation, consequently correcting the contact area between the material and the tip.

$$h_c = h_p + \frac{h_1 + h_2 + h_3}{3} \tag{7.1}$$

$$\sigma_C = H(\frac{A_0}{A} - 1) \tag{7.2}$$

$$\sigma_T = \frac{H}{sin\alpha}(1 - \frac{A_0}{A}) \tag{7.3}$$

Compressive and tensile residual stress were calculated with Eq7.2-7.3(respectively). A stress is determined to be compressive or tensile by comparing the load of the shot peened condition to the stress-free condition, if the load is larger the stress is compressive. To get average surface hardness measurements, Vickers hardness was performed on the target surfaces before and after SP. A Zygo optical profilometer was used to measure surface roughness changes caused by SP. Lastly, the corrosion resistance of alloys was measured using cyclic potentiodynamic anodic polarization as described in ASTM G61. A three electrode set up using a saturated calomel reference electrode and a platinum counter. Hank's solution (see Table.7.2) was used as the electrolyte where samples were immersed because it is a well-established representative media for body conditions. The solution was maintained at 37°C and deaerated by bubbling N_2 gas into the solution for 1 hr. The specimen was immersed in the solution for 2 hours to stabilize the open circuit potential. The measured pH of the solution was 7.4.

Table 7.2.
Hank's solution composition. Composition expressed in g/L [75].

Species	Concentration
NaCl	8.0
CaCl2	0.14
KCl	0.4
MgCl˙26H2O	0.1
MgSO˙47H2O	0.1
NaHCO3	0.35
Na2HPO412H2O	0.12
KH2PO4	0.06
Phenol red	0.02
Glucose	1.0

7.3.1 Results and Discussion

Surface contamination and Reisdual stress comparison

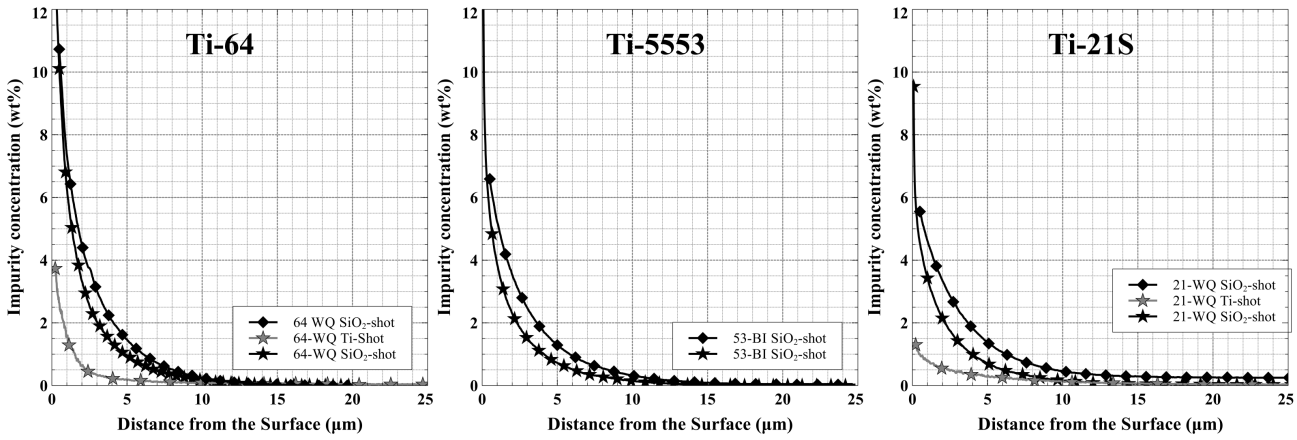

Fig. 7.2. Chemical depth profiles performed with GDS on Ti specimens that were subjected to SP with SiO_2 and Ti-shot .curves dotted with diamonds are measurements of Si, and curves dotted with stars are measurements of O.

GDS examination of SP surfaces (see Fig.7.2)) shows a clear change in surface chemistry for all specimens. The specimens peened with SiO_2 show an increased Si content, a consequence of deposition of shot materials during SP process. Surprisingly, the elevated Si content has penetrated several microns into the substrate , on average 13 μm from the surface across all alloys and conditions. The point of maximum penetration is defined as the point where the This uniform penetration of Si indicates that penetration of contamination is independent on initial surface hardness because the varied initial surfaces harness of each specimen resulted in similar contamination penetrations between $\sim$12-$\sim$14 μm. Specimens peened with Ti shows that the magnitude and maximum depth reached by contaminating species is significantly decreased. One can see(Fig.7.2) that the contamination incurred by Ti-shot is seen as an increase in O content within the first 5-8 μm. Additionally,

the increased O on the surface will not produce an oxide layer but will instead go into solution with the rest of the material upon subsequent heating, and because the magnitude and extent of penetration is small it may not affect precipitation of α-Ti, i.e. form an α-case. Thus indicating that the Ti-shot has successfully decreased the contamination incurred through SP, but more importantly argues that self-peening , i.e. peening a material with shot made of a similar material would remove the need for further cleaning steps after SP . The residual stress profiles (see Fig.3) produced by SP with Ti-shot and SiO_2-shot show that similar profiles have been produced from the use of both SiO_2 and Ti. This would suggest that the density of shot is critical in determining the residual stress. Previous works state that particle size of media is the processing parameter to control [105], but they have used the same material for SP media. In the present work, when all processing parameters (coverage, propelling pressure), and material conditions (composition, surface hardness and microstructure) are kept the same one can see that depth profile from a small shot with larger density(Ti-shot) can achieve similar RS profile to that of a lower density shot with larger size (SiO_2).

Table 7.3.
Measurements of hardness and contamination penetration in relation to shot media.

Specimen	Label	Surface hardness(HV0.5)		Shot Media	Contamination
		Untreated	SP Treated		Penetration (μm)
Ti-64 martensite	61	348+/-11	433+/-48	SiO_2	12.3
Ti-64 martensite	T61	338+/-7	389+/-14	Ti	5.2
Ti-5553 Bimodal	53	358+/-12	437+/-25	SiO_2	14.3
Ti-21S Fully β	21	301+/-12	389+/-15	SiO_2	13.8
Ti-21S Fully β	T21	296+/-13	344+/-16	Ti	7.8

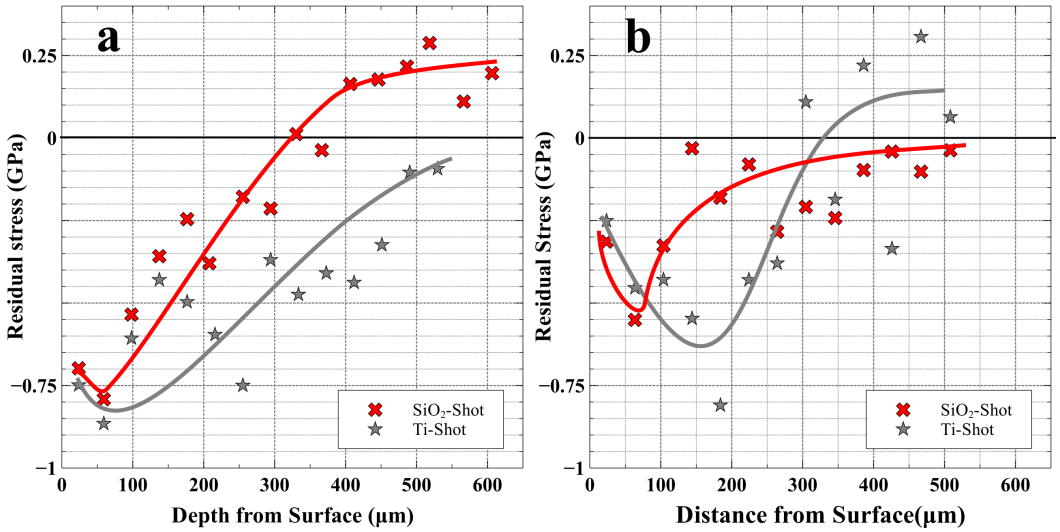

Fig. 7.3. Residual stress depth profiles measured in (a) Ti64 and (b) Ti21S, the marks on each curve identify the shot media used a cross for SiO_2 and a star for Ti.

Surface Hardness and Roughness

The peened surfaces showed increased hardness, this is due to the plastic deformation of the surface and is not affected by the elastic residual stress imposed on the material during SP (see table.4). Fig.4-a shows that increasing initial surface hardness decreases surface roughness (ra) show a lesser surface roughness. However, there is a clearer relation between surface roughness to shot size, as all specimens peened with SiO_2 displays a larger Ra than the specimens peened with Ti-shot, and the magnitude of Ra produced by each shot media is similar when for samples peened with the same media. Previous works state that increasing size of shot media increases surface roughness, residual stress imparted on the piece and depth of penetration caused by the SP process [67, 105]. The surface roughness results (see Fig.4) would suggest that the roughness of the part after SP is solely due to the size of the particles used, but when comparing the RS depth profiles one can see that similar magnitudes were achieved

with Ti and SiO_2 shot. This means that the density of shot in combination with shot velocity (determiend by propelling pressure) determines magnitude of RS and depth of profile. Interestingly the surface roughness obtained from SP process, which in aerospace applications would be undesirable, could lead to improvements in medical applications. Hsu et al. [106] reported that a surface roughness on Ti specimens with arithmetic average roughness between 1-2 μm showed improved osteointegration.

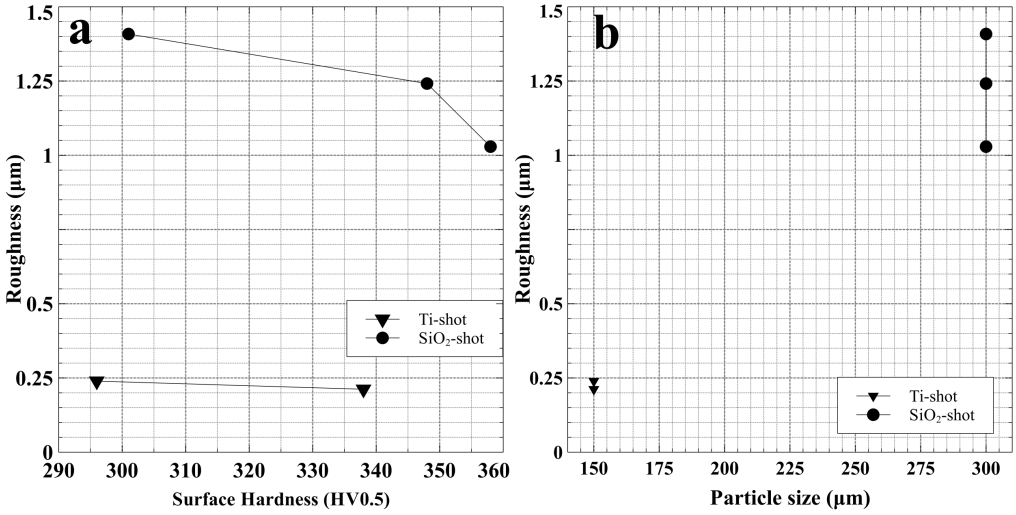

Fig. 7.4. Graphs showing (a) the arithmetic average roughness of the SP surfaces treated with Ti-Shot and SiO_2-shot vs initial surface hardness expressed in Vickers hardness, and (b) arithmetic average roughness of the SP surfaces treated with Ti-Shot and SiO_2-shot vs average shot diameter.

UFG layers

Peened specimens of Ti-64, Ti-5553, and Ti-21S that showed clear signs of plastic deformation near the surface (see Fig.5) were selected to perform a heat-treatment. Plastic deformation manifested itself Ti-64 specimens (64-WQ and T64-WQ) in the form of bent or distorted α-laths (see Fig.5-a,c). In Ti-5553 bimodal (53-BI) plastic deformation is seen by the distortion of α-laths at the surface, and the decrease of fine α-precipitates near the surface(see Fig.5-e). Ti-21S shows the formation shear bands

along the surface of the material (see Fig.5-g), it should be noted that the fully-β microstructure of Ti-21S shows deeper penetration of plastic deformation markers . The layer of ultra-fine grains produced in all Ti-64 specimens (See Fig.5) distinguishes itself morphologically from the microstructure of the bulk material because it is comprised entirely of a mixture of α+β equiaxed grains. This is in contrast to previous works that used ECAP [107] who reported a drop in β-phase fraction resulting from the severe plastic deformation, the work presented here shows clearly that the phase fraction of the UFG layers is dominated by α-Ti in Ti-64, but decreases in Ti-5553 and Ti21S as β-stabilizer content increases. Similarly, the β-alloys Ti-5553 produced an equiaxed mixture of α+β grains; however, Ti-21S shows 2 distinct morphologies of equiaxed grains to β-grains surrounded by grain boundary-α. The formation of equiaxed grains is commonly seen in other surface treatment, and tend to have a sharp boundary between the UFG layer and the bulk microstructure [81]. Nanoindentation was perfromed to measure hardness and modulus of the UFG layers in comparison with the underlying material. All specimens showed an increased hardness within the UFG layer with 64-WQ showing the largest increase in hardness from3.63 GPa to 5.08 GPa; followed by 21-WQ which went from 3.93 GPa to 5.00 GPa. Additionally, modulus measurements done on the UFG layers and the bulk material revealed that modulus did not change significantly showing Ti-64 having a modulus decrease 0.5% in comparison to the untreated condition, Ti-5553 decreased by 12%, and Ti-21S increased 5%. This is in contrast with Huang et al [63], who reported that modulus increased by 16% in specimens of CP-Ti treated with SMAT. An increase in modulus would be a deleterious effect of Sp based processes for medical applications because it would exacerbate the modulus mismatch that is already present between Ti-64($\sim$112GPa [4]) and bone ($\sim$20 GPa [108]). The modulus results would suggest that β-alloys treated with SP and heat-treatment to produce UFG layers would maintain a lower modulus while improving the hardness of the surface. This would suggest that newer TNZT alloys that exhibit lower modulus and higher β-stabilizer

content than Ti-64 could be processed in a similar manner as described in this study to improve surface properties without causing a detriment to stress shielding.

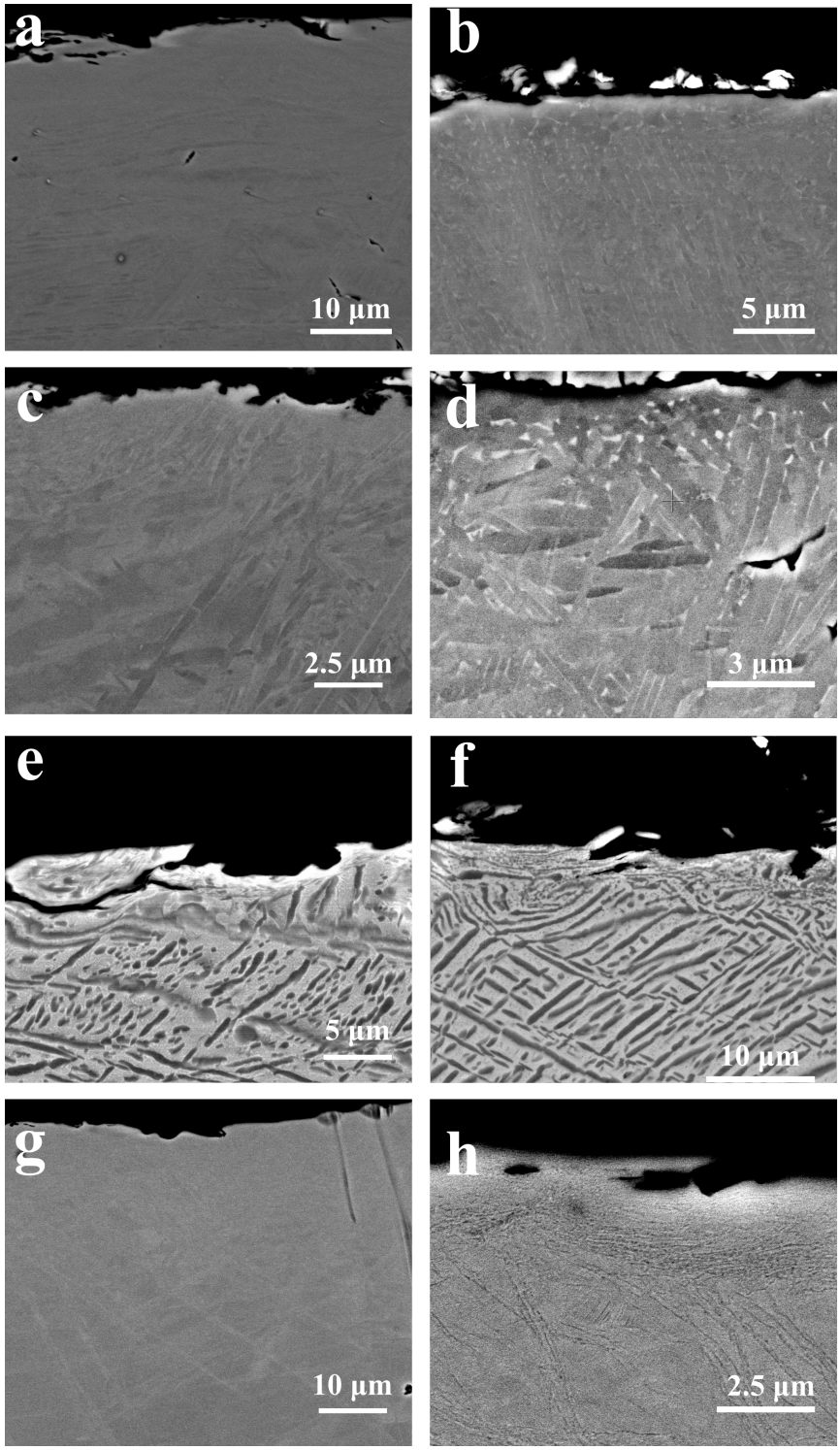

Fig. 7.5. SEM backscattered images showing peened (a) 64-WQ,(c)T61-WQ,(e) 53-BI, (g) 21-WQ, and post peening heat treated specimens showing UFG layers on (b) 64-WQ,(d)T61-WQ,(f) 53-BI, (h) 21-WQ.

Corrosion Resistance

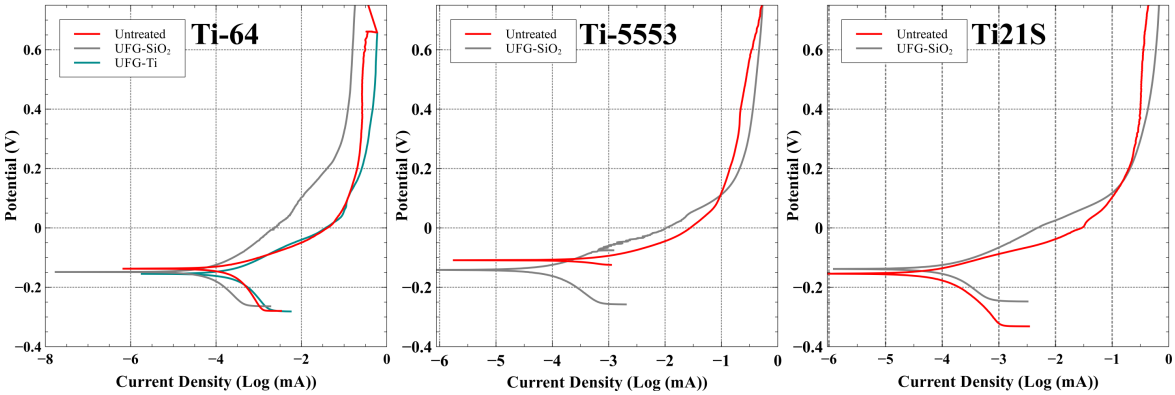

Fig. 7.6. Cyclic potentiodynamic polarization curves for specimens of Ti-64,Ti-5553 and Ti-21S treated to produce UFG layers through the use of SP with SiO_2 and Ti shot.

Potentiodynamic anodic polarization curves were produced for specimens that were processed to create the UFG layers(see Fig.5) with the intention of determining if the surface modification has affected the corrosion resistance of the material. Curves for treated Ti-64 samples seemed to become slightly more active than the untreated control sample as seen by the more negative E_{corr} (see Table.5); however, passivation is seen to take place evidenced by the lack of current change as potential increases. Interestingly the corrosion rates calculated through Tafel fit show no significant change corrosion rate. Results for Ti-21S showed similar trend to Ti-64 in that E_{corr} of the treated specimen became more negative, but the corrosion rate remained virtually unchanged. 53-BI showed a clear decrease in E_corr in comparison with the Ti-5553 control, but the corrosion rate has decreased in comparison to the control. The decrease in E_{corr} could be caused by the increased roughness of the specimens because the rougher surfaces tend to lower H overpotential making the surface more vulnerable to corrosion attack [28]. Additionally the rougher surfaces can decrease critical pitting temperature, consequently easing the formation of

pits [109]. The corrosion rate of all specimens analyzed did not show a significant increase of corrosion rate. Additionally, the grain refinement caused on the surface produces a larger concentration of interfaces at the surface that would normally be expected to severely deteriorate corrosion resistance; however, corrosion resistance of titanium alloys with UFG and NC features tends to be improved in comparison to their coarse grained counter-parts [9, 110, 111]. The reason for the increased corrosion resistance in UFG/NC Ti could be due to the increased short circuit diffusion paths created by the large concentration of grain boundaries adjacent to the surface that ease passivation of the surface in the event of passive film breakdown because of fast diffusional supply of Ti atoms. This is supported by previous authors [110–113] who looked at variations in grain size in relation to corrosion current densities, where they posit that the formation of an oxide layer (passivation) during anodic reactions requires ionic diffusion that would be facilitated by the increased density of interfaces at the surface. However, from the data presented here suggests that the fine grain structures are not having any effect on the corrosion resistance of the material, and further studies would have to be conducted to definitively state if the corrosion resistance remaining contestant is actual attributable to the grain size.

Table 7.4.
Comparison of polarization measurements.

Specimen	Shot media	OCP (mv)	E_{corr}	Corrosion rate (μm per year
Ti-64 untreated	N/A	-141	-138	0.45
61	SiO_2	-133	-147	0.25
T61	Ti	-138	-157	0.23
Ti-5553 untreated	N/A	-58	-63	16
53	SiO_2	-128	-144	9.40
Ti-21S untreated	N/A	-146	-160	7.05
21	SiO_2	-127	-143	7.57

7.3.2 Conclusions

The present study has compared the effects of shot peening Ti alloys with conventional (SiO_2) and new (Ti) shot media. The main findings of the study are summarized as follows:

1. Use of Ti-based shot has resulted in a marked decrease in magnitude of surface contamination and penetration into the material as demonstrated by the decreased magnitude and penetration of O in specimens peened with Ti-shot. This clearly shows the advantage of performing SP with shot media similar to the target , .i.e. self-peening, materials can eliminate the need for rigorous cleaning processes after SP.

2. Comparison of shot media effects show that density of shot is a key processing parameter for shot peening. The increased density of Ti shot produced similar residual stress profiles to those produced by SiO_2 shot, and the decreased size of the Ti shot decreased overall surface roughness.

3. The use of both Ti-based and SiO_2 shot media produced enough plastic deformation at the surface to allow grain refinement through recrystallization during post SP heat-treatments

4. Anodic potentiodynamic polarization curves showed that the UFG surfaces produced became more active, but the corrosion rate did not change as a result of the decreased average grain size on the surface. Consequently, the corrosion resistance did not deteriorate as a result of the UFG structure formed on the surface of the alloys , in spite of the increase surface roughness.

8. OVERALL CONCLUSIONS AND FUTURE WORKS

The application of conventional shot peening surface processing has been performed on Ti-64, Ti-5553, and Ti-21s. These alloys were selected because they provide a wide range of molybdenum equivalent content,a parameter that differentiates Ti alloys through chemical composition and the microstructures that can be formed within these alloys. The present study showed how several microstructural conditions in both $\alpha + \beta$ and β-alloys, microstructural responses can be described as follows:

- Uniform microstructures produced through solutionization and quenching in all alloys (referred in the text as quenched) readily deformed under the peening conditions used in this study. Additionally, all quenched conditions of the alloys showed deep and well defined residual stress profiles

- Lamellar conditions across all alloys showed little to no signs of deformation with exception of Ti-64 basket-weave structure. Similarly the residual stress stored in the material was low in magnitude and shallow in penetration.Comparing colony and basket-weave TI-64 microstructures showed a clear distinction between these structures, a fact that has been largely ignored in literature.

- Bimodal structures in Ti-64 and Ti-5553 showed clear signs of deformation in both alloys, and similar accommodation of residual stress.

The clear deformation of surface layers was shown to be an exploitable feature of the shot peening process that allows for the formation of greatly refined grain sizes at the surface, effectively creating a layer on the surface once it is heat treated to induce recrystallization. In all alloys the UFG layer was comprised of α plus β equiaxed grains, and were shown to be significantly harder than the original material. An unforeseen consequence of the post shot peening heat -treatment was the gradation

of volume fraction of α-Ti precipitates, which was exclusively seen in β-Ti alloys. Fully-β conditions of Ti-5553 and Ti-21S, showed this behavior after being treated, and the decrease of volume fraction α-Ti coincides with the decreasing residual stress. This would suggest that it is possible to produce tunealbe subsurface structures by producing selected residual stress profiles and then using the residual stress to induce precipitation.

The study has clearly succeeded in producing Ti-based shot peening media, and used it to perform self-peening of titanium alloys. Comparing the surface contamination of samples peened with SiO_2 vs Ti-shot showed a significant decrease in oxygen present at the surface and a lesser penetration of contaminants. This would suggest that further cleaning steps/processes would not be needed for self-peened parts. Additionally, the practice of self peening would avoid the previously reported deterioration of performance(corrosion resistance) due to shot contamination of the surface. The surface roughness created with the Ti-shot was significantly reduced in comparison to the SiO_2 shot, reinforcing previous works that show surface toughness is dependent on particle size. The residual stress from Ti-shot was similar magnitude and penetration in to the material showing that density of a key factor when selecting shot media.

The UFG layers produced on the surfaces of all the alloys were subjected to potentiondynamic polarization testing in an environment that simulated body conditions. This was done to determine if the UFG layers that were shown to increase surface hardness would have a deleterious effect on performance of a medical implant material. Results showed no significant change to corrosion resistance as corrosion rates did not increase, in spite of increased surface roughness on all treated surfaces

8.0.1 Future works

Throughout this study it was the author's intention to call attention to β-Ti alloys because of the promising mechanical properties that they display, and could make β-

Ti alloys better suited for applications in which Ti-64 or CP-Ti are currently being used.

Regarding surface microstructural refinement

If the effort to improve Ti-alloys for medical applications is to continue, newer titanium alloys that have been specifically developed to produce low modulus alloys should be investigated and processed in a similar manner to the treatments described in this study to produce UFG layers. Ti-Nb based alloys have shown promising performance in several studies present in literature. Alloys containing large amounts of Mo (namely Ti-15Mo) seem to have a similar effect, but will have a higher density.

It should be noted that the UFG layers produced in this study may improve materials' performance for other applications. The nature of the refined structures can be expected to have a lowered thermal stability, as many studies have shown coarsening of fine structures at low temperatures. This means that the thermal stability of the UFG layers should be investigated to determine the viability of the UFG-layers in applications the are above room temperature (T>200°C) Regardless of thermal stability, it is recommended that future effort investigate Ti-Al (Ti alumindes) since these materials are becoming popular in aerospace industry due to their high strength low density and retention of properties at high temperatures.

Regarding Precipitate gradient

The increased α-Ti phase fraction with increasing residual stress in the material suggests that by controlling the residual stress imparted on the part one can not only produce a UFG layer , but also create an adjustable precipitate layer beneath the UFG layer. The precipitate gradient effect should be evaluated in other alloy systems that can form a supersaturated solid solution(as is the case with the β structures seen in this study).

Additionally, the nature of shot peening allows for selection of surfaces to peen. Thus it would be interesting to understand the effect of a graded precipitate layer that are produced in selected areas of a singular part by considering the loading it experiences.

Regarding residual stress

As seen by the precipitation gradient, the residual stress is "used up" to allow precipitation ofα-Ti; however, this study has not shown evidence that this is a worthwhile exchange. Efforts should be done to determine if the fatigue life proerpties of specimens treated in the same manner as detailed in this study will decrease fatigue life in comparison to conventionally shot peened specimens

Regarding Self Peening

The success of self-peening on titanium would suggest that other valve materials such as Zr, V,Ta,etc could be processed in a similar manner to produce shot and carry out self-peening.

REFERENCES

[1] R. Boyer, "An overview on the use of titanium in the aerospace industry," *Materials Science and Engineering: A*, vol. 213, no. 1-2, pp. 103–114, 1996.

[2] B. D. Ratner, A. S. Hoffman, F. J. Schoen, and J. E. Lemons, *Biomaterials science: an introduction to materials in medicine*. Elsevier, 2004.

[3] D. M. Brunette, P. Tengvall, M. Textor, and P. Thomsen, *Titanium in medicine: material science, surface science, engineering, biological responses and medical applications*. Springer Science & Business Media, 2012.

[4] G. Welsch, R. Boyer, and E. Collings, *Materials properties handbook: titanium alloys*. ASM international, 1993.

[5] M. Niinomi and M. Nakai, "Titanium-based biomaterials for preventing stress shielding between implant devices and bone," *International journal of biomaterials*, vol. 2011, 2011.

[6] "Allvac ti-15mo (beta-rich alpha-beta alloy)."

[7] X. Yang and C. R. Hutchinson, "Corrosion-wear of -ti alloy tmzf (ti-12mo-6zr-2fe) in simulated body fluid," *Acta Biomaterialia*, vol. 42, pp. 429 – 439, 2016. [Online]. Available: http://www.sciencedirect.com/science/article/pii/S1742706116303245

[8] L. M. Ricciardi and H. Umezawa, "Brain and physics of many-body problems," *Kybernetik*, vol. 4, no. 2, pp. 44–48, 1967.

[9] S. Bagheri and M. Guagliano, "Review of shot peening processes to obtain nanocrystalline surfaces in metal alloys," *Surface Engineering*, vol. 25, no. 1, pp. 3–14, 2009.

[10] G. Lütjering and J. C. Williams, *Titanium*. Springer Science & Business Media, 2007.

[11] J. Murray and H. Wriedt, "The o- ti (oxygen-titanium) system," *Journal of Phase Equilibria*, vol. 8, no. 2, pp. 148–165, 1987.

[12] D. Brice, P. Samimi, I. Ghamarian, Y. Liu, R. Brice, R. Reidy, J. Cotton, M. Kaufman, and P. C. Collins, "Oxidation behavior and microstructural decomposition of ti-6al-4v and ti-6al-4v-1b sheet," *Corrosion Science*, vol. 112, pp. 338–346, 2016.

[13] S. Banerjee and P. Mukhopadhyay, *Phase transformations: examples from titanium and zirconium alloys*. Elsevier, 2010, vol. 12.

[14] G. Ghosh, "Thermodynamic and kinetic modeling of the cr-ti-v system," *Journal of phase equilibria*, vol. 23, no. 4, p. 310, 2002.

[15] B. Predel, "Mo-ti (molybdenum-titanium)," in *Li-Mg–Nd-Zr*. Springer, 1997, pp. 1–3.

[16] D. Brice, P. Samimi, I. Ghamarian, Y. Liu, M. Mendoza, M. J. Kenney, R. Reidy, M. Garcia-Avila, and P. C. Collins, "On the eutectoid transformation behavior of the ti-zn system and its metastable phases," *Journal of Alloys and Compounds*, vol. 718, pp. 22–27, 2017.

[17] G. Franti, J. Williams, and H. Aaronson, "A survey of eutectoid decomposition in ten ti-x systems," *Metallurgical Transactions A*, vol. 9, no. 11, pp. 1641–1649, 1978.

[18] S. Nag, R. Banerjee, R. Srinivasan, J. Hwang, M. Harper, and H. Fraser, "ω-assisted nucleation and growth of α precipitates in the ti–5al–5mo–5v–3cr–0.5 fe β titanium alloy," *Acta Materialia*, vol. 57, no. 7, pp. 2136–2147, 2009.

[19] D. Brice, *An assessment of uncommon titanium binary systems: Ti-Zn, Ti-Cu, and Ti-Sb*. University of North Texas, 2015.

[20] G. Lütjering, "Influence of processing on microstructure and mechanical properties of (α+ β) titanium alloys," *Materials Science and Engineering: A*, vol. 243, no. 1-2, pp. 32–45, 1998.

[21] G. E. Dieter and D. J. Bacon, *Mechanical metallurgy*. McGraw-hill New York, 1986, vol. 3.

[22] R. E. Reed-Hill, R. Abbaschian, and R. Abbaschian, "Physical metallurgy principles," 1973.

[23] D. Eylon and J. Hall, "Fatigue behavior of beta processed titanium alloy imi 685," *Metallurgical Transactions A*, vol. 8, no. 6, pp. 981–990, 1977.

[24] S. Semiatin, V. Seetharaman, and I. Weiss, "The thermomechanical processing of alpha/beta titanium alloys," *Jom*, vol. 49, no. 6, pp. 33–39, 1997.

[25] J. D. Cotton, R. D. Briggs, R. R. Boyer, S. Tamirisakandala, P. Russo, N. Shchetnikov, and J. C. Fanning, "State of the art in beta titanium alloys for airframe applications," *Jom*, vol. 67, no. 6, pp. 1281–1303, 2015.

[26] S. Nyakana, J. Fanning, and R. Boyer, "Quick reference guide for β titanium alloys in the 00s," *Journal of materials engineering and performance*, vol. 14, no. 6, pp. 799–811, 2005.

[27] D. Brice, "Unpublished work on ti-alloys. university of north texas."

[28] R. W. Revie, *Corrosion and corrosion control: an introduction to corrosion science and engineering*. John Wiley & Sons, 2008.

[29] H. Okamoto, "O-ti (oxygen-titanium)," *Journal of Phase Equilibria and Diffusion*, vol. 32, no. 5, pp. 473–474, 2011.

[30] R. Padma, K. Ramkumar, and M. Satyam, "Growth of titanium oxide overlayers by thermal oxidation of titanium," *Journal of materials science*, vol. 23, no. 5, pp. 1591–1597, 1988.

[31] P. Samimi, D. Brice, R. Banerjee, M. Kaufman, and P. C. Collins, "On the influence of alloy composition on the oxidation performance and oxygen-induced phase transformations in ti–(0–8) wt% al alloys," *Journal of materials science*, vol. 51, no. 8, pp. 3684–3692, 2016.

[32] T. A. Wallace, R. K. Clark, and K. E. Wiedemann, "Oxidation characteristics of beta-21s in air in the temperature range 600 to 800 c," 1992.

[33] P. Samimi, Y. Liu, I. Ghamarian, D. A. Brice, and P. C. Collins, "A new combinatorial approach to assess the influence of alloy composition on the oxidation behavior and concurrent oxygen-induced phase transformations for binary ti–xcr alloys at 650 c," *Corrosion Science*, vol. 97, pp. 150–160, 2015.

[34] H. Dong, P. H. Morton, A. Bloyce, and T. Bell, "Method of case hardening," Dec. 21 2004, uS Patent 6,833,197.

[35] H. Dong and X. Li, "Oxygen boost diffusion for the deep-case hardening of titanium alloys," *Materials Science and Engineering: A*, vol. 280, no. 2, pp. 303–310, 2000.

[36] B. Sarma and K. R. Chandran, "Recent advances in surface hardening of titanium," *JOM*, vol. 63, no. 2, pp. 85–92, 2011.

[37] C. Koch, "Optimization of strength and ductility in nanocrystalline and ultrafine grained metals," *Scripta Materialia*, vol. 49, no. 7, pp. 657–662, 2003.

[38] H. Gleiter, "Nanocrystalline materials," *Progress in Materials Science*, vol. 33, no. 4, pp. 223 – 315, 1989. [Online]. Available: http://www.sciencedirect.com/science/article/pii/0079642589900017

[39] ——, "Nanocrystalline materials," in *Advanced Structural and Functional Materials*. Springer, 1991, pp. 1–37.

[40] R. Valiev, "Nanostructuring of metals by severe plastic deformation for advanced properties," *Nature materials*, vol. 3, no. 8, p. 511, 2004.

[41] R. Z. Valiev, R. K. Islamgaliev, and I. V. Alexandrov, "Bulk nanostructured materials from severe plastic deformation," *Progress in materials science*, vol. 45, no. 2, pp. 103–189, 2000.

[42] Y. Wang, M. Chen, F. Zhou, and E. Ma, "High tensile ductility in a nanostructured metal," *Nature*, vol. 419, no. 6910, p. 912, 2002.

[43] A. Vinogradov and S. Hashimoto, "Multiscale phenomena in fatigue of ultrafine grain materials—an overview," *Materials Transactions*, vol. 42, no. 1, pp. 74–84, 2001.

[44] K. Zhu, A. Vassel, F. Brisset, K. Lu, and J. Lu, "Nanostructure formation mechanism of α-titanium using smat," *Acta Materialia*, vol. 52, no. 14, pp. 4101–4110, 2004.

[45] A. Rosochowski, *Severe plastic deformation technology*. Whittles Publishing, 2017.

[46] A. Azushima, R. Kopp, A. Korhonen, D. Yang, F. Micari, G. Lahoti, P. Groche, J. Yanagimoto, N. Tsuji, A. Rosochowski *et al.*, "Severe plastic deformation (spd) processes for metals," *CIRP Annals*, vol. 57, no. 2, pp. 716–735, 2008.

[47] L. Wagner, "Mechanical surface treatments on titanium, aluminum and magnesium alloys," *Materials Science and Engineering: A*, vol. 263, no. 2, pp. 210–216, 1999.

[48] Y. Todaka, M. Umemoto, Y. Watanabe, and K. Tsuchiya, "Formation of nanocrystalline structure by shot peening," in *Materials Science Forum*, vol. 503. Trans Tech Publ, 2006, pp. 669–674.

[49] W. Zinn, J. Schulz, R. Kopp, and B. Scholtes, "The influence of the velocity of a peening medium on the almen intensities and residual stress states of shot peened specimens," *Shot Peening*, pp. 161–166, 2002.

[50] *SAE J444 Cast Shot and Grit Size Specifications for Peening and Cleaning*.

[51] D. Kirk and M. Abyaneh, "Theoretical basis of shot peening coverage control," *Shot Peener(USA)*, vol. 9, no. 2, pp. 28–30, 1995.

[52] P. Prevey and J. Cammett, "The effect of shot peening coverage on residual stress," *Cold Work and Fatigue in a Ni-Cr-Mo Low Alloy Steel, Shot Peening (L. Wagner, ed.) Wiley-VCH (2003)*, vol. 295, 2003.

[53] D. Kirk, "Shot peening," *Aircraft Engineering and Aerospace Technology*, vol. 71, no. 4, pp. 349–361, 1999.

[54] *ASTM-B851 Standard Specification for Automated Controlled Shot Peening of Metallic Articles Prior to Nickel, Autocatalytic Nickel, or Chromium Plating, or as Final Finish1*.

[55] *SAE-J2277 Shot Peening Coverage Determination*.

[56] G. Salishchev, S. Y. Mironov, and S. Zherebtsov, "Mechanisms of submicron grain formation in titanium and two-phase titanium alloy during large strain warm working," in *Nanostructured Materials by High-Pressure Severe Plastic Deformation*. Springer, 2006, pp. 47–54.

[57] L. Saitova, I. Semenova, G. Raab, R. Valiev, T. Lowe, and Y. Zhu, "Improving the mechanical properties of ti-6al-4v alloy by equal channel angular pressing," in *Nanostructured Materials by High-Pressure Severe Plastic Deformation*. Springer, 2006, pp. 241–246.

[58] E. Ma, "Instabilities and ductility of nanocrystalline and ultrafine-grained metals," *Scripta Materialia*, vol. 49, no. 7, pp. 663–668, 2003.

[59] T. Fang, W. Li, N. Tao, and K. Lu, "Revealing extraordinary intrinsic tensile plasticity in gradient nano-grained copper," *Science*, vol. 331, no. 6024, pp. 1587–1590, 2011.

[60] N. Akhmadeev, N. Kobelev, R. Mulyukov, Y. Soifer, and R. Valiev, "The effect of heat treatment on the elastic and dissipative properties of copper with the submicrocrystalline structure," *Acta Metallurgica et Materialia*, vol. 41, no. 4, pp. 1041 – 1046, 1993. [Online]. Available: http://www.sciencedirect.com/science/article/pii/095671519390153J

[61] A. Lebedev, S. Pulnev, V. Kopylov, Y. Burenkov, V. Vetrov, and O. Vylegzhanin, "Thermal stability of submicrocrystalline copper and cu: Zro2 composite," *Scripta Materialia*, vol. 35, no. 9, pp. 1077 – 1081, 1996. [Online]. Available: http://www.sciencedirect.com/science/article/pii/1359646296002618

[62] R. Mulyukov, M. Weller, R. Valiev, T. Gessmann, and H.-E. Schaefer, "Internal friction and shear modulus in submicrograined cu," *Nanostructured Materials*, vol. 6, no. 5, pp. 577 – 580, 1995, proceedings of the Second International Conference on Nanostructured Materials. [Online]. Available: http://www.sciencedirect.com/science/article/pii/0965977395001247

[63] L. Huang, J. Lu, and M. Troyon, "Nanomechanical properties of nanostructured titanium prepared by smat," *Surface and Coatings Technology*, vol. 201, no. 1, pp. 208 – 213, 2006. [Online]. Available: http://www.sciencedirect.com/science/article/pii/S0257897205012934

[64] V. Lacaille, G. Kermouche, D. T. Spinel, E. Feulvarch, C. Morel, and J. Bergheau, "Modeling nitriding enhancement resulting from the nanopeening treatment of a pure iron," in *IOP Conference Series: Materials Science and Engineering*, vol. 63, no. 1. IOP Publishing, 2014, p. 012124.

[65] V. V. Stolyarov, Y. T. Zhu, I. V. Alexandrov, T. C. Lowe, and R. Z. Valiev, "Influence of ecap routes on the microstructure and properties of pure ti," *Materials Science and Engineering: A*, vol. 299, no. 1-2, pp. 59–67, 2001.

[66] P. Shewmon, *Diffusion in solids*. Springer, 2016.

[67] E. Maleki, O. Unal, and K. R. Kashyzadeh, "Effects of conventional, severe, over, and re-shot peening processes on the fatigue behavior of mild carbon steel," *Surface and Coatings Technology*, vol. 344, pp. 62–74, 2018.

[68] M.-C. Berger and J. Gregory, "Residual stress relaxation in shot peened timetal 21s," *Materials Science and Engineering: A*, vol. 263, no. 2, pp. 200–204, 1999.

[69] , *Shot Peening Coverage Determination*, apr 2013. [Online]. Available: https://doi.org/10.4271/J2277˙201304

[70] A. C. Fischer-Cripps, *Introduction to contact mechanics*. Springer, 2000, vol. 87.

[71] *ASTM E92-17 Standard Test Methods for Vickers Hardness and Knoop Hardness of Metallic Materials, ASTM International, West Conshohocken, PA, 2017.*

[72] R. Payling and T. Nelis, *Glow discharge optical emission spectroscopy: a practical guide*. Royal Society of Chemistry, 2007.

[73] R. Baboian and G. Haynes, "Cyclic polarization measurements—experimental procedure and evaluation of test data," in *Electrochemical corrosion testing*. ASTM International, 1981.

[74] A. S. for Testing and P. Materials (Filadelfia, "Astm g5-14: Standard reference test method for making potentiodynamic anodic polarization measurements." ASTM, 2014.

[75] A. International, "Astm f2129-17b-standard test method for conducting cyclic potentiodynamic polarization measurements to determine the corrosion susceptibility of small implant devices," 2017.

[76] M. Geetha, A. K. Singh, R. Asokamani, and A. K. Gogia, "Ti based biomaterials, the ultimate choice for orthopaedic implants–a review," *Progress in materials science*, vol. 54, no. 3, pp. 397–425, 2009.

[77] J. Fanning, "Properties of timetal 555 (ti-5al-5mo-5v-3cr-0.6 fe)," *Journal of Materials Engineering and Performance*, vol. 14, no. 6, pp. 788–791, 2005.

[78] ——, "Timetal 21s property datasheet."

[79] ——, "Timetal reg-sign 21s property data," in *Beta Titanium Alloys in the 1990's*, 1993.

[80] C. Leyens and M. Peters, *Titanium and titanium alloys: fundamentals and applications*. John Wiley & Sons, 2003.

[81] S. Bagherifard and M. Guagliano, "Fatigue behavior of a low-alloy steel with nanostructured surface obtained by severe shot peening," *Engineering Fracture Mechanics*, vol. 81, pp. 56–68, 2012.

[82] E. Ma, "Eight routes to improve the tensile ductility of bulk nanostructured metals and alloys," *Jom*, vol. 58, no. 4, pp. 49–53, 2006.

[83] Y. Wang and E. Ma, "Three strategies to achieve uniform tensile deformation in a nanostructured metal," *Acta Materialia*, vol. 52, no. 6, pp. 1699–1709, 2004.

[84] P. S. Prevey and J. T. Cammett, "The effect of shot peening coverage on residual stress, cold work and fatigue in a ni-cr-mo low alloy steel," *Shot peening*, pp. 295–304, 2003.

[85] S. Ghanbari, M. D. Sangid, and D. F. Bahr, "Residual stress asymmetry in thin sheets of double-sided shot peened aluminum," *Journal of Materials Engineering and Performance*, vol. 28, no. 5, pp. 3094–3104, 2019.

[86] B. R. Bhat, M. Jayalakshmi, and K. U. Bhat, "Effect of shot peening coverage on surface nanostructuring of 316l stainless steel and its influence on low temperature plasma-nitriding," *Materials Performance and Characterization*, vol. 6, no. 4, pp. 561–570, 2017.

[87] I. Weiss, F. Froes, D. Eylon, and G. Welsch, "Modification of alpha morphology in ti-6al-4v by thermomechanical processing," *Metallurgical Transactions A*, vol. 17, no. 11, pp. 1935–1947, 1986.

[88] P. Samimi, *Combinatorial assessment of the influence of composition and exposure time on the oxidation behavior and concurrent oxygeninduced phase transformations of binary Ti-x systems*. University of North Texas, 2015.

[89] P. Samimi, Y. Liu, I. Ghamarian, and P. C. Collins, "A novel tool to assess the influence of alloy composition on the oxidation behavior and concurrent oxygen-induced phase transformations for binary ti–xmo alloys at 650 c," *Corrosion Science*, vol. 89, pp. 295–306, 2014.

[90] S. Bagherifard, R. Ghelichi, and M. Guagliano, "On the shot peening surface coverage and its assessment by means of finite element simulation: a critical review and some original developments," *Applied Surface Science*, vol. 259, pp. 186–194, 2012.

[91] P. Hutmann, "The application of mechanical surface treatment in the passenger car industry," *Shot peening*, p. 3, 2006.

[92] W. König, "Life enhancement of aero engine components by shot peening: opportunities and risks," in *Shot peening*. Wiley-VCH, Weinheim, 2003, pp. 1–22.

[93] Q. Sun, Q. Han, X. Liu, W. Xu, and J. Li, "The effect of surface contamination on corrosion performance of ultrasonic shot peened 7150 al alloy," *Surface and Coatings Technology*, vol. 328, pp. 469–479, 2017.

[94] C. Muller and R. Rodriguez, "Influence of shot peening on the fatigue and corrosion behavior of the die cast magnesium alloy az91 hp. conf," *Proc. ICSP–8*, pp. 271–277, 2002.

[95] P. Zhang, J. Lindemann, and C. Leyens, "Shot peening on the high-strength wrought magnesium alloy az80—effect of peening media," *Journal of Materials Processing Technology*, vol. 210, no. 3, pp. 445–450, 2010.

[96] A. Schuh, U. Holzwarth, G. ZEILER, W. Kachler, J. GÖSKE, T. KNETSCH, and B. EIGEN-MANN, "Shot peening of a titanium alloy for medical implant applications with zirconia shot," in *Shot peening–Proc. 9th Int. Conf., IITT Int., Noisy-le-Grand*, 2005, pp. 54–59.

[97] C. Suryanarayana and M. G. Norton, *X-ray diffraction: a practical approach*. Springer Science & Business Media, 2013.

[98] S. Garg, N. Krishnamurthy, A. Awasthi, and M. Venkatraman, "The o-ta (oxygen-tantalum) system," *Journal of phase equilibria*, vol. 17, no. 1, pp. 63–77, 1996.

[99] H. Wriedt, "The ov (oxygen-vanadium) system," *Bulletin of Alloy Phase Diagrams*, vol. 10, no. 3, pp. 271–277, 1989.

[100] C. Wang, M. Zinkevich, and F. Aldinger, "On the thermodynamic modeling of the zr–o system," *Calphad*, vol. 28, no. 3, pp. 281–292, 2004.

[101] D. Shin, R. Arróyave, and Z.-K. Liu, "Thermodynamic modeling of the hf–si–o system," *Calphad*, vol. 30, no. 4, pp. 375–386, 2006.

[102] M. Long and H. Rack, "Titanium alloys in total joint replacement—a materials science perspective," *Biomaterials*, vol. 19, no. 18, pp. 1621–1639, 1998.

[103] D. R. Sumner and J. O. Galante, "Determinants of stress shielding," *Clin. Orthop. Relat. Res*, vol. 274, pp. 202–212, 1991.

[104] D. Brice, R. Rahimi, and D. Bahr, "Hardening particulate ti media through controlled oxidation," *Metallurgical and Materials Transactions A*, pp. 1–5.

[105] V. Schulze, "Characteristics of surface layers produced by shot peening," in *Proceeding of the Eighth International Conference on Shot Peening ICSP-8 in Garmisch-Partenkirchen DGM*. Citeseer, 2002, pp. 145–160.

[106] S.-h. Hsu, B.-S. Liu, W.-H. Lin, H.-C. Chiang, S.-C. Huang, and S.-S. Cheng, "Characterization and biocompatibility of a titanium dental implant with a laser irradiated and dual-acid etched surface," *Bio-medical materials and engineering*, vol. 17, no. 1, pp. 53–68, 2007.

[107] I. Semenova, G. Raab, L. Saitova, and R. Valiev, "The effect of equal-channel angular pressing on the structure and mechanical behavior of ti–6al–4v alloy," *Materials Science and Engineering: A*, vol. 387, pp. 805–808, 2004.

[108] D. M. Brunette, P. Tengvall, M. Textor, and P. Thomsen, *Titanium in medicine: material science, surface science, engineering, biological responses and medical applications*. Springer Science & Business Media, 2012.

[109] S. Esmailzadeh, M. Aliofkhazraei, and H. Sarlak, "Interpretation of cyclic potentiodynamic polarization test results for study of corrosion behavior of metals: A review," *Protection of Metals and Physical Chemistry of Surfaces*, vol. 54, no. 5, pp. 976–989, 2018.

[110] K. Ralston and N. Birbilis, "Effect of grain size on corrosion: a review," *Corrosion*, vol. 66, no. 7, pp. 075 005–075 005, 2010.

[111] K. Ralston, N. Birbilis, and C. Davies, "Revealing the relationship between grain size and corrosion rate of metals," *Scripta Materialia*, vol. 63, no. 12, pp. 1201–1204, 2010.

[112] S. Lee and H. S. White, "Dissolution of the native oxide film on polycrystalline and single-crystal aluminum in nacl solutions," *Journal of The Electrochemical Society*, vol. 151, no. 8, pp. B479–B483, 2004.

[113] M.-K. Chung, Y.-S. Choi, J.-G. Kim, Y.-M. Kim, and J.-C. Lee, "Effect of the number of ecap pass time on the electrochemical properties of 1050 al alloys," *Materials Science and Engineering: A*, vol. 366, no. 2, pp. 282–291, 2004.